UNIVERSITA' DI SIENA

DIPARTIMENTO DI MEDICINA MOLECOLARE E DELLO SVILUPPO

DOTTORATO DI RICERCA IN MEDICINA MOLECOLARE

CICLO XXXV

COORDINATORE Vincenzo Sorrentino

Pacemaking and pacemaker current in cardiac and neuronal cells: a multi-method electrophysiological approach for evaluating innovative blockers and modulatory signals

SETTORE SCIENTIFICO-DISCIPLINARE: BIO/14

DOTTORANDA

Valentina Balducci

Digitally signed by BALDUCCI VALENTINA
C=IT

TUTOR

Prof.ssa Elisabetta Cerbai

ANNO ACCADEMICO: 2021/2022

CHAPTER I.
INTRODUCTION

1. Pacemaking and pacemaker current

Cardiac pacemaking can be considered the most relevant cardiac function; however, pacemaker function is also widely present in the nervous system.

In the heart pacemaking takes place in peculiar regions, located in the wall of the right atrium and named sinoatrial node (SAN). SAN cells have the capacity to generate spontaneous action potentials, propagate them to the rest of the cardiac muscle and drive the rhythmic cardiac contraction (Barbuti *et al.*, 2007). In the central and peripheric nervous system pacemaking neurons are located in many different regions, where they regulate a number of diverse functions including synaptic transmission, dendritic integration, learning and memory, visual and pain perceptions (Pape, 1996; Robinson and Siegelbaum, 2003).

The slow diastolic depolarization (phase 4 of the cardiac action potential) is the result of a net inward ionic current, which leads to a positive and progressive voltage increase between the end of one action potential and the beginning of the next one. Several mechanisms underlie this phenomenon (Noma, 1996), but the major role is played by the hyperpolarization-activated cyclic-nucleotide gated current (or *funny* current, I_f). Since its first description in the rabbit cardiac SAN (Brown et al., 1979), I_f drew the attention of many researchers because of several unusual features (hence the term “funny”) that have been highlighted in some pioneer works (Brown and Di Francesco, 1981; Di Francesco, 1993; Di Francesco, 1999). The first unusual feature is its voltage dependence: I_f is activated by hyperpolarization with a threshold of -40/-60 mV in the SAN. At the termination of an action potential, the pacemaker depolarization slowly brings the membrane voltage up to threshold for initiation of a new action potential, thus producing repetitive activity (Accili et al., 2002; DiFrancesco, 2006). The second feature of I_f is the mixed permeability to sodium (Na^+) and potassium (K^+). In fact, studies have shown that the I_f is fully activated at about -100/-110 mV and its reversal potential is about -10/-20 mV, which indicates the mixed ionic nature of the current (Freemantle et al., 1999; Mengesha et al., 2017). Another unusual feature is the direct activation by cyclic adenosine monophosphate (cAMP). I_f thus represents a unique ion current, which is dually regulated by voltage and direct cAMP binding. As cAMP acts as a second messenger, there exist several endogenous mediators and molecules that can influence I_f kinetics by using this cyclic nucleotide in their intracellular pathways: for example acetylcholine and catecholamines modulate I_f by shifting its activation curve along the voltage axis in negative and positive direction, respectively (DiFrancesco and Tortora, 1991).

Besides the heart, I_f has been investigated also in non-cardiac tissues. In particular, the current has been described in different types of neurons, where it takes the name of I_h, which displays main biophysical properties similar to those described in the cardiac pacemakers (see below) (Pape, 1996; Robinson and Siegelbaum, 2003).

1.1 Hyperpolarization-activated Cyclic Nucleotide-gated (HCN) channels

In the late 1990s three different research groups cloned the genes responsible for the pacemaker currents (Gauss et al., 1998; Ludwig et al., 1998; Santoro et al., 1998). The corresponding proteins turned out to be ion channels whose properties were closely related

to the current they generate, hence the name of Hyperpolarization-activated Cyclic Nucleotide gated (HCN) channels.

In mammalians, four HCN isoforms have been cloned (HCN1-4). The first three were identified in the mouse brain (Ludwig et al., 1998; Santoro et al., 1998), while the fourth isoform was revealed during a cDNA library screening from human heart (Ludwig et al., 1999). Human genes coding for the four isoforms are all located in different chromosomes (Vaccari et al., 1999; Seifert et al., 1999). The main features of HCN channels follow the same ones we already attributed to I_f/I_h: activation upon membrane hyperpolarization, mixed Na^+ and K^+ permeability and modulation by cyclic nucleotides (mainly cAMP). Furthermore, all isoforms are blocked in a voltage-dependent way by millimolar concentrations of extracellular cesium (Cs^+), although different isoforms show slight differences in Cs^+ concentrations required to block 50% of current (Accili et al., 2002).

1.1.1 Structure and properties

HCN channels belong to the subgroup of cyclic nucleotide-regulated cation channels within the large super family of the pore-loop cation channels (Biel and Michalakis, 2007). The core unit of HCN consists of four subunits arranged around the centrally located pore. Different subunit isoforms have been identified; these subunits can form four different homotetramers with distinct biophysical properties (Ishii et al., 1999). However, there is evidence that the number of potential HCN channel types is increased *in vivo* by the formation of heterotetramers (Altomare et al., 2003; Baruscotti et al., 2010). Each subunit contains two structural modules: the transmembrane core and the cytosolic C-terminal domain (Figure 1).

The transmembrane core hosts the gating machinery and the ion conducting pore, the cytosolic C-terminal domain confers modulation by cyclic nucleotides. Both modules allosterically cooperate with each other during channel activation (Wahl Schott and Biel, 2009). The transmembrane core is composed of six α-helical segments (S1-S6), of which S1-S4 represent the voltage-sensing domains and S5 and S6 constitute the ion conducting pore loops or pore domains. A highly conserved asparagine residue in the extracellular loop between S5 and the pore loop is glycosylated. This post-translational modification seems to be crucial for normal cell surface expression (Much et al., 2003). The pore loop contains a glycine-tyrosine-glycine (GYG) motif, which represents the typical selectivity filter for the K^+ selective voltage-dependent channels (K_v) (Biel et al., 2009). However, HCN channels show scarce selectivity, conducting both Na^+ and K^+. In the tetrameric HCN channel complex, GYG motifs are coordinated in a less rigid fashion than in K_v channel, and Na^+ ions can easily permeate the pore without binding, while K^+ forms a singlebound within the pore region (Lee and MacKinnon, 2017). Na^+ entry and K^+ exit occur with a ratio ranging from 1:3 to 1:5 (Biel et al., 2009). Surprisingly, HCN channels also seem to display a small permeability for calcium (Ca^{2+}), but their fractional calcium current is small compared with other Ca^{2+} permeable channels. At 2.5 mM external Ca^{2+}, the fractional current of HCN2 and HCN4 is about 0.5% (Yu et al., 2004).

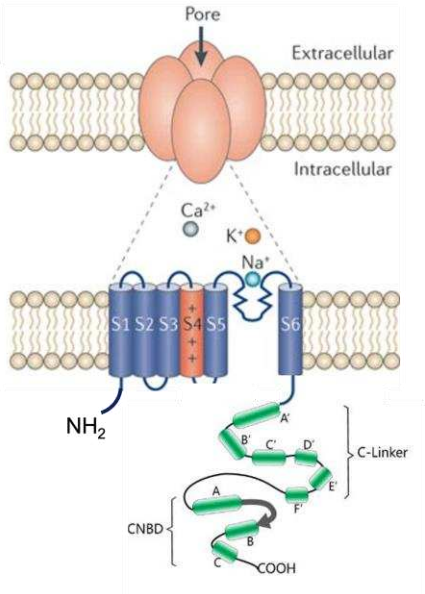

Figure 1. Transmembrane topology of HCN channels. The HCN channels are tetramers (upper panel). Each subunit is composed of six transmembrane segments (S1-S6), which include the voltage sensor (S4) and the selectivity filter at the pore loop (S5-S6 linker), and the cytosolic C-terminal. The C-linker, displaying six α-helices (A'-F'), connects the transmembrane core to the Cyclic Nucleotide Binding Domain (CNBD), which contains three α-helices (A-C) and a β-roll (arrow) between A- and B-helix. (Modified by Postea and Biel, 2011).

The voltage sensor resides in the positively charged S4 helix, where nine arginine or lysin residues are regularly spaced at every third position (Chen et al., 2000). This standard voltage sensor is very similar to depolarization-activated channels, but the reverse voltage dependence may be explained by the recent hypothesis Lee and MacKinnon (2017) provided in their structural study. Two features need to be highlighted: S4 interacts with S5-S6 segments in a packed conformation, and S4 segment is extremely long (two additional helices extend from the membrane into the cytoplasm) so that the S4-S5 linker interacts with the C-linker (a structural component of the C-terminal domain). When the membrane is depolarized, this conformation compresses the pore in a closed state, but the inward movement of S4, driven by hyperpolarization, displaces the S4-S5 linker and releases the constraints imposed on the C-linker and S6, allowing the pore to open like a zipper (Figure 2).

The C-terminal portion contains a cyclic nucleotide binding domain (CNBD) and the C-linker region that connects the CNBD to the S6 segment of the transmembrane core. Together, C-linker and CNBD can be referred to as the cAMP sensing domain (CSD), because they are of functional importance for the cAMP-induced positive shift of HCN voltage-dependent activation (He et al., 2014). CNBD shows a highly conserved region for cyclic nucleotide binding; it is composed of 120 amino acids forming three α-helices (A-C) and an eight stranded antiparallel β-roll between A and B-helices. C-linker (80 amino acids) consists of six α-helices (A'-F') of variable length.

Direct binding of cAMP to the CNBD does not open the channel in the absence of membrane hyperpolarization, but speeds up channel opening by increasing the open state probability and shifts the activation curve to more positive voltages (Wahl Schott et al., 2009). The binding is more likely to occur when channels are in the open state, thus stabilizing the open configuration (DiFrancesco, 1999). It is largely accepted that cAMP exerts the activation effect by removing the inhibition conferred by C-linker-CNBD (CL-CNBD) configuration. Binding of cAMP induces a conformational change in the CNBD involving the C-helix, which in turn is then coupled to the C-linker that occupies a looser conformation leading to an alteration of

the inter-subunit interface between helices of neighboring subunits (Biel et al., 2009). It is worth mentioning that most of the subunit interactions in the tetramer complex are mediated by the C-linker residues (Flynn et al., 2007). Embedded in a network of interactions between adjacent subunits, opposite subunits in HCN channels are functionally coupled by the residue K464 of the C-linker, that stabilizes the closed state of the HCN channels. The introduction of a charge inversion by a K464 variant at the elbow structure of C-linker weakens the autoinhibitory effect of the unoccupied CL-CNBD region, inducing a rotation of the intracellular domain relative to the channel pore, which is similar to the cAMP-induced rotation. This suggests that the CL-CNBD rotation is involved in activation-induced affinity increase and indirectly involved in gate modulation of HCN channels (Kondapuram et al., 2022).

The finding that cAMP promotes HCN channels activation by affecting the voltage dependence suggests that both gating mechanisms, operated by hyperpolarization and by cAMP, might be closely related to each other and the allosteric hypothesis introduced for the cAMP modulation might be extended to include the voltage dependence gating (Figure 2). This model suggests that voltage and cAMP use a common mechanism to increase the channel open probability. According to this model, channel opening is a two-step process: 1) first, the dislocation of the four voltage sensors, 2) then, a concerted rearrangement of all subunits leading to a closed to open allosteric transition (Altomare et al., 2001). The allosteric hypothesis of gating might account for some of the current kinetic features which could not be explained by simple Hodgkin-Huxley model (exponential function) (Accili et al., 2002).

Finally, CNBD turns out to be important for normal cell surface expression of HCN channel. In HCN2 a four-residue motif (EEYP) in the B-helix is supposed to promote channel export from the endoplasmic reticulum to reach cell membrane (Nazzari et al., 2008).

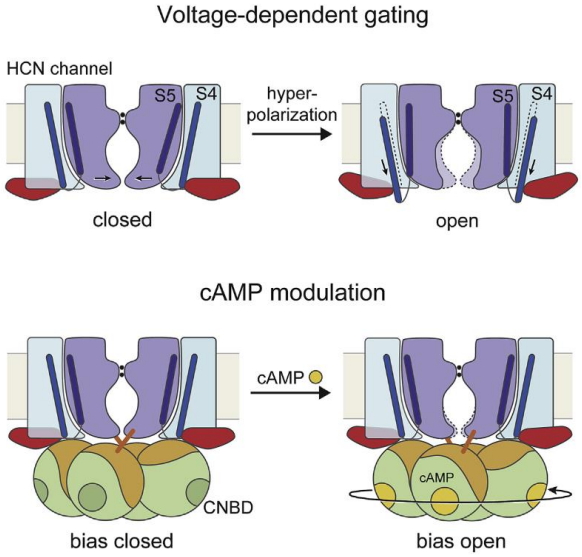

Figure 2. Representation of voltage-dependent gating and cAMP modulation of HCN channels. When the channel is in the closed state, S4 interacts with S5-S6 segments in a packed conformation, and S4 segment is extremely long so that the S4-S5 linker interacts with the C-linker. The inward movement of S4, driven by hyperpolarization, displaces the S4-S5 linker releasing the constraints imposed on the C-linker and S6 allowing the pore to open (on top). cAMP binding induces local conformational changes that are propagated to the channel. These induce a rotation of the gate-forming inner helices toward opening (on bottom) (modified by Lee and MacKinnon, 2017).

The main biophysical features of HCN channels retrace the ones already reported for native I_f/I_h. They include voltage dependent activation kinetics and modulation by cAMP. All four HCN isoforms display these principal features, but they do quantitatively differ from each other.

Voltage-dependent activation

HCN channels activate at hyperpolarizing potentials. Typically, two kinetic components can be distinguished upon activation: a minor initial and instantaneous current (Proenza et al., 2002) and the major slow time dependent component (DiFrancesco and Noble, 1985). The former is activated within few milliseconds and its amplitude is usually small; however, instantaneous phase is not consistently detected in all measurements and its nature and roles are a matter of current dispute. Differently, the slow component reaches the full activation within a range of tens of milliseconds to several seconds under hyperpolarizing conditions (Biel et al., 2009). The two components may result from different open state configurations of HCN channels (Wemhöner et al., 2012). Depending on the cell type, activation of time dependent current is usually fitted by either mono- or bi-exponential functions. Midpoint of activation values ($V_{1/2}$) reported in literature are variable (Ludwig et al., 1998; Ishii et al., 1999; Chen et al., 2001), but in general they indicate HCN1 with the less negative values and HCN2 with the most negative ones.

Recently, Flynn and Zagotta (2018) defined a new model of the mechanism underlying hyperpolarization-dependent activation of HCN channels, in which the S4–S5 linker, the covalent linkage between the voltage-sensing domain and the pore domain, is not required for hyperpolarization-dependent activation or ligand-dependent gating, as previously thought. In fact, according to this model, the S4 C-terminal region ($S4_{C\text{-}term}$) of the voltage-sensing domain is autoinhibitory on the pore domain. Pore domain and voltage-sensing domain are coupled by S5 N-terminal region ($S5_{N\text{-}term}$), that is involved in holding the pore closed. The movement of the S4 voltage sensor, caused by hyperpolarizing voltages, relieves an allosteric inhibitory effect on the pore domain produced by the S4 C-terminal region ($S4_{C\text{-}term}$) of the voltage-sensing domain. This allows the pore to open. Pore opening is further stabilized by the binding of cAMP to the CNBD (Flynn and Zagotta, 2018). Moreover, Flynn and Zagotta (2018) demonstrated that in HCN channels this hyperpolarization-dependent activation is a separate process from the depolarization-dependent recovery from inactivation, whose mechanism is still unknown.

Activation kinetics

Kinetics of activation can be considered a hallmark to differentiate between isoforms. HCN1 is the fastest activating channel with an activation time constant (τ) in the range of 30-300 ms (Santoro et al., 1998), whereas HCN4 represents the most slowly activating isoform with τ ranging from 300 ms to several seconds (Ludwig et al., 1999). HCN2 and HCN3 display intermediate activation kinetics. The reported values are strongly influenced by the potential used to activate the channel (that means the more negative the voltage step, the faster the activation), but also depend on the experimental recording parameters, including temperature, pH, concentration of modulatory factors, expression system, patch configuration, ionic composition of the solution, etc.

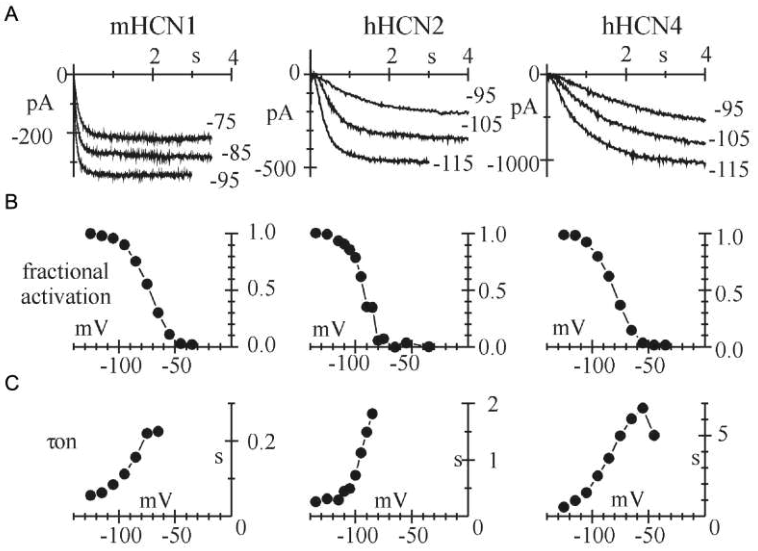

Figure 3. Properties of different HCN isoforms. (A) Whole-cell current recordings on hyperpolarization to the voltages specified from a holding potential of -35 mV in HEK293 cells transfected with mouse HCN1, human HCN2 and human HCN4 channels. (B) Mean activation curves, with lines drawn through points and fitted by a Boltzmann function. (C) Mean time constants of activation (τ) (modified by Accili et al., 2002).

Modulation by cyclic nucleotides

Although the basic channel activation mechanism is likely to be the same, another key difference between isoforms is the differential efficacy of cAMP action. HCN1 is the far less responsive isoform to cAMP modulation, with maximal shifts of the activation curve of 2-7 mV (Santoro et al., 1998). By contrast, HCN2 and HCN4 are more sensitive to cAMP, with $V_{1/2}$ shifts ranging from 10 to 25 mV (Moroni et al., 2000; Moosmang et al., 2001). Reduced cAMP sensitivity of HCN1 might be explained by a low basal inhibition of the CNBD on gating for this channel isoform (Wainger et al., 2001). Interestingly, HCN3 isoform seems to be totally unaffected by cAMP modulation (Wahl Schott and Biel, 2009) (Figure 4).

Like cAMP, also cGMP shifts the voltage dependence of activation to more positive values. At saturating concentrations, the extent of the shift is similar for both cyclic nucleotides. However, cGMP displays a 10 fold lower potency for HCN channel if compared to cAMP (Ludwig et al., 1998).

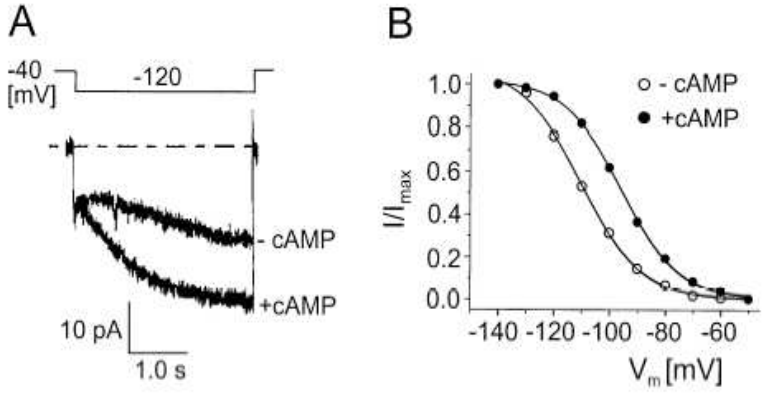

Figure 4. Modulation of HCN channel by cAMP action. (A) I_f traces acquired in HEK293 cells expressing HCN4 channels at -120 mV, in absence (-cAMP) and in presence (+cAMP) of cAMP at saturating concentration (10 μM). Increase of the current amplitude after perfusion of cAMP is evident. (B) Activation curves of HCN4 currents measured in the whole-cell mode, in absence and presence of 1mM cAMP. The $V_{1/2}$ is shifted by cAMP of about 15 mV to more positive potentials (Biel et al., 2002).

Voltage hysteresis

At the end of '90s an interesting aspect of I_f voltage activation was observed in HCN channels expressed in the sea urchin sperm (spHCN) (Gauss et al., 1998). This was then confirmed in mammalian HCN1 channel (Männikkö et al., 2005), demonstrating that HCN1 can shift between two modes depending on the previous activity. In mode I, gating and channel opening occur at very negative potentials; while in mode II, both processes are shifted to over 50 mV more positive potential. The voltage dependence of channel activity is dynamically modulated by the activity itself: persistent channel opening (long hyperpolarizing steps) favors the transition from mode I to mode II, while closed channels (long depolarizations) promote the transition from mode II to mode I. This gating behavior and the different sensitivity to the direction of the voltage change lead to the so called voltage hysteresis (Männikkö et al., 2005; Villalba Galea and Chiem, 2020). The hysteretic phenomenon is probably the result of a slow conformational change of the channel due to lateral movement of the voltage sensor that stabilizes its inward position upon hyperpolarization. In HCN1 channels, hysteresis strongly affects the voltage dependence and the deactivation kinetics (Männikkö et al., 2005). HCN2 displays hysteresis as well and the effects of the mode shift on the deactivation kinetics are present, but the process is far less pronounced. For HCN4, changes in deactivation kinetics are observed only under certain conditions using high K^+ concentrations in the extracellular recording solution (Wahl Schott and Biel, 2009). Voltage hysteresis and the two modes model may explain the different voltage dependence of HCN channel during different phases in the pacemaker cycle. Furthermore, in silico experiments suggest that hysteretic behavior of HCN channels may represent a protective factor against arrhythmic phenomena in pacemaker cells (Männikkö et al., 2005).

1.1.2 Regulation of HCN channels

Heterologous expression of various HCN isoforms, either alone or in combination, cannot fully recapitulate native pacemaker current properties (Barbuti et al., 2007). This observation suggests that I_f features cannot be determined only by HCN subunits; the environment in which channels are preferentially located drives efficient interactions with specific accessory proteins and signaling molecules (in addition to cAMP, as mentioned previously). HCN channels are regulated by interacting proteins as well as low molecular-weight factors in the cytosol and the extracellular space. These molecules regulate important channel features, such as functional properties, quantitative membrane expression and localization in specific subcellular compartments.

Regulation by interacting proteins

Several regulatory proteins take part in macromolecular complexes with HCN channel subunits. Within them, the HCN channel core (transmembrane pore and regulatory C-terminal domain) forms the α-subunit of the native f-channels described since the first studies, while a growing number of ancillary proteins participate in constituting the β-subunits.

MinK-related peptide 1 (MiRP1), encoded by kcne2 gene, is a single-transmembrane domain protein that was reported to interact with different cardiac ion channels, including HCN channels (Wahl-Schott et al., 2009). Co-expression experiments show high levels of MiRP1 associated to HCN subunits in mammalian SAN (Accili et al., 2002) and lower, but still present,

levels in atrial and ventricular myocytes (Stillitano et al., 2008). In these regions, modification of I_f, related to diseases or postnatal maturation, is most likely associated with transcriptional regulation of both HCN and MiRP1 subunits. MiRP1 accelerates kinetics of activation of HCN1 and HCN2 but does not affect the voltage-dependence. By contrast, the protein slows down HCN4 kinetics and shifts $V_{1/2}$ to more negative potentials (Sartiani et al., 2017).

The K^+ channel regulator protein 1 (KCR1), expressed both in the brain and the heart, is a transmembrane protein which serves as an auxiliary subunit of several K_v as well as HCN channels. It was reported to interact with HCN2 in heterologous expression systems, reducing current density and shifting the midpoint of activation to more negative potentials (Michels et al., 2008). The inhibitory action of KCR1 is also observed in cultured neonatal cardiac myocytes, where it reduces cardiac automaticity (Wahl-Schott and Biel, 2009), but further experiments are needed to verify the hypothesis also in vivo.

Moreover, different scaffold proteins (mainly neuronal) interact with the C-terminus of HCN channels. They may have a crucial role in targeting the channel protein to distinct subcellular compartments. TRIP8b (Tetratricopeptide repeat-containing Rab8b-interacting protein) is a member of the Rab family of the small GTPase proteins, and it is localized in the cytosol of many neurons, where it contributes to vesicle trafficking (Biel et al., 2009). TRIP8b was found to interact with HCN C-terminus through a conserved tripeptide-sequence (Santoro et al., 2004). In cortical and hippocampal pyramidal neurons, TRIP8b colocalizes with HCN1 and promotes an active trafficking of the channels from soma to dendrites, thus contributing to modulate spike firing and synaptic potential (Sartiani et al., 2017). Another neuronal scaffold protein involved in trafficking of the HCN1 (but not the other isoforms) channel is filamin A, which binds the channel via a 22 amino acid sequence downstream of the CNBD. Filamin A anchors ion channels to the actin cytoskeleton and cluster them to restricted regions of the cell membrane, reducing both the channel density and the whole-cell conductance (Gravante et al., 2004). Furthermore, the protein is able to reversibly internalize HCN1 channels and to redistribute them on the cell surface by accumulation of channels in endosomal compartments (Noam et al., 2014; Sartiani et al., 2017).

HCN2 interacts with three other neuronal scaffold proteins, namely Tamalin, Mint2 and S-SCAM, through distinct protein-binding domains (Biel et al., 2009). Tamalin contributes to assembly of multimolecular proteins: it forms a protein complex with several receptors and scaffold proteins, such as S-SCAM, to organize a postsynaptic signal-processing machinery; it associates with protein-trafficking scaffold proteins, such as Mint2 (Kitano et al., 2003). HCN2 levels are increased upon coexpression with Mint2 in heterologous systems, suggesting that this protein may be a positive regulator of cell surface expression of HCN channels (Kimura et al., 2004).

On the cardiac side, a crucial interaction is exerted by caveolin 3 (cav-3), a marker protein of a distinct type of lipid raft called caveolae. In pacemaker cells and HEK293, caveolae are membrane microdomains where HCN channels are preferentially localized; cholesterol depletion, which typically causes the disruption of these lipid rafts, induces a redistribution of HCN channels within the membrane and affects the channel kinetic properties (Fürst and D'Avanzo, 2015). In SAN cells, the interaction between HCN4 and cav-3 promotes a shift of $V_{1/2}$ to more negative potentials; it also modifies HCN4 current kinetics by accelerating channel deactivation (Barbuti et al., 2004; Sartiani et al., 2017). Experimental evidence indicates that the confinement of HCN channels within caveolae has a role in adrenergic modulation. In fact, β2-AR, rather than β1, are more expressed in caveolar spaces and that facilitates the adrenergic enhancement of I_f, hence the rise of heart rate (Barbuti et al., 2007).

Regulation by kinases

Phosphorylation status affects the HCN channel properties and represent an additional regulatory mechanism. Both tyrosine and serine/threonine kinases take part in this type of modulation.

Src binds to the C-linker-CNBD via its SH3 domain and leads to the phosphorylation of a tyrosine (Tyr476) that is located in the C-linker: as a result, channel activation kinetics is enhanced (Herrmann et al., 2015). Despite the fact this action is exerted both in HCN2 and HCN4, a stimulation of kinetics has been proven only for the latter (Sartiani et al., 2017). In contrast, HCN1 is not modulated by Src kinase (Yu et al., 2004). Regulation by tyrosine phosphorylation via Src has been demonstrated under physiological conditions in SAN cells of murine and rat heart as well as in neurons (Biel et al., 2009). Src inhibition reduces heart rate in Langendorff-perfused mouse hearts (Li et al., 2008).

In neurons, HCN channels are also phosphorylated by serine/threonine kinases, such as p38-MAP (mitogen activated protein) kinase and calcium/calmodulin-dependent protein kinase II (CaMKII). In hippocampal pyramidal circuits, activation of p38-MAP kinase significantly shifts the voltage-dependent activation to more positive potentials; however, it is not clear if this effect results by a direct phosphorylation or by phosphorylation of another protein interacting with the HCN channel (Wahl-Schott and Biel, 2009). The action of p38-MAP kinase is reduced in epileptic animal models (He et al., 2014).

In hippocampal pyramidal neurons, CaMKII controls activity-dependent HCN channels trafficking and surface expression: it increases surface expression through the interacting protein TRIP8b or reduces the HCN gene transcription via Neuronal Restrictive Silencing Factor (NRSF) in pathological conditions, such as vascular dementia (He et al., 2014; Luo and Guo, 2015).

Regulation by membrane phosphoinositides

Phosphatidylinositol-4,5-biphosphate (PIP_2) is a constitutive membrane component and it is the major membrane lipid able to allosterically regulate HCN channels. PIP_2 acts as an intracellular allosteric ligand and increases the channel opening probability. Its interaction with the channel causes a rightward shift of the voltage activation by about 20 mV (Biel et al., 2009). Modulation by PIP_2 is independent of cyclic nucleotides and, at variance with cAMP, is equally effective on $V_{1/2}$ shifting in all four isoforms (Zolles et al., 2006). Experiments using spHCN channel indicate that PIP_2 exerts its effect, at least in part, by stabilizing the activated state of the voltage sensor S4 (Herrmann et al., 2015). PIP_2-mediated regulation may be of a key importance for the physiological regulation of channel gating both in neurons and in cardiomyocytes (Sartiani et al., 2017).

Similar effects are shown with two phosphoinositides derivates, namely phosphatidic acid and arachidonic acid, which promote HCN channel gating by shifting the midpoint of activation curve to more positive potentials (Sartiani et al., 2017).

Regulation by protons

Intracellular protons, whose concentrations reflect the intracellular pH (pH_i), modulate the HCN channel activity by shifting the voltage-dependence of activation to more negative values and slowing down the opening kinetics. In murine HCN2, pH_i sensitivity is found to be conferred by the presence of a protonable histidine residue (His321), localized between the voltage-sensing S4 segment and the cytoplasmic S4-S5 linker (Zong et al., 2001). Modulation

by intracellular protons may play a key role in controlling physiological activities of HCN channels in the brain, such as the regulation of thalamic oscillations and the respiratory frequency (Wahl-Schott et al., 2009).

Also extracellular protons regulate HCN channel activity, but in the opposite way. Acidic extracellular pH (pHe) activates I_h by profoundly shifting the voltage-dependence of channel activation to more positive potentials. This mechanism was shown to contribute to sour taste transduction in a subset of rat taste cells (Stevens et al., 2001).

Regulation by chloride

Despite its cationic permeability, I_h conductance is affected by concentrations of small anions, notably Cl^- (Biel et al., 2009). Extracellular Cl^- affects the steady-state conductance of I_h and this effect is more pronounced for HCN2 and HCN4, rather than HCN1. The molecular determinant of the extracellular Cl^- sensitivity is identified as a single amino acid residue in the pore region: an arginine residue for HCN2 and HCN4, an alanine residue for HCN1. This difference may explain the stronger influence of chloride on HCN2/4 over HCN1 (Wahl-Schott et al., 2005). The regulation of HCN channel by Cl^- is likely to be relevant for cardiac pathophysiology. In hypochloremia, a reduction of amplitude of SAN I_f, carried by HCN2 and HCN4, can be responsible for the generation of arrhythmias that are frequently observed in this condition (Wahl-Schott and Biel, 2009).

Also, intracellular Cl^- affects HCN channel activity. An increase of the ion concentrations up to 140 mM almost completely abolishes the instantaneous component of I_h, while no effects are observed on the steady-state current (Mistrik et al., 2006). Further experiments are needed to determine the physiological relevance of this regulation.

1.2 Role of HCN channels in cardiac physiology and pathologies

1.2.1 Function of HCN channels in cardiac action potential

The cardiac rhythm is generated in the sinoatrial node (SAN) by specific cells, the pacemaker cells, from which it propagates to the atria and the atrioventricular node (AVN). Following a brief pause in AVN, that allows complete contraction of the atria, bundle of His leads the stimulus along both sides of the interventricular septum to excite both ventricles. The bundle of His ends in Purkinje fibers, millions of small fibers that project the stimulus throughout the myocardium, allowing its contraction (Renwick et al., 1993; Nerbonne and Kass, 2005; Anderson et al., 2009).

The action potential (AP), the electrical stimulation that generates the cardiac rhythm, is created by a sequence of ion fluxes through specialized channels present in the sarcolemma of cardiomyocytes, which lead to their contraction (Nerbonne and Kass, 2005). In the heart, the AP displays differences between the working atrial and ventricular cardiomyocytes and the pacemaker cells. These differences allow cells to accomplish substantially different tasks: the

pacemaker cells are responsible for the generation and the propagation of the electrical pulse, while working cells must contract in order to maintain the pulsatile activity of the heart.

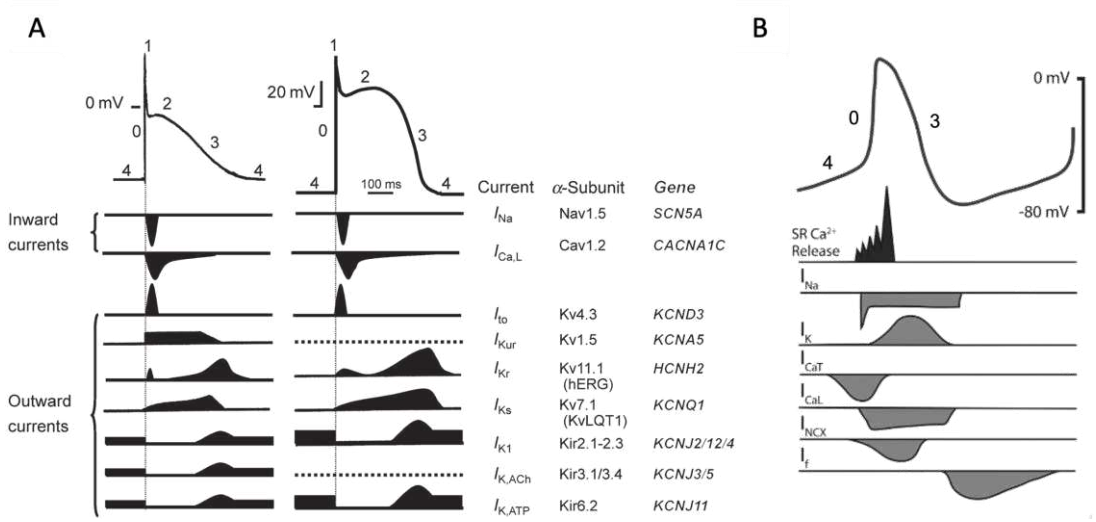

Figure 5. Action potential traces in atrial and ventricular cardiomyocytes and in pacemaker cells. (A) At the top, the traces of atrial (on left) and ventricular (on right) action potentials with respective phases. At the bottom, inward depolarizing and outward repolarizing currents that characterize each respective action potential (from Ravens and Cerbai, 2008). (B) Trace of pacemaker cell AP and relative currents involved in its generation (modified from Bartos et al., 2015).

The atrial and ventricular AP is consisted of the following five phases (Nerbonne and Kass, 2005) (Figure 5A).

- Phase 0: it is a fast depolarizing upstroke, due to a quick inflow of a depolarizing Na^+ current from voltage-gated Na^+ (Nav) channels. The membrane potential shifts from hyperpolarized to depolarized values. The trigger for this channels activation is the depolarization wave spread by the cardiac conduction system. In the SAN and AVN this phase is markedly slower than in atria and ventricles.
- Phase 1: it is a transient and rapid repolarization, resulting from Na^+ channels inactivation and an increase of chloride (Cl^-) flux and transient potassium (K^+) flux due to the activation of fast transient voltage-gated outward K^+ current (I_{to}). This repolarization is quite important in ventricular cells and influences the height and duration of the next plateau phase of AP.
- Phase 2: the L-type voltage-gated Ca^{2+} (Cav) channels are activated by membrane depolarization, leading an influx of Ca^{2+} that is the main trigger for excitation-contraction coupling in the working myocardium (Bers and Perez-Reyes, 1999; Fabiato and Fabiato, 1979). The inward L-type Ca^{2+} current (I_{CaL}) is counteracted by the ultrapid outward current (I_{Kur}, present only in the atria (Ravens and Cerbai, 2008), and the rapidly (I_{Kr}) and the slowly (I_{Ks}) activating delayed rectifier K^+ currents.
- Phase 3: with the gradual Cav channels inactivation, the outward K^+ currents predominate, resulting in repolarization towards diastolic potential. In addition, the inward-rectifier K^+ current (I_{KIR}), which was inactivated during the depolarization phase, is activated.
- Phase 4: the membrane potential is maintained at the resting voltage of around -75/-85 mV (diastolic phase), primarily by the I_{K1}, an inward K^+ current, present in the

working cells. The resting state is preserved until another electrical stimulus brings the voltage up to the threshold for the activation of Nav channels.

Since the pacemaker cells are able to generate and transmit rhythmically the electrical impulse throughout the heart, their AP lacks the plateau (phase 1-2) and of the stable resting phase (phase 4). Indeed, while in the working myocytes (whose task is to contract) the voltage remains stable at the resting membrane potential, in the pacemaker cells the potential gradually changes toward the positive values. This process is called spontaneous slow depolarization (phase 4; Figure 5B), which allows to generate spontaneous APs with a certain cycle length (Varrò et al., 2021). In particular, thanks to the repolarization phase (phase 3), the membrane potential of pacemaker cells reaches the maximal diastolic potential (MDP), defined as the most negative value (around -40/-60 mV) reached during the entire cycle. In this range of voltages, the activation of I_f leads the next slow diastolic depolarization phase. Following this activation, a steady-state inward current drives membrane potential (-70/-40 mV, depending on cells) to depolarize toward the threshold required to generate a spontaneous AP (DiFrancesco et al., 1986), activating the T-type Ca^{2+} current (I_{CaT}) and finally the I_{CaL} (late phase of diastolic depolarization) (Noma, 1996).

During the impulse propagation, the cell that first reaches the AP threshold and generates the AP (source cell) charges the neighboring cell (sink), in which the membrane potential is below threshold (Wahl-Schott et al., 2014). In case of deletion of HCN channels, more current and more time are required for a cell to charge the sarcolemma of an adjacent cell to reach the threshold potential for AP. This condition leads to slow down conduction of SAN AP with consequent bradycardia, as observed in mouse with HCN1 deletion (Figure 6) (Fenske et al., 2013; Wahl-Schott et al., 2014).

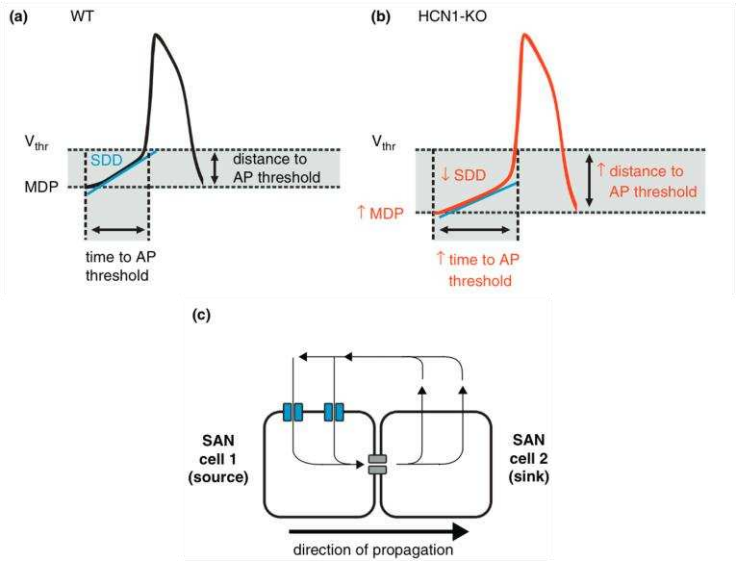

Figure 6. Role of HCN channels for impulse formation and impulse conduction in the SAN node. Schematic pacemaker potential in sinoatrial node cells of wild type (a) and $HCN1^{-/-}$ mice (b). HCN channels contribute to the slow diastolic depolarization. The absence of HCN1 decreases the slope of slow diastolic depolarization and increases the time to threshold for an action potential. HCN channels decrease the maximal diastolic potential, that increases in the absence of HCN1. This results in an increased distance and time to threshold for a new action potential and a decrease in impulse propagation. (c) Direction of intracellular and extracellular current flow during propagation of an action potential from depolarized (source) to resting cells (sink) (modified by Wahl-Schott et al., 2014).

It is hypothesized that the spontaneous electrical activity in SAN is driven by an interplay between the voltage clock, sustained by inward/outward membrane conductances (including I_f), and the Ca^{2+} clock, mainly sustained by Ca^{2+} release from sarcoplasmic reticulum. During the diastolic phase, the depolarization of membrane potential, necessary to generate a spontaneous AP, takes place thanks to I_f flow that leads to a simultaneous or sequential work of ion conductances, mainly, NCX, I_{CaT}, I_{CaL}, Na^+/K^+ ATPase, voltage-dependent K^+ and background Na^+ currents (voltage/membrane clock) (DiFrancesco and Noble, 2012). At the same time the diastolic phase is caused by the periodic, spontaneous submembrane Ca^{2+} release from sarcoplasmic reticulum, that triggers Ca^{2+} extrusion via NCX current, depolarizes the membrane and activates I_{CaT} and I_{CaL}, triggering finally APs (Ca^{2+} clock) (Vinogradova et al., 2010; Maltsev and Lakatta, 2012).

In conclusion, HCN channels play an important role in the generation of pacemaker activity of cardiac sinoatrial node cells and immature cardiomyocytes. However, f-channels are present also in atrial and ventricle cardiomyocytes, where the physiological role is currently under investigation while that carried out in cardiac pathologies (such as hypertrophy, failure and atrial fibrillation, see paragraph 1.4) is supposed to be linked to arrhythmogenesis (Cerbai and Mugelli, 2006; Sartiani et al., 2015; Sartiani et al., 2017).

1.2.2 Function of HCN channels in cardiac pacemakers and working myocardium

The pacemaker mechanism in the heart was originally interpreted as resulting from the decay of an outward K^+ current during the diastolic depolarization of SAN AP (Noble and Tsien, 1968). Only in late 70s the discovery of funny current re-evaluated the theory and provided a new interpretation of pacemaking, according to which the pacemaker depolarization was generated by activation of the inward I_f during diastole (DiFrancesco, 1981). I_f flows almost exclusively during the diastole, with channels opening during terminal repolarization following an AP, and deactivating rapidly upon subsequent AP depolarization (Robinson et al., 2006). For this reason, among the mechanisms involved in pacemaking, the funny current has properties most specifically fitting the requirements for the roles that the current itself plays: the generation of pacemaker automaticity and the autonomic-mediated modulation.

Regarding the pacemaker generation, basic evidence includes the observation that the current activation range approximately overlaps that of diastolic depolarization (Brown and DiFrancesco, 1980; DiFrancesco, 1986), implying that I_f activation contributes to initiating and controlling the rate of development of this phase. Contribution of the funny current to the diastolic depolarization can be described simply on the basis of the current properties. During depolarization, at positive voltages, I_f is completely turned off; when the voltage goes down below -40/-45 mV, during repolarization, the current switches on and progressively increases, first opposing to and then stopping the repolarization process, and finally initiating the diastolic depolarization. The I_f contribution terminates when, in the late part of diastolic depolarization, Ca^{2+}-dependent mechanisms take over and the threshold for the action potential firing is reached (DiFrancesco, 2010).

The current is also involved in the pacemaking modulation, mediating the chronotropic action of neurotransmitters. Adrenaline stimulation acts by accelerating the heart rate:

activation of β adrenergic receptor (β-AR) increase cAMP levels via adenylate cyclase, that therefore increase the opening probability of HCN channels. Sympathetic stimulation shifts the I_f activation curve to more positive voltages, thus providing more inward current and steepening the slope of diastolic de polarization (DiFrancesco and Tromba, 1988). The adrenaline induced rate acceleration is almost attributable to the shortening of the diastolic duration associated with a faster slope of diastolic depolarization, whereas only minimal changes occur in the action potential shape and duration (DiFrancesco, 2010). The opposite event occurs with vagal stimulation, which therefore slows rate via muscarinic induced decrease of adenylate cyclase activity, reduced cAMP levels and negative shifts of the I_f activation curve (DiFrancesco and Tromba, 1988) (Figure 7). Acetylcholine concentration required to inhibit the I_f are very low (up to 0.03 µmol/L), 20 fold lower than those necessary to activate the acetylcholine dependent K^+ current (DiFrancesco et al., 1989).

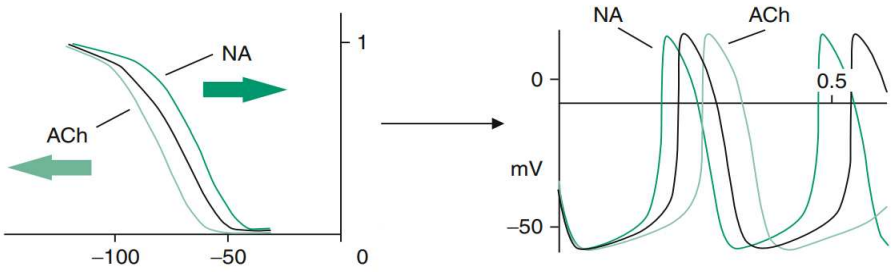

Figure 7. Modulation of the I_f activation curve. (on the left) and the diastolic depolarization phase of the pacemaker action potential (on the right) by noradrenaline (NA) and acetylcholine (ACh) actions. (Modified by DiFrancesco and Borer, 2007).

1.2.3 HCN channels in cardiac pathologies

Funny current and heart rate are correlated both in normal physiological conditions and in the framework of cardiac pathologies involving pacemaker alterations. During fetal and neonatal stages of heart development funny channels are highly expressed in all cardiac regions, but soon after the birth their expression in the working myocardium decreases (Cerbai et al., 1999; Robinson et al., 1997) and the voltage range of activation shifts to values that are more negative than the resting potential (Robinson et al., 1999), avoiding that I_f contributes to normal electrical activity. Nevertheless, in specific pathological condition (such as cardiac hypertrophy or heart failure), expression levels of the funny channels can newly rise, as observed in animal models (i.e., spontaneously hypertensive rat) (Cerbai et al., 1994) and in explanted human hearts with dilated or ischemic cardiomyopathy (Cerbai et al., 1997; Hoppe et al., 1998). Mislocalized expression and/or overexpression of HCN channels are a consequence of the so-called cardiac remodelling, a phenomenon associated with a huge variety of clinical conditions (such as hypertension and ischemic cardiomyopathy but also diabetes or B6 vitamin deficiency) (Swynghedauw, 1999). During cardiac remodelling a fetal gene re-expression program occurs and new transcripts include that of HCN channels. Often, during the conditions underlying the remodelling, chronic activation of renin-angiotensin system occurs, playing a pivotal role in this process (Kim and Iwao, 2000). In particular, consequent increased plasmatic and/or tissutal levels of angiotensin II determine hyperactivation of angiotensin II type I receptor (AT1), which mediates (directly or indirectly)

signalling pathways driving the switching on/off of I_f (Sadoshima and Izumo, 1993; Kajstura et al., 1997). The I_f recorded in these non-pacemaker regions shows similar electrophysiological features (from the qualitative point of view) to those described in SAN cells from DiFrancesco in his first studies (Cerbai and Mugelli, 2006).

In ventricular myocytes I_f may act as an arrhythmogenic mechanism, especially in an enhanced sympathetic drive condition (Cerbai and Mugelli, 2006); this altered sympathetic drive can eventually lead to heart failure, condition associated with a high risk for sudden death. At variance with ventricular myocytes, I_f is constitutively present in atrial myocytes (Thuringer et al., 1992; Porciatti et al., 1997), but its role in atrial electrogenesis still remains not fully understood (Michels et al., 2005). Although I_f conductance in human atrium is not large enough to depolarize the membrane and generate spontaneous activity, pathological conditions (e.g., atrial fibrillation) and several neurohumoral signals (e.g. serotonin and atrial natriuretic peptide) may amplify the current, so that I_f can influence cell excitability and put at risk for or worsen/reinforce atrial arrhythmias (Opthof, 1998; Workman, 1998).

1.3 Function and dysfunction of HCN channels in the central and peripheral nervous system

Accumulating evidence over the past decades have investigated the role of HCN channels in nervous cells (He et al., 2014; Shah, 2016). Aiming to provide a simple and brief overview of HCN channel function in neuronal physiology, it is important to remind that action of HCN channels arise from four fundamental properties, which have been already described in the previous sections and namely: 1) selectivity for Na^+ and K^+; 2) activation curve at potentials close to firing threshold;
3) reversal potential at depolarized values (≈ -35 mV) with respect to resting membrane potential; 4) slow gating kinetics. Because of these properties, HCN channels generate a tonic depolarizing current, which drives the neuron membrane potential toward firing threshold. Importantly, HCN current is able to compensate both negative and positive perturbations of membrane potential by responding with increased activation or deactivation, respectively. Additionally, the slow kinetics of HCN current provide a filtering action that is effective for low-frequency oscillatory inputs (high-pass filtering).

Thanks to these properties, HCN current in neurons accomplish different tasks:

1. regulation of resting membrane potential and intrinsic excitability (Kase and Imoto, 2012; McCormick and Pape, 1990b; Maccaferri et al., 1993; Gasparini and DiFrancesco, 1997; Nolan et al., 2003; Ko et al., 2016; Hawkins et al., 2015). This action of HCN current on neurons has been proved in many diverse brain areas and control important traits of learning, circadian rhythm, and sleep/wakefulness state;
2. rhythmogenesis in a functional interplay with other conductances, which may eventually generate AP firing (Alonso and Llinas, 1989; Moser et al., 2015; Giocomo and Hasselmo, 2009; Giocomo et al., 2011). This function in thalamocortical neurons is effective during wakefulness and rapid eye movement sleep (McCormick and Pape, 1990a, b), while it is disrupted in absence seizure and some form of epilepsy (Ludwig et al., 2003; Ying et al., 2011);

3. synaptic excitability and plasticity (Bender et al., 2001; Lörincz et al., 2002; Harnett et al., 2015). This function controls many important abilities, including long-term potentiation and associated cognitive functions, learning and memory performance (Nolan et al., 2004; Wang et al., 2007; Arnsten and Jin, 2014; Sheets et al., 2011);
4. resonance properties, the ability to respond preferentially to inputs at a certain frequency, and thus determines to what extent the neuron responds to synchronous network activity (Bedard et al., 2006; Hutcheon et al., 1996; Nolan et al., 2004);
5. neurotransmitter release of GABAergic terminals (Boyes et al., 2007) as well as glutamatergic terminals (Huang et al., 2011).

To date, abundant number of works evidences the role of I_h in influencing the neuronal excitability and the generation of AP firing in sensory neurons (Tu et al., 2004; Luo et al., 2007; Momin et al., 2008). I_h contributes to electrophysiological properties such as membrane potential (Tu et al., 2004), adaptation (Spain et al., 1987; Takigawa et al., 1998) and after hyperpolarization (McCormick and Pape, 1990; Womble and Moises, 1993), and eventually they influence membrane excitability. The current is highly expressed in primary afferent somatosensory neurons, including the nociceptors, whose body resides in the DRG; the ionic channels that mediate this current, in fact, have been reported to participate in the pain process (Chaplan et al., 2003). Beyond the painful stimuli, peripheral sensory neurons can also detect muscle stretch, touch and pressure; I_h may thus influence sensation associated with all these (Gao et al., 2012). Sensory afferent nerve fibres can be classified into three main categories: large and fast-conducting myelinated Aβ-fibres; medium-sized and slow-conducting myelinated Aδ-fibres; small and slowest conducting unmyelinated C-fibres. The majority of studies has been conducted in neonatal rats, in which the cell body sizes criterion follows these references: large (> 35 μm), medium (25-35 μm) and small (< 25 μm) (Momin et al., 2008). A general finding is that large and medium sized neurons express greater I_h and with faster activation times whereas only half of small DRG neurons shows a functional I_h current (Scroggs et al., 1994). However, according to different experimental studies a current intensity over 50 pA is detected in less than half of the large DRG neurons, but the fraction increases going towards the medium fibres, up to the small neurons where approximately the totality of them expresses these values of I_h intensity (Scroggs et al., 1994; Yagi and Sumino, 1998; Momin et al., 2008).

The intensity of sensation in all sensory systems is determined mostly by the frequency of AP firing in the afferent fibres (Momin et al., 2008). Among these systems nociceptors are unique because the sensitivity to noxious stimuli is enhanced in inflammatory hyperalgesia by the action of pro inflammatory mediators (e.g., bradykinin, nerve growth factor and prostaglandin E_2) (Coutaux et al., 2005). One of the mechanisms by which inflammatory mediators are able to increase the frequency of AP provoked by a given inward current is acting on the voltage dependence of I_h activation, by increasing intracellular cAMP levels and shifting the activation curve to less negative membrane potentials. This shift has the effect both of increasing the amplitude of inward current and of increasing the rate of activation (Ingram and Williams, 1994; Gold et al., 1996). However, I_h in large and medium sized DRG neurons shows low sensitivity to cAMP as compared to the characteristic of the current in small diameter neurons (Gao et al., 2012): these data are consistent with the electrophysiological findings of a faster and slower activation times of medium large and small neurons, respectively (Villiere and McLachlan, 1996; Doan and Kunze, 1999).

Disfunctions of I_h in the central and peripheral nervous system

Given the strong connection between the presence of I_h in neurons and the dynamic modulation of physiologic processes, HCN gene polymorphisms and altered function/expression of the current in the CNS might lead to pathological conditions, e.g. autism, schizophrenia, epilepsy, neurodegenerative diseases or mood disorders (Lewis and Chetkovich, 2011; Chen et al., 2022). Among them, epilepsy is the neurologic disorder which is lately receiving most attention from researchers. Studies support the evidence of a relation between channelopathy and epilepsy, but there is no suggestion of a univocal cause and effect link (Sartiani et al., 2017). Both up and downregulation of I_h can be associated with an increased neuronal excitability, which is largely determined by the pathophysiological context and subcellular location of the dysregulated I_h (Dyhrfjeld-Johnsen et al., 2009).

Physiologic roles of I_h in DRG are not clearly understood. On the other hand, the current function seems to be related to pathologic states, such as neuronal damage and inflammatory insults (Papp et al., 2010; Acosta et al., 2012). Although a prominent role of CNS sensory processing is likely in these pathologies, discharges from the injured peripheral nerve are believed to be critical to the initiation and the maintenance of neuropathic pain syndromes (Chaplan et al., 2003; Yao et al., 2003). Nociceptor hyperexcitability, which is associated with hyperalgesia and allodynia, is attributed to an increased activity of I_h in the pain sensing pathway (Herrmann et al., 2015). Among the several mechanisms that underlie this phenomenon, most important include the overexpression and mutation of HCN ion channel (Papp et al., 2010; Resta et al., 2018; Dini et al., 2018), the PIP_2 mediated pathway modulation (Pian et al., 2006), the PKA channel hyperactivation (Cheng and Zhou, 2013) and the elevated cAMP levels triggered by inflammatory substances, which increase HCN-current (Momin et al., 2008).

1.4 Uncanonical roles of the pacemaker current

HCN channels are mainly expressed in the nervous system and the heart, but they are also present in some other tissues. In the case of the retina, all four HCN channel isoforms are expressed and I_h plays a role in the shaping of retinal responses to light (Ivanova and Mueller, 2006). Patients during prolonged treatment with HCN inhibitor (see “Pharmacology of HCN channels”) experienced visual symptoms such as phosphenes (visual perceptions evoked by stimuli other than changes in light) or photopsia (light flashes) (Cervetto et al., 2007). Other tissues which express HCNs are auditory neurons, olfactory pathways, B cells of pancreatic Langerhans islets, enteric, lymphatic smooth muscle, uterine smooth muscle, smooth muscle cells of the bladder or portal vein, testis, and the enteric nervous system (Wahl-Schott and Biel, 2009), but for the low levels of channels expression it is not easy to define the physiological role of I_h.

Recently it was also found that HCN channels, mostly HCN3, are located in kidney mitochondria which are important organelles for cell viability, since they produce energy for the cells as ATP, via oxidative phosphorylation. HCN3 protein expression was found in rat kidney mitochondria and in HEK293 mitochondria, where function has been studied by patch-clamp recordings (León-Aparicio et al., 2019).

1.5 Pharmacology of HCN channels

Molecules that specifically interfere with HCN channels represent an important tool in the characterization of their structural and functional properties, as well as drugs and prototypes effective to modify HCN channel function in pathological conditions. High heart rate is closely related with an increased mortality in various cardiovascular diseases, such as heart failure, artery hypertension, and ischemic heart disease (Benetos et al., 1999; Seccareccia et al., 2001); therefore, given the role of HCN channels in the SAN, the use of drugs targeting these channels and aiming to a heart rate reduction is a valid therapeutical approach for those patients.

Furthermore, findings demonstrating that I_h activation plays a facilitating role in neuropathic pain, hyperalgesia or allodynia path the way for HCN channel blockers as innovative drugs.

To date, several compounds have been developed, with substantial differences in their chemical structures and, consequently, in their interactions with the channel. From the chemical point of view, these molecules belong to three different classes: imidazolines, aminopyrimidines, and phenylalkylamines (Romanelli et al., 2016). Of note, development of phenylalkylamines, which derivate from the calcium-antagonist verapamil structure, has gained interesting goals.

Ivabradine

Ivabradine (Figure 9), developed by Servier, is currently the only specific heart rate-lowering agent approved for the clinical practice. European Medicines Agency indicates ivabradine for the treatment of uncontrolled chronic angina pectoris in patients with contraindicated or not tolerated beta-blocker therapy (or as an add-on therapy when adequate heart rate control is not achieved) and with heart rate >70 bpm. Later, Food and Drug Administration approved ivabradine also as a second-line therapy for severe heart failure in patients with reduced ejection fraction and heart rate >75 bpm.

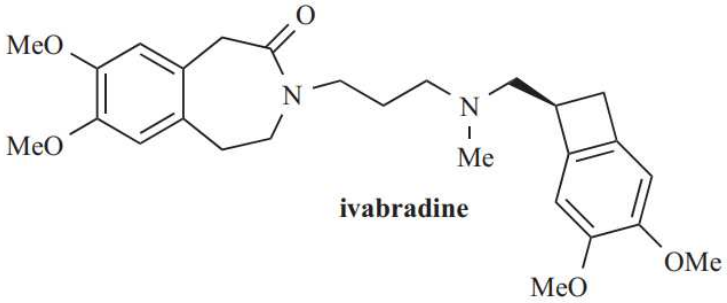

ivabradine

Figure 9. Two-dimensional structure of ivabradine

Block of HCN channel is accomplished from the intracellular side. Ivabradine binds the channel inner pore when the channel is in the open state, hence showing a use-dependence feature (Herrmann et al., 2015). This implies that hyperpolarization must be applied in order for the drug to reach its binding site, but, at the same time, the block is stronger at depolarized voltages (DiFrancesco, 2015). Experimental studies show how the ivabradine-induced block on HCN channel is quite atypical because it depends on the direction of the current flow rather than the voltage itself (Bucchi et al., 2002). This “current dependence” is a unique property of

ivabradine, not shared with any other heart rate-lowering agent. Use-dependence is a remarkable attribute of this drug, as it implies a more prominent effect of ivabradine when the frequency of channel opening (related to the heart rate) is increased, and at the same time minimizes the risk for severe bradycardia. Ivabradine blocks HCN4 and HCN1 with IC50 in the low micromolar range (1-2 μM). However, at higher concentrations, ivabradine interacts with other ion channels, like hKv1.5 (Delpon et al., 1996) and hERG K^+ channels (Sartiani et al., 2017). An interesting finding obtained in heterologous expression system, demonstrates that ivabradine blocks HCN1 preferentially in the closed state, or during the transition between the open and the closed state, while blocking HCN4 in the open state, as expected (Bucchi et al., 2006). The overall effect of ivabradine is to inhibit the maximal conductance and to reduce the amplitude of I_f without affecting the voltage-dependence of current activation (Baruscotti et al., 2015).

Beneficial effects of ivabradine's bradycardic properties emerged in the SHIFT and in the BEAUTIFUL clinical trials, where patients with chronic stable angina took advantage of lowered heart rate, because of the associated improved myocardial perfusion and the reduced oxygen demand (Fox et al., 2008; Böhm et al., 2010). Furthermore, ivabradine does not cross the blood-brain barrier (Young et al., 2014), so that its effects mainly occur at heart level. Unfortunately, also adverse effects emerged from the trials, among which excessive bradycardia, atrial fibrillation and visual disturbances (phosphenes) (Fox et al., 2014). These complications derive from the block of cardiac and retinal HCN channels, and they may represent a limiting factor in ivabradine use.

A recent and small clinical study performed in diabetic patients with neuropathic pain has demonstrated ivabradine is effective, well tolerated in patients and thus considered of potential merit for further investigation in clinical trials (Bernard Healey et al., 2021).

Zatebradine, cilobradine and other specific HCN antagonists

Zatebradine and cilobradine (Figure 10) are phenylalkylamines designed from the L-type Ca^{2+} channel blocker verapamil. Both compounds share the binding of HCN channel from the intracellular side as mechanism of action, and they inhibit the current at low micromolar concentrations (IC50 0,5-2 μM) in a use-dependent fashion (Baruscotti et al., 2005). In SAN myocytes, cilobradine was found to induce a more effective and faster block, if compared to zatebradine (Van Bogaert and Pittoors, 2003). Like ivabradine, zatebradine and cilobradine do not shift the position of the I_f activation curve but reduce the maximal conductance. Zatebradine has been the first of this class of compounds facing a clinical trial, with evidence of reduced heart rate both at rest and during exercise, but its development was stopped due to the adverse effects (Frishman et al., 1995). However, chemical manipulation of the zatebradine's structure led to the development of a series of analogues, including ivabradine, with a reduced conformational flexibility, and some of them show interesting features in terms of potency and channel selectivity.

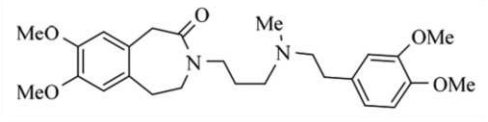

(A) Zatebradine

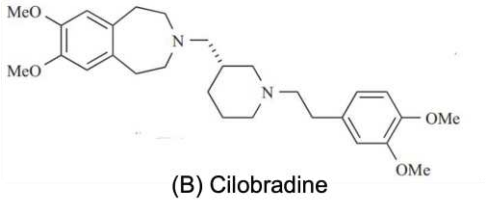

(B) Cilobradine

Figure 10. Two-dimensional structure of Zatebradine (A) and Cilobradine (B).

EC18 (Figure 11) derives from the insertion of the propane chain of zatebradine into a cyclohexane ring. When tested on recombinant homomeric HCN channels, EC18 exhibited a 5-fold preference for HCN4 isoform over HCN1 and HCN2 (Del Lungo et al., 2012; Romanelli et al., 2019). This HCN4-preferring compound blocks HCN4 channels with a potency comparable to that of ivabradine (Bucchi et al., 2013). This preference found in recombinant systems was observed also in native tissues, such as guinea pig SAN and DRG neurons (Del Lungo et al., 2012). Therefore, EC18 can be considered an effective tool to study HCN4 channels in both heart and nervous system.

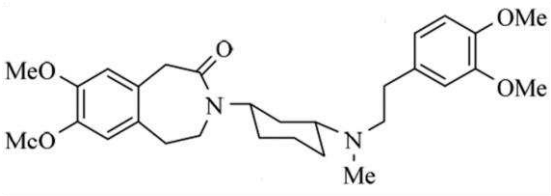

EC18

Figure 11. Two-dimensional structure of EC18

MEL55A (R enantiomer), another semi-rigid analogue of zatebradine, is characterized by the replacement of the propane chain with a cis-butene moiety and the introduction of a methyl group in the ethyl linker (Figure 12). MEL55A shows a strong preference towards HCN1 and HCN2 over HCN4 (Melchiorre et al., 2010; Dini et al., 2018). The compound was tested both in vitro, by patch clamp recordings on mouse DRG neurons, and in vivo, on mouse models of oxaliplatin-induced neuropathy by means of thermal hypersensitivity. MEL55A demonstrated to preferentially block HCN1 and HCN2, therefore reducing the I_h amplitude and the cell excitability in cultured DRG with similar effects to that observed with ivabradine, and to relieve the chemotherapy-induced neuropathic pain (Dini et al., 2018). For these observations, MEL55A could constitute a valid tool in the assessment of the pharmacological impact of HCN modulation in pain nociception.

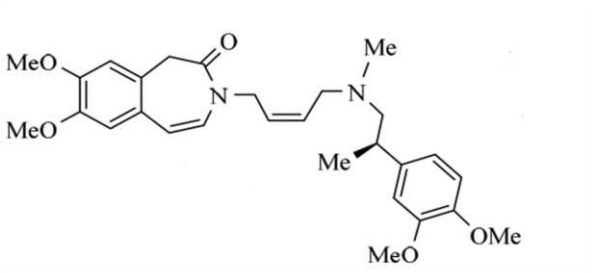

MEL55A

Figure 12. Two-dimensional structure of MEL55A

MEL57A (Figure 13) is an unwieldy product found during the synthesis of MEL55A. Unexpectedly, MEL57A was found to display a 39- and a 230-fold preference for HCN1 over HCN2 and HCN4, respectively (Del Lungo et al., 2012). In rat models of CIPN (Chemotherapy-Induced Peripheral Neuropathy), where MiRP1 is upregulated and an HCN1 gain of function occurs, the molecule was able to reduce hyperalgesia and allodynia without cardiac side effects, and proves itself to be a more selective HCN1 inhibitor (Resta et al., 2018). Given the lack of specific therapies, CIPN patients are treated with the same pharmacological approaches employed in other types of chronic pain, but MEL57A may represent a promising compound to further develop a new generation of analgesic drugs.

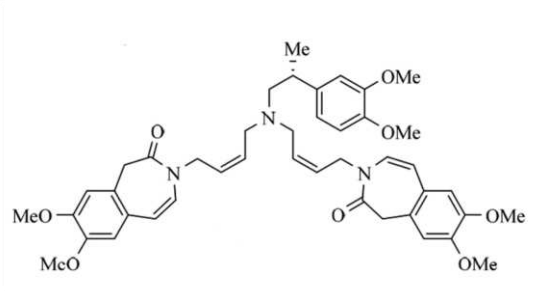

MEL57A

Figure 13. Two-dimensional structure of MEL57A

Another HCN channel blocker is ZD7288 (Figure 13), a pyridinium derivative structurally unrelated to zatebradine. ZD7288 is probably the most widely used experimental blocker of I_f/I_h (Biel et al., 2009) and like other agents discussed so far, it blocks the channel from the intracellular side (Shin et al., 2001). However, the block is not use-dependent (Biel et al., 2009). The current inhibitory effect of ZD7288 consists of a negative shift of the $V_{1/2}$ of about 15 mV and a decrease of the maximal channel conductance (Baruscotti et al., 2005). Early data in guinea pig SAN and right atria showed that the compound reduced spontaneous rate without modifying the contractile force (Marshall et al., 1993; BoSmith et al., 1993). The effects of ZD7288 were evaluated also in CNS, resulting in a substantial block of I_h in various neuronal structures (Baruscotti et al., 2005). Moreover, local or systemic administration of ZD7288 reduces the neuropathic behaviour in animal models of peripheral nerve injury (Ramirez et al., 2018). Despite the high selectivity for HCN channel, ZD7288 has been reported to block T-type calcium channels in rat hippocampal pyramidal cells (Sanchez Alonso et al., 2008); then, in rat DRG neurons, it blocks Na^+ current with a higher potency than that exerted on I_h (with IC50 of 1,17 µM and 15 µM, respectively) (Wu et al., 2012).

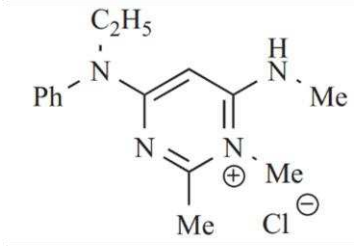

ZD7288

Figure 13. Two-dimensional structure of ZD7288

Finally, alinidine is an imidazoline compound derived from the antihypertensive drug clonidine. Although the two molecules structurally differ from each other in a very slight fashion, alinidine display distinct pharmacological effects, including analgesia and bradycardia (Baruscotti et al., 2005). Alinidine has been the first compound to be investigated for its bradycardic activity. In rabbit SAN, 0,3 µg/ml alinidine slow the spontaneous activity by shifting the I_f activation curve to more negative values (by 7-8 mV) and by reducing its fully activated conductance (by 27%). No use-or frequency-dependence was observed (Satoh and Hashimoto, 1986). However, further experiments demonstrated that alinidine was able to induce little prolongation of action potential duration, and therefore to be proarrhythmic (Snyders and Van Bogaert, 1987).

Other drugs showing HCN modulation activity

Clonidine is a α2-agonist used in clinic for several indications including analgesia. It blocks HCN4 with an IC50 of about 10 µM. At variance with ivabradine and the other compounds described above, clonidine binds the HCN channel from the extracellular side and shifts the activation curve by 10-20 mV to more hyperpolarized voltages (Postea and Biel, 2011). As its neuronal effects (analgesia and sedation) are mediated by central α2-adrenoreceptors, clonidine cannot be adopted as a bradycardic drug.

Loperamide is a µ-opioid receptor agonist, indicated for the treatment of diarrhea. Its capacity of binding to the HCN channel, which occurs by the extracellular side of the plasma membrane, was found during a screening library of known ion channel modulators. This has been hypothesized to be involved in the analgesic and antihyperalgesic effects of the drug (Vasilyev et al., 2007). In DRG neurons, loperamide inhibits I_h with a IC50 of 5-10 µM depending on the DRG sizes (Biel et al., 2009).

Eugenol is an analgesic agent, used in dentistry to relieve tooth pain, and its activity is associated with block of Na^+ and Ca^{2+} voltage-dependent channels. This drug was also found to inhibit I_h in medium and large trigeminal ganglion neurons, which mainly express HCN1 and HCN2, and this property may contribute to its analgesic activity (Romanelli et al., 2016). HCN channel blockade by eugenol occurs at concentrations lower than those required to block voltage-gated Na^+ channels (Yeon et al., 2011). Attenuation of the eugenol's effects in presence of cAMP analogues (e.g. 8-Br-cAMP) suggests a competition of these molecules for the binding site on the CNBD (Romanelli et al., 2016).

Propofol is a well-documented general anaesthetic agent, with additional antiemetic and antiepileptic properties (Sartiani et al., 2017; He et al., 2019). In several types of neurons, it inhibits I_h and HCN1 seems to be the most sensitive channel isoform (Cacheaux et al., 2005), therefore suggesting an antihyperalgesic action of this drug. Of note, some analogues of

propofol (alkylphenols) are found to be more potent HCN1 antagonists than propofol itself (Tibbs et al., 2013).

Lidocaine is a local anesthetic and antiarrhythmic drug. Its capacity of blocking HCN channels was tested on recombinant systems and native cardiac and neuronal tissues. On all isoforms, lidocaine causes a decrease of maximal conductance and slows current activation kinetics; only for HCN1 it produces a leftward shift in voltage dependence of activation (Sartiani et al., 2017). HCN channel blockade by lidocaine has been suggested to contribute to the drug effects during epidural and spinal anaesthesia (Zhou et al., 2015).

Challenges in structure-based drug design

Rational drug design targeting ion channels with specific properties is a constantly evolving research field. Structure-based methods and computational tools are two" driving forces" which offer the possibility to develop new therapeutic drugs. These approaches help the researcher to predict the position of small molecules within a three-dimensional representation of a protein. In this process, structural, physical-chemical and pharmacological properties of ligands and targets are critical to gain high potency and binding affinity.

The design of novel HCN channel antagonists also fits into this context, and three crucial points should be taken into account. First, there is a need of compounds with higher affinity: ideal molecules should act in the nanomolar range to lower the risk of off-target and noxious side effects. Second, also the localization of the drug binding site is of a key importance. Most of known blockers target the intracellular side of the channel, often in the inner ion-conducting pore: that implies not only the need of penetration of plasma membrane by the compound, but also a very slow deactivation kinetics, due to the fact that the molecule is trapped within the pore. Furthermore, as occurs with ZD7288 (Rothberg et al., 2002), the block can be irreversible. It would be desirable to design compounds which bind to the HCN channel in a reversible manner from the external side of the membrane: in this regard, clonidine could serve as a sample for such a drug. Third, probably the most important goal in the development of drugs targeting HCN channels will be the design of isoform-specific blockers, as the only commercially used drug, ivabradine, does not discriminate between different isoforms. Drugs selective for HCN4 would be effective in lowering heart rate without the side effects associated with vision that are typical of nonspecific HCN channel blockers. Similarly, selective inhibitors of HCN1 and/or HCN2 would have no major effects on cardiac pacemaker function but could be used as analgesic agents.

2. Role of inflammation and cytokines in cardiac electrogenesis

Inflammation is an important defence mechanism of the body. It occurs during several physiologic and pathologic processes and it is triggered by stimuli and harmful conditions, such as infections and tissue injury (Kumar et al., 2003; Medzhitov, 2008). According to duration, this mechanism is classified in acute and chronic inflammation. Acute inflammation is a primary and physiological response and is controlled by the organism with the aim to defend from infections and immediately repress the effects of the causative agent, in order to restore tissue homeostasis (Woodroofe, 1995; Nathan et al., 2002). Acute inflammation is triggered by innate immune system, which occurs at the tissue level and consists of a vascular and leukocyte response. Macrophages and mast cells present in the tissues and/or tissue cells produce a series of mediators, such as chemokines, cytokines, vasoactive amines, eicosanoids and products of the proteolytic cascades, that recruit neutrophils and eventually impair the function of tissues and organs. Different immune cells in this process upon activation release the toxic content present within their granules in order to eliminate the causative agents. When the acute inflammatory responses are successful, the tissue, damaged by resident macrophages, is consequently repaired (Serhan and Savill, 2005; Medzhitov, 2008). However, it is possible that the inflammation persists even after elimination of the cause, establishing a chronic systemic inflammation. If not adequately controlled, the chronic inflammation can assume large size and contribute to the occurrence of chronic diseases.

2.1 Cytokines as effectors of the inflammatory process

Important effectors of the inflammatory process are the cytokines, no antigen-specific soluble polypeptide mediators (8-60 kDa) of the immune system. Cytokines act as paracrine and/or endocrine carriers of messages between the cells of the immune system and/or between immune cells and cells distant from the production site of cytokines, respectively (Abbas et al., 2005). Cytokines are also responsible for the regulation of maturation, growth and reactivity of the immune cells and affect almost all biological processes, such as embryonic development, pathogenesis of many diseases, no-specific response to infections, specific response to an antigen, changes in cognitive functions and progression of degenerative processes during aging (Dinarello, 2007).

Cytokines are produced by several cell types, mainly by lymphocytes, activated macrophages, mononucleate phagocytes and other antigen presenting cells (APCs), following the phagocytosis, elaboration and presentation to T-helper lymphocytes from APCs, but also by endothelial, epithelial and connective tissue cells (Kumar et al., 2003).

Cytokines can be divided in pro- and anti- inflammatory according to their role as mediator or inhibitor, respectively, of immune system and inflammatory responses (Kim et al., 2016). Cytokines include tumor necrosis factor α (TNF-α) and several interleukin molecules (IL) known as IL-1, IL-6, IL-8, IL-12, IL-15, IL-18 and IL-23, that exert several roles, such as activation

of leukocytes and induction of acute response resulting in local recall of cells fighting infection and repairing tissues (Borish and Steinke, 2003; Medzhitov et al., 2008) (Figure 14).

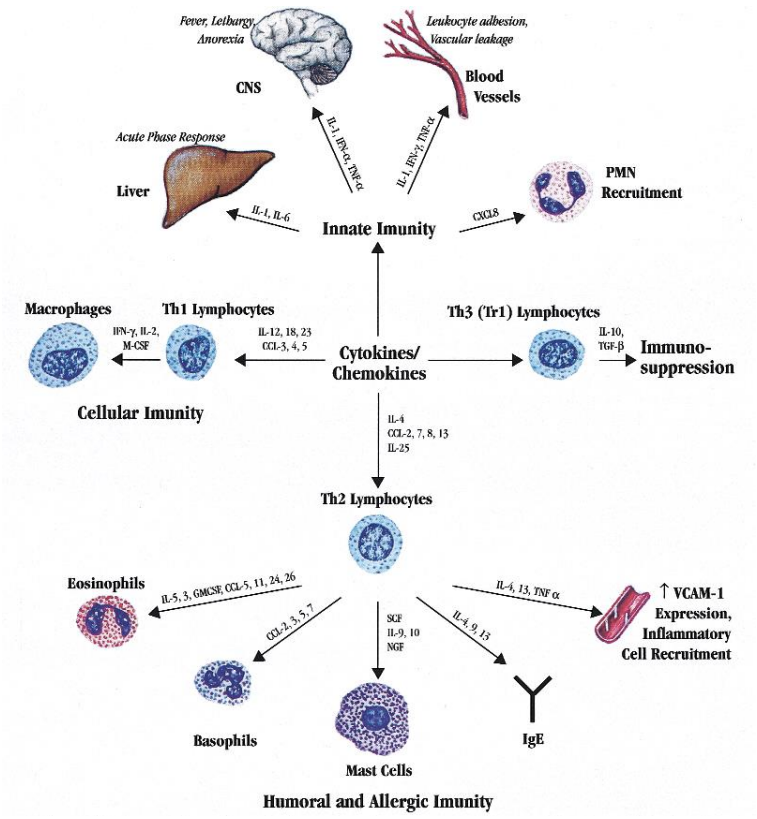

Figure 14. Summary of actions of cytokines and chemokines. Cytokines derived mainly from mononuclear phagocytic cells. They are important in innate immunity, initiate immune responses and generate symptoms associated with infections and inflammatory disorders. The responding T-helper 1 and 2-like (TH1, TH2) lymphocytes contribute to cellular immunity and humoral and allergic responses, respectively, and produce IFN-γ, IL-4, IL-5, IL-9 and IL-13 in response of immune system. TH3-like lymphocytes have immunosuppressive tendencies and are characterized by their production of IL-10 and TGF-β. (from Borish and Steinke, 2003).

Based on their concentrations, effects of cytokines can be beneficial and harmful: generally, beneficial effects occur at lower and/or physiological concentrations, while the harmful effects are observed mainly when cells are exposed to relatively high concentrations of cytokines. In this last case, several experimental and clinical studies demonstrated that the massive release of proinflammatory cytokines into the systemic circulation causes cardiovascular disorders associated to inflammatory conditions, such as rheumatoid arthritis or viral infections (such as COVID-19). It was demonstrated that circulating levels of IL-6, IL-1, and TNF-α are directly associated with pro-arhythmic changes in the heart, such as increased duration of the electrocardiographic QT interval (see “cardiac arrhythmogenic effects of inflammatory cytokines”).

TNF-α is derived from mononucleated phagocytes. Its production can be induced by lipopolysaccharide, following the recognition of pathogen proteins. TNF-α is a potent neutrophil activator, mediating adhesion, chemotaxis, degranulation and oxidizing reactions (Borish and Steinke, 2003). Its biological effects of TNF-α are mediated by two surface receptors, the TNF receptor type 1 (TNFR1) and type 2 (TNFR2), both expressed in cardiomyocytes, cardiac fibroblasts and endothelium cells. The increased levels of TNF-α can cause arrhythmic events. Moreover, TNF-α induces adhesion molecules, such as intracellular

adhesion molecule 1 (ICAM-1), vascular cell adhesion molecule 1 (VCAM-1) and E-selectin, in endothelial cells, permitting the entry of granulocytes into inflamed tissues and induces anticancer immunity (hence the name) through direct cytotoxic effects on cancerous cells (Borish and Steinke, 2003).

IL-1 family consists of 11 cytokines and 10 receptors (Dinarello, 2018). IL-1 production by several cells, such as mononucleate phagocytes, endothelial cells, keratinocytes, synovial cells, osteoblasts, neutrophils, glial cells, is stimulated by endotoxins, other cytokines, microorganisms and antigens. IL-1 has several biological activities: IL-1 activates T cells, increases the production of B cells and the synthesis of immunoglobulins, stimulates the production of acute inflammation proteins, such as reactive C protein and complement proteins, and mediates the adhesion of leukocytes to endothelial cells, increasing the expression of adhesion molecules (Borish and Steinke, 2003). IL-1 has also several effects on cardiomyocytes, where it decreases their contractile strength, acting on Ca^{2+} homeostasis or suppressing β-adrenergic response; it also exerts pro-apoptotic actions and stimulates and supports the inflammatory response, inducing the mobilization and activation of leukocytes (Hanna and Frangogiannis, 2020).

IL-6 family consists of several cytokines, including IL-6, IL-11, oncostatin and cardiotropin. It is involved in the regulation of the acute inflammatory phase, after a result of a harmful stimulus. These cytokines activate the target genes involved in differentiation, survival, apoptosis and proliferation. Moreover, the cytokines of this family have pro-and anti-inflammatory properties and play an important role in haematopoiesis, in the acute phase of inflammation and in immune responses of the body (Heinrich et al., 2003). IL-6 is a pleiotropic cytokine produced by several cell types, such as lymphocytes, monocytes, fibroblasts, keratinocytes, endothelial cells and cardiomyocytes, like the other cytokines. It binds its specific receptor (IL-6R) and gp130, which homodimerizes and activates Januse Kinase (JAK), the intracellular effector able to initiate the cellular and organ response (see “interleukin-6 and ion channels”). In this way, IL-6 influences various cell types and has multiple biological activities. IL-6 is produced transiently in response to infections and tissue lesions, in order to stimulate the acute response, haematopoiesis and immune reactions (Mihara et al., 2012). IL-6 induces the differentiation of CD8 T cells into cytotoxic T cells and of activated B cells into plasma cells (Tanaka et al., 2014); it is involved in neutrophil recall, angiogenesis, lipid and bone metabolism (Mihara et al., 2012). Elevated concentrations of this cytokine contribute to genesis of several autoimmune and inflammatory diseases; in line with this tocilizumab, a humanized monoclonal anti-human IL-6R antibody, is effective to improve symptoms of rheumatoid arthritis and of juvenile idiopathic arthritis (Mihara et al., 2012).

2.2 Interleukin-6 acts as modulator of cardiac ion channels

IL-6 mediates its effects by binding its membrane-bound receptor, IL-6R α subunit (classical signalling), or the soluble receptor (sIL6R). The latter interacts with the signal transduction protein glycoprotein 130 (gp130) forming a dimeric complex (IL-6-IL-6R-gp130) and leading to the activation of intracellular signaling pathways (Akira et al., 1990; Akira et al.,

1994; Naka et al., 1997; Taga and Kishimoto, 1997; Heinrich et al. 2003; Fontes et al., 2015; Alì et al., 2019) (Figure15).

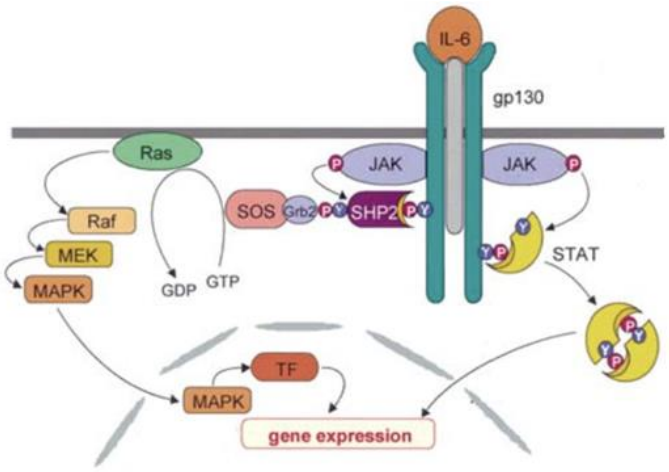

Figure 15. IL-6 signalling pathway in cells expressing IL-6R and gp130. IL-6 binds its non-signalling receptor, IL-6R, that in turn interacts with gp130 subunits, the signal transduction receptor for IL-6. The formation of the complex IL-6-IL-6R-gp130 can induce the activation of tyrosine kinases of JAK family, promoting the phosphorylation of STAT1 and STAT3, which dimerize and migrate into the nucleus to induce the transcription od target genes. However, the complex IL-6-IL-6R-gp130 can active the Ras-Raf-MAPK pathway (modified by Heinrich et al., 2003).

In one of the activated signalling pathways, IL-6 recruits tyrosine phosphatase protein 2 (SHP2), that triggers the activation of the GTPase Ras pathway and its Raf effector, with subsequent activation of the mitogen-activated protein kinase cascade (MAPK), responsible for controlling cell proliferation and differentiation. Otherwise, the activation of tyrosine kinases of the JAK family may occur (Lutticken et al., 1994; Stahl et al., 1994). Activated JAK recruits and subsequently phosphorylates transcriptional factors belonging to the STAT family (STAT1, STAT3 and, less frequently, STAT5) (Hirano et al., 1997; Yamanaka et al., 1996). Phosphorylated STAT dimerizes and subsequently migrates into the nucleus to induce the transcription of target genes (Yoshida et al., 1996).

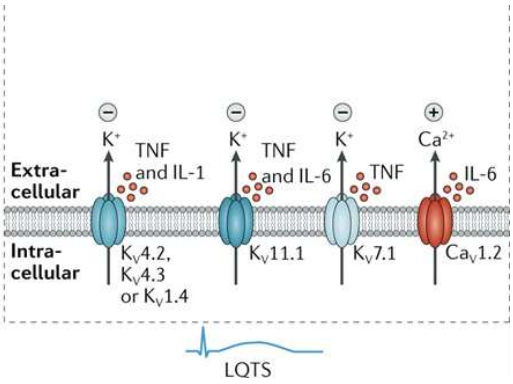

Figure 16. Role of the inflammatory cytokines on the modulation of ionic channels and the development of arrhythmias. IL-6 acts on the L-type Ca^{2+} channels ($Ca_V1.2$), increasing I_{CaL} in ventricular cardiomyocytes, and inhibits the rapid component of the delayed rectifier K current, I_{Kr} (modified by Aromolaran et al., 2018).

Among the several effects of IL-6, several studies demonstrated the interaction of IL-6 with cardiac ionic channels. In particular, IL-6 is able to induce an increase of L-Type Ca^{2+} current

(I_{CaL}) through phosphorylation of $Ca_{V1.2}$ subunit and to inhibit the rapid component of the delayed rectifier K^+ current (I_{Kr}) through activation of JAK pathway (Armolaran et al., 2018) (Figure 16). These modulations are critically involved in cardiac instabilities, that ultimately predisposes to arrhythmic disorders and cardiomyopathies (Alì et al., 2019).

Hagiwara and coworkers (2007) demonstrated that IL-6 induces the phosphorylation of $Ca_{V1.2}$, increasing the density of L-Type Ca^{2+} current (I_{CaL}). This study was performed in mouse ventricular cardiomyocytes, where mouse gp130 gene was replaced with human gp130 mutant cDNAs in order to disrupt the SHP2/MAPK signal and active the JAK/STAT3 cascade. For the study, the authors considered the leukemia inhibitory factor (LIF), a cardiac hypertrophic cytokine belonging to the IL-6 family (Metcalf, 1992), that activates its signaling pathway binding the IL-6R. It was demonstrated that LIF increased I_{CaL} and intracellular Ca^{2+} concentrations in the cardiomyocytes via SHP2/MAPK pathway. In addition, LIF induces the phosphorylation of the extracellular serine 1829 in the $Ca_{v1.2}$ subunit, increasing I_{CaL} in the cardiomyocytes (Takahashi et al., 2004). Therefore, it is hypothesized that the increase of IL6- and LIF-induced intracellular Ca^{2+} concentrations may induce cardiac arrhythmias. In fact, it was reported that increasing IL-6 in patients is one of the risk factors, that predicts sudden cardiac death during coronary artery disease.

The effect of IL-6 on I_{Kr} was demonstrated by Aromolaran and coworkers (2018) on HEK293 cells stably expressing ether-á-go-go-related gene (hERG) channels and on adult guinea-pig ventricular myocytes by electrophysiological and biochemical assays. In particular, Aromolaran and coworkers demonstrated that the increase of circulating levels of IL-6 induces a decrease of I_{Kr} with subsequent prolongation of the duration of the action potential. This effect of IL-6 is prevented by using an inhibitory mouse monoclonal anti-IL6R antibody and a JAK-inhibitor, and induces a delayed repolarization which may set the basis for the development of ventricular arrhythmias. Further experiments in guinea pig heart showed a reduction in mRNA and protein expression of the hERG channels (Aromolaran et al., 2018).

Despite many experimental evidence indicate IL-6 and other inflammatory cytokines exert direct and indirect effects on cardiac ion channels and electrogenesis, no information are available on the effects of IL-6 on cardiac pacemaking function and on the associated ionic mechanisms.

Cardiac arrhythmogenic effects of inflammatory cytokines

Several experimental and clinical studies have shown that inflammatory conditions, such as rheumatoid arthritis, or viral infections, such as COVID-19, are associated with cardiovascular disorders, caused by the massive release of proinflammatory cytokines into the systemic circulation. In particular, inflammatory cytokines play a key role in the genesis and maintenance cardiac arrhythmogenesis, such as atrial fibrillation (AF), promoting the electrical (hours to days after exposure to cytokines) and structural (over weeks or months) remodelling of the atrial myocardium (Lazzerini et al., 2022). These changes occur through different mechanisms, ranging from the activation of fibroblasts to myofibroblasts, to the alteration of the gap junctions (the main proteins for electrical conduction in the myocardium) and to the induction of abnormalities of Ca^{2+} ion regulation in cardiomyocytes. Overall, these modifications are suggested to induce both the formation of fibrosis and occurrence of electrical abnormalities (Lazzerini et al., 2017; Hanna and Frangogiannis, 2020) (Figure 17).

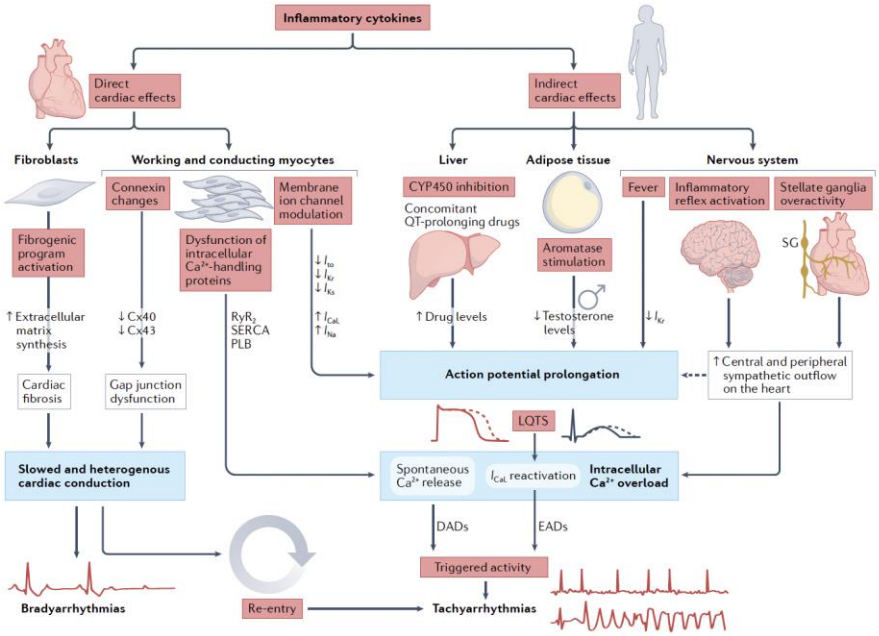

Figure 17. Arrhythmogenic effects of inflammatory cytokines.
(from Lazzerini et al., 2022).

The cardiac proarrhythmic changes are directly associated to high circulating levels of cytokines, which as mentioned previously for IL-6 (see "interleukin-6 and ion channels"), may alter the duration of action potential and increases the QT electrocardiographic interval. In the ventricle, the above-mentioned modifications increases the propensity to develop dangerous polymorphic ventricular tachycardias, such as *Torsades de Pointes* (TdP), that can evolve in ventricular fibrillation (VF) (Lazzerini et al., 2017; Aromolaran et al., 2018).

In murine cardiomyocytes, experimental data have demonstrated the occurrence of interactions between several ionic channels and cytokines such us TNF-α and IL-1 β. TNF-α, like IL-6, increases I_{CaL} and decreases I_{Kr}, prolonging the action potential durations (Rozansky, 1993; Wang et al., 2004); differently, IL-1β induces the prolongation of the action potential through a decrease of the I_{to} and an increase of Ca^{2+} current, thus increasing the risk of developing arrhythmias (Monnerat et al., 2016).

In addition, overexpression of TNF-α in murine hearts may increase predisposition to AF associated with decreased contractile function of the heart muscle and changes in Ca^{2+} homeostasis of cardiomyocytes (Saba et al., 2005; Scott et al., 2019). Moreover, TNF-α can also trigger an apoptotic response in the myocardium, activating specific intrinsic cell death pathways (Haudek et al., 2007).

Recently, Wu and coworkers (2013) demonstrated a close correlation between IL-6 and the incidence of AF and its recurrences after electrical cardioversion or catheter ablation. In addition, Lazzerini and coworkers (2019) demonstrated that high levels of IL-6 derived from systemic inflammation are closely linked with transient electrical remodelling at atrial level due to decreased expression of some connexins. This event disrupts normal cardiac conduction. In fact, *in vitro* experiments have shown that the incubation of mouse atrial HL-1 cardiomyocytes with IL-6 is associated with a significant decrease in protein expression of both connexin 40 and connexin 43 (Lazzerini et al., 2019).

Other effects of IL-6 that have been demonstrated in different experimental models are the induction of cardiac hypertrophy and heart failure associated to enhanced fibrosis and

increase of Atrial Natriuretic Peptide (ANP), known marker of hypertrophy (Zhao et al., 2020; Huo et al., 2021). Altogether these findings corroborate the notion of an important role played by IL-6 in myocardial dysfunctions associated to arrhythmias. In line with this observation, high levels of circulating IL-6 have been recently associated with an increased arrhythmic risk in patients with COVID-19 (Lazzerini et al., 2020).

COVID-19 and cardiac arrhythmias

Coronavirus disease (COVID-19) is an infectious disease caused by the SARS-CoV-2 virus and can cause severe acute respiratory syndrome (Driggin et al., 2020). This condition is characterized by viral tissue invasion and an exaggerated response of the immune system (cytokinin storm). This response is often followed by a multiorgan dysfunction. In fact, patients with COVID-19 present high levels of circulating cytokines, in particular of IL-6, associated with an increase in morbidity and mortality for cardiovascular disease. The latter often arise from development of arrhythmic events, such as malignant ventricular arrhythmias (VA), or ventricular tachycardia/fibrillation (VT/VF) (Driggins et al., 2020; Lazzerini et al., 2020) and AF (Bhatla et al., 2020; Ip et al., 2021). Although the mechanisms of COVID-19-induced myocardial damage are unknown, it is hypothesized that the viral infection induces a cellular and (subsequently) tissue damage, caused by a cytokinin storm, promoting the development of cardiac arrhythmias in the patients. Indeed, Lazzerini and coworkers (2019) observed that patients with severe disease and higher incidence of VT/VF presented also an increase of levels of Troponin T, correlated with a damage of cardiac myocytes. The risk of developing arrhythmias is determined not only by myocardial damage, but also by other factors such as pharmacological treatments used against virus infection and replication, that can, however, cause the prolongation of the QT interval and, therefore, the appearance of TdP. Capecchi's team demonstrated that the characteristic inflammatory state of COVID-19 may be a potential risk factor in inducing arrhythmogenic events, such as QT prolongation and TdP, caused by the interaction of cytokines (IL-6, TNF and IL-1) with the ion channels. In addition, the research team demonstrated that inflammatory cytokines can cause hyperactivation of the cardiac sympathetic system, through the hypothalamus-modulated pathways, inducing the appearance of arrhythmic events (Lazzerini et al., 2017; Lazzerini et al., 2019; Lazzerini et al., 2022). High levels of IL-6 inhibit hERG channels, prolonging the duration of action potential in ventricular myocytes (Lazzerini et al., 2019), and cytochrome p450, causing an increase in the bioavailability of several drugs used for the treatment of patients with COVID-19. Subsequently, the inhibition of the inflammatory response in COVID-19 patients may also be useful in reducing cardiovascular events. In fact, the treatment with tocilizumab (mentioned previously) induces beneficial effects on the survival of patients with COVID-19, inducing a reduction of the QT interval, related to decrease of C-reactive protein and cytokine levels (Lazzerini et al., 2020). These data suggest that the administration of anti-IL-6 therapies in patients with COVID-19 could represent a useful approach for the recovery of multiorgan dysfunction and to reduce the high arrhythmic risk that is associated.

3 Human induced pluripotent stem cells to model cardiac pacemaker function and diseases

At the beginning of 20s, Takahashi and Yamanaka (2006) demonstrated that pluripotent stem cells can be directly generated from somatic cell cultures by the only introduction of few factors (Oct3/4, Sox2, c-Myc andKfl4). These cells were called induced pluripotent stem cells (iPSCs) and exhibit the morphology and growth properties of embryonic stem cells (ESCs) and express ES cell marker genes (Takahashi and Yamanaka, 2006). This discovery allowed the possibility to create *in vitro* models of healthy and diseased human differentiated cells from iPSCs, among which cardiomyocytes.

Thanks to their pluripotency, iPSCs have the ability to differentiate in all cell types belonging to the three germ layers (endoderm, mesoderm and ectoderm). Among them, the human iPSC-derived cardiomyocytes (hiPSC-CMs) have generated much interest: thanks to their unlimited source, their use is broad from *in vitro* applications (i.e., cardiotoxicity screening, drug discovery, disease modelling) to *in vivo* applications (i.e., cell replacement therapy) (Pourrier and Fedida, 2020). In fact, the hiPSC-CMs are used as an alternative tool to better understand basic cellular, molecular and genetic mechanisms in physiological and pathological events; they provide an *in vitro* model that can be used in drug development and safety, efficacy testing and in clinical applications for diagnosis and personalized treatment to predict therapeutic responses in individual patients with cardiac diseases, such as arrhythmogenic syndromes (Knollmann, 2013; Sala et al., 2019).

The possibility to obtain hiPSCs from human somatic cells provides a way to capture the heterogeneity developing from gender, ethnicity and biological patient-specific variability (Bellin et al., 2012).

There are different protocols to differentiate hiPSC in cardiomyocytes, as the one described later in this thesis (see “Materials and methods”), that include a variety of stimuli and culture media (Shiba et al., 2009; Yoshida and Yamanaka, 2011; Burridge et al., 2014; Smith et al., 2017). Usually a mixed population of ventricular-like (generally in the majority), atrial-like and sinoatrial node-like hiPSC-CMs is generated (Itzhaki et al., 2011; Ma et al., 2011; Burridge et al., 2012; Devalla et al., 2015; Protze et al., 2017), in which the subtype specific cell type is confirmed through differences in electrophysiological characteristics (i.e., action potential morphology and duration) and calcium handling (duration and kinetics of calcium transients).

One of the most valuable use of hiPSC-CMs is to model inherited cardiac diseases, such as arrhythmogenic diseases (i.e., hypertrophy cardiomyopathy, dilated cardiomyopathy, short or long QT syndromes, Brugada syndrome, catecholaminergic polymorphic ventricular tachycardia, arrhythmogenic right ventricular cardiomyopathy, etc.), by using patient-specific cells, editing the genome of healthy cells or overexpressing mutated ion channels (Figure 18).

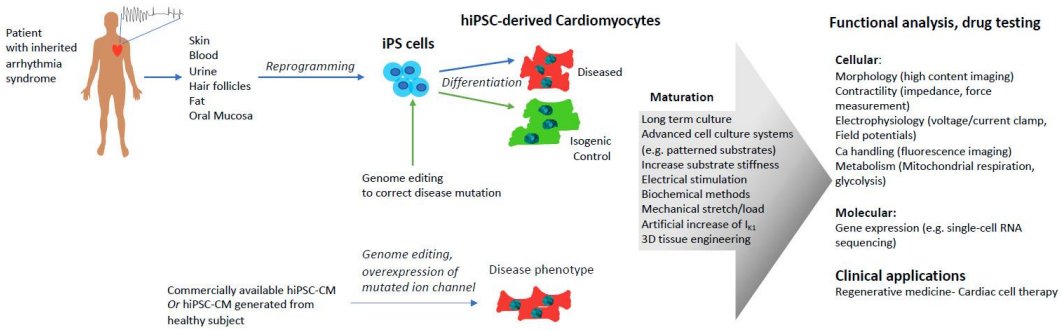

Figure 18. Approaches to model cardiac diseases using hiPSC-derived cardiomyocytes. (Pourrier and Fedida, 2020).

The possibility to generate patient-specific iPSC represents a critical preclinical model system for investigating the genetic basis of human cardiac diseases and studing patient-specific therapies. In this way, hiPSC-CMs are closely genetically matched to patients with a particular disease, unlike animal models. Among the most broadly studied diseases there are arrhythmic disorders caused by mutations in ion channel-related proteins, modulatory proteins and structural proteins; functional characterization is mostly obtained via patch clamp electrophysiological techniques and/or high throughput techniques (Pourrier and Fedida, 2020).

The emergence of genome editing techniques resolved an important limitation of patient specific iPSC lines, the lack of their isogenic control, that is reflective of the patient genetic background and epigenetic modifications induced by epidemiological and environmental factors. In additional, genome editing tools (clustered regularly interspaced short palindromic repeats (CRISPR/Cas9), zinc finger nucleases (ZFN), adenoviral vectors, and transcription activator-like effector nucleases (TALEN)) allow the generation of new cell lines, introducing in hiPSC lines desired mutations or other variants (Moehle et al., 2007; Mussolino et al., 2011; Cong et al., 2013; Corrigan-Curay et al., 2015; Matsa et al., 2016; Seeger et al., 2017; Strong and Musunuru, 2017), in order to study variants modifying disease in the same genetic background.

Phenotypic profile of hiPSC-CMs

Generally, hiPSC-CMs are a predictive tool in the context of drug testing and as a promising alternative to animal testing with regard to disease modelling, despite their differences in electrophysiological characteristics with adult human myocytes (Pourrier and Fedida, 2020).

hiPSC-CMs are electrophysiologically immature when compared to isolated adult human cardiomyocytes, as reflected by a more positive maximal diastolic potential (MDP), a large phase 4 depolarization, a slower upstroke velocity, and almost absent notch (Ma et al., 2011; Hoekstra et al., 2012; Gibson et al., 2014). Spontaneous beating ventricular-like and atrial-like hiPSC-CMs, a characteristic of fetal human cardiomyocytes, is due to a less negative resting membrane potential, caused in turn by a small I_{K1}, and the presence of the pacemaker current (Figure 19). As reported by Zhao and coworkers (2018), most ion channels (such as I_{Na}, I_{CaL}, I_{CaT}, I_f, I_{NCX}, I_{K1}, I_{to}, I_{Kr}, I_{Ks}, I_{KATP}, $I_{K\text{-}pH}$), present in adult healthy or diseased cardiomyocytes, are also expressed in hiPSC-CMs, contributing to action potential morphology and presenting a regulation by adrenergic and cholinergic modulation (Ma et al., 2011; Gibson et al., 2014; Zhao et al., 2018).

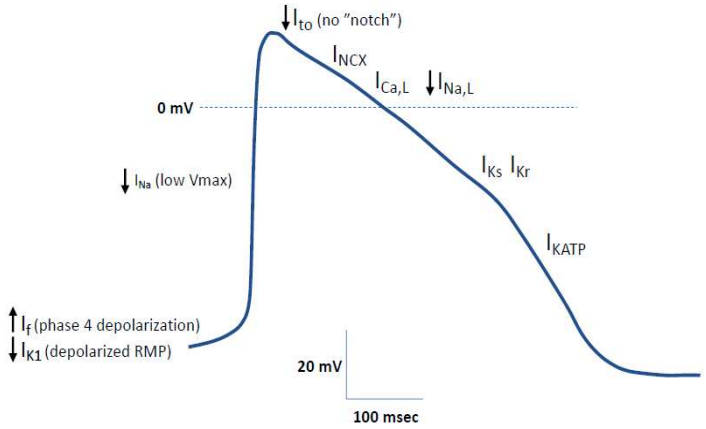

Figure 19. Representation of a typical action potential recorded from a ventricular-like hiPSC-CM. In the graph shows the function ionic currents. Arrows indicate reported up and down regulation in comparison to adult human ventricular myocytes (from Pourrier and Fedida, 2020).

In addition, the immature Ca^{2+} handling of hiPSC-CMs is due to the lack of T-tubules, resulting in poor coupling between the Ca^{2+} entry through I_{CaL} and Ca^{2+} release from the sarcoplasmic reticulum through cardiac ryanodine receptor type 2 (RyR2) (Lieu et al., 2009; Hwang et al., 2015). Random structures of the myofibrils indicate a high disorganization of contractile proteins (Lundy et al., 2013) and mitochondria present immature structural and functional properties (Feric et al., 2016; Scuderi and Butcher, 2017). Lastly, the hiPSC-CMs metabolism depend on glycolytic pathways for energy production, in contrast to adult cardiomyocytes that depend on fatty oxidation (Karakikes et al., 2015).

Despite their immature phenotype, in several studies hiPSC-CMs recapitulated the clinical phenotypes observed in the donors and the expected phenotypes associated with drug effects (Crumb et al., 2016; Pourrier and Fedida, 2020). Several strategies have been developed in order to improve the maturation of hiPSC-CMs (Yang et al., 2014; Keung et al., 2014; Jiang et al., 2018; Ribeiro et al., 2019): enhancing the function or expression level of I_{K1} (Li et al., 2017; Vaidyanathan et al., 2016); a long term culture (Lewandowski et al., 2018); specific biochemical differentiation enhancing tools such as the hormone triiodothyronine (Yang et al., 2014) or fatty acids (Yang et al., 2019); generation of engineered three-dimensional human cardiac tissue and application of electrical stimulation or mechanical strain to improve structural and functional maturation (Nunes et al., 2013). Moreover, in the last years, new protocols to improve the ability to derive specific cardiac subtypes have been developed (Zhang et al., 2011; Xu, 2012; Karakikes et al., 2014; Weng et al., 2014; Devalla et al., 2015; Cyganek et al., 2018), enabling a more comprehensive approach to disease modelling, drug screening and widening the potential applications of hiPSC-CMs in preclinical studies (Smith et al., 2017; Pourrier and Fedida, 2020).

However as mentioned previously, spontaneous electrical activity of cardiomyocytes differentiated from hiPSC typically is due to a robust expression of I_f, which has also been described in cardiomyocytes differentiated from hESC (Sartiani et al. 2017). For this reason and for the aim of this thesis we used cardiomyocytes differentiated from hiPSC to study the effect of innovative HCN channel blockers and test their potential as bradycardic agent.

CHAPTER II.
AIM OF STUDY

Cardiac pacemaker activity arising from the sinoatrial node (SAN) cells is caused by the concerted function of different ion channels and pumps, among which the Hyperpolarized-activated Cyclic Nucleotide-gated (HCN) channels play a prominent role. In line with this function in the heart, pacemaker activity in neurons is also sustained by HCN channels, that control many different functions, including pain perception passing through dorsal root ganglia.

HCN channel family comprises four homologous members (HCN1-4), differently expressed in the heart and the nervous system, which have been characterized for their different structure, biophysical properties, regulatory pathways, and pharmacology. Because of these characteristics, HCN channels represent valuable targets to identify novel pharmacological molecules and endogenous mediators of potential interest to modulate their physiological function or their dysfunction in cardiac and neuronal pathologies. In further details, research interest in the field of HCN channel blockers has remarkably grown up during the last decades, since the discovery of ivabradine. This is the only HCN blocker employed in the clinical use as specific bradycardic agent that is utilized in patients with stable angina and heart failure, intolerant or not responsive to β-blockers. However, as well as other HCN antagonists (i.e., zatebradine and cilobradine), ivabradine lacks HCN isoform selectivity and tissue specificity, leading to the occurrence of side effects (i.e., phosphenes) in patients. Furthermore, the function of distinct HCN isoforms in the central and peripheral nervous system opened to new applications of drugs able to reduce their activity. In particular, molecular prototypes showing higher selectivity toward HCN1/HCN2 isoforms have been successfully tested in animal models of neuropathic pain, while others, showing higher selectivity for HCN4 isoforms have been experimentally tested against some forms of epilepsy. Finally, a recent clinical study has indicated ivabradine as effective drug for neuropathic pain relief, further confirming the potentials of HCN blockers as innovative drugs.

In the last decades, the research group I joined during the PhD course, has done considerable efforts to characterize new HCN blockers with the ultimate aim to discriminate among different HCN channel isoforms. Main results of this research have identified lead compounds endowed with isoform selective/preferential blockade for specific HCN isoform; for these reasons they are currently employed as pharmacological tools to study the role of single channel isoforms in physiological and pathological conditions. Moreover, these molecules could represent a starting point to develop innovative drugs effective to prevent or treat cardiac or extra-cardiac diseases, characterized by enhanced and/or altered function of single or all HCN channel isoforms.

A different but still connected investigation performed in my thesis, concerned the modulatory signals of pacemaker function and the optimization of the experimental approaches to study it. In particular, a number of experimental and clinical literature data prompted us to study the potential effects of IL-6 on cardiac pacemaker function, since the cytokine is involved in cardiac arrhythmic disturbance via interactions with different ion channels in the heart. This notion consolidated the idea that IL-6 may play a role as a direct modulator of cardiac pacemaker activity acting as multichannel modulators.

Following on this premise in this thesis I studied the effects of two new zatebradine analogues, PK9 and PK19, synthesized by Prof. Romanelli and co-workers (Department of NEUROFARBA, University of Florence). To this aim I used three different *in vitro* cellular models: HEK293 cells expressing recombinant homo-tetrameric mouse HCN1, mouse HCN2 and human HCN4 channel isoforms; rat Dorsal Root Ganglia (rDRG) neurons; hiPSC-derived cardiomyocytes (hiPSC-CMs). HEK293 and rDRG models have been used to study the

electrophysiological effects of PK9 and PK19 on HCN-mediated current by using single-cell patch-clamp recordings (whole-cell configuration). In addition, hiPSC-CMs have been used to study the effects of both zatebradine analogues on spontaneous action potentials and pacemaker activity. To perform this phase of experiments, in collaboration with Prof. Sacconi and Dr. Credi (European Laboratory for Non-linear Spectroscopy), I developed a High Throughput System MULTIPLE that is able to perform high-throughput fluorescence recordings of cardiomyocytes exhibiting spontaneous electrical activity. Using this approach, I studied the two zatebradine analogues as well as the effect of human IL-6 using growing concentrations in the sub-μM and μM ranges, respectively. As concerns HEK cells and DRG neurons, PK9 and PK19 effects on HCN-mediated current were analyzed in terms of concentration-dependence of blockade, potency of current blockade, and channel use- and state-dependence of blockade. Differently, experiments on hiPSC-CMs were used to investigate the effects on frequency of spontaneous action potentials, amplitude, maximal diastolic potential and duration of the repolarization phase.

Finally, based on the concern that cardiomyocytes differentiated from hiPSC are currently one of the best platforms to study human cardiac pacemaker function and related modulatory signals, during six months of my PhD I carried out a research period at the University Medical Center of Utrecht (The Netherlands) in collaboration with Prof. Francesca Stillitano (aiming to establish novel hiPSC lines able to differentiate toward the cardiomyocyte lineage). The overall training done in this phase of research enabled me to substantially advance the knowledge in stem cell technology, through the assessment on cell quality and pluripotency, the Sendai virus handling, the trilineage differentiation technique, karyotyping and cross-contaminations.

CHAPTER III.
MATERIALS AND METHODS

1. Culture and isolation of HEK293 expressing cardiac HCN isoforms

Human embryonic kidney cells (HEK293 cells DSMZ, Braunschweig, Germany), transfected with mouse HCN1 (mHCN1), mouse HCN2 (mHCN2) and human HCN4 (hHCN4) cDNA (provided by Prof. M. Biel, University of München), were cultured in T25 flasks and incubated at 37◦C with 5% CO_2 as previously described (Del Lungo et al. 2012). The culture medium consisted of Dulbecco's modified Eagle's medium, High Glucose (DMEM + GlutaMax-I x1, Gibco, Italy), supplemented with 10% fetal bovine serum (FBS), 100 units/ml penicillin, 100 µg/ml streptomycin, 200 µg/ml geneticin (G418, Gibco, Italy). At confluence (3-5 days after plating), cells were detached by enzymatic dissociation with trypsin-EDTA. Digestion was stopped by adding complete medium and the cells were centrifuged at 1200 rpm for 5 minutes. The sedimented cells were either replated or used for electrophysiological measurements. To measure I-HCN, HEK293 cells were dissociated with diluted trypsin in Phosphate-Buffered Saline (PBS) solution (1:10) and then were incubated in Tyrode's solution (see "Solutions") supplemented with 300µM $CaCl_2$ and Bovine Serum Albumin (10 mg/mL; Sigma-Aldrich, A9647) for 2–3 h at room temperature (Balducci et al., 2021).

2. Preparation of Rat Dorsal Root Ganglia neurons

Male Sprague Dawley rats (Envigo, Varese, Italy), housed in a temperature- and humidity-controlled vivarium (12 h dark/light cycle, free access to food and water), were sacrificed by cervical dislocation at 22-30 days of age. DRG were isolated from the entire length of the spinal column following removal of the spinal cord, then used for primary cultures. After incubation in collagenase (2.5 mg/ml, Sigma-Aldrich) and trypsin (1 mg/ml, Sigma-Aldrich) for 1 h at 37°C, ganglia were mechanically triturated with a 45 µm sterile needle (Dini et al., 2018). The cell suspension was filtered in 40 µm Nylon filter (BD Falcon) then centrifugated and re-suspended in Dulbecco's modified Eagle's medium (DMEM, Gibco, Italy) supplemented with 50 units/ml penicillin and 0.05 mg/ml streptomycin (Invitrogen), 1% L-glutamine (Invitrogen), 10% FBS (Gibco, Italy), 50 ng/ml nerve growth factor (NGF, Promega) and 1.25 µg/ml cytosine β-D-arabinofuranoside (Ara-C, Sigma, Italy) (Dini et al., 2018). DRG neurons were plated onto 13 mm borosilicate cover glass previously coated with polyL-lysine (1000 µg/ml, Sigma, Italy) and laminin (10 µg/ml, Sigma, Italy). The medium was changed after 24 h. Electrophysiological recording were made within 48 h from dissociation.

3. Human induced Pluripotent Stem Cells (hiPSCs)

Human induced pluripotent stem cells (hiPSCs) show features similar to embryonic stem cells (ESC). This makes them an invaluable source of pluripotent cells for drug discovery, cell therapy and basis research.

3.1 Reprogramming and Cell culture

There are several methods to generate hiPSCs, including retrovirus-mediated gene transduction and chemical induction. The retroviral vectors require integration into chromosomes of the somatic cell to express pluripotency genes; DNA-based vectors, such as adeno-associated virus, adenovirus and plasmid vectors do not integrate into host genome.

All hiPSCs lines, used to obtain data shown in the paragraph "establishment and phenotypic characterization of novel hiPSCs lines" (see Results), were reprogrammed from peripheral blood mononuclear cells (PBMCs) using Sendai virus carrying Yamanaka factors (Oct, SOX2, Klf4 and c-Myc) (CytoTune™-iPS 2.0 Sendai Reprogramming Kit, Invitrogen). This vector is a non-transmissible form virus that remains in host cell cytoplasm without integration into host genome. For the reprogramming with Sendai virus, PBMCs were isolated from blood of five asymptomatic patients with the R14del mutation in the phospholamban (PLN) gene. PBMCs were cultured in a 12-well plate and expanded with PBMC medium that consists of StemPro™-34 medium (Thermo Fisher Scientific) supplemented with 1% penicillin and streptomycin, 100 ng/mL SCF, 100 ng/mL FLT-3, 20 ng/mL IL-3 and 20 ng/mL IL-6 (PeproTech). The medium was refreshed every day. The day of the transduction (day 0), the cells were incubated for 24h with the Sendai virus, following the manufacturer's instructions. After three days, the reprogrammed cells were plated on vitronectin-coated 24-well plate and cultured in StemPro™-34 medium without cytokines (changed two days). At day 7 from transduction, the medium was changed to Essential 8 Medium (E8 medium, Thermo Fisher Scientific), that was then changed every two days. The emergence of cell clumps, indicating of reprogrammed cells, was observed at around 10 days from the transduction. When these clumps were grown up to form a colony, they were picked up and splitted in more wells of a Matrigel-coated 12-well plate to be expanded (Figure 20). Five/six clones from each line were selected and expanded under feeder-free conditions at 37 °C, 5% CO_2.

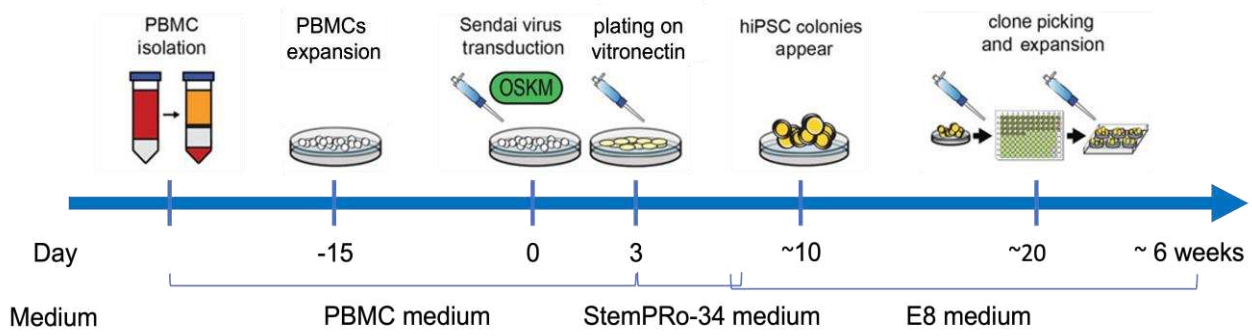

Figure 20. Schematic timeline of new hiPSCs reprogramming from Peripheral Blood Mononuclear Cells (PBMCs) using Sendai Virus. PBMCs isolated from blood are expanded for around 15 days. At day 0, PBMCs are infected with Sendai virus to introduce pluripotency genes into the cells. At day 3, reprogrammed cells are plated on vitronectin-coated well and the PBMC medium is changed with StemPro-24 medium. This is replaced after 4 days (day 7) by E8 medium, in which the reprogrammed cells (iPSCs) are maintained in culture. When new iPSCs form a colony, this one is picked up and expanded (modified from Sharma et al., 2018).

hiPS cells (WTC11, a healthy hiPSC line that was engineered by Dr. Bruce Conklin at the Gladstone Institute) were maintained in mTeSR Plus medium (Stem Cell Technolgies, Vancouver, Canada) on a Corning®Matrigel matrix (Matrigel®hESC-Qualified Matrix, Corning®, New York, NY, USA) and regularly passaged every 4–5 days.

3.2 Characterization

Immunofluorescence staining

To observes pluripotency markers (SOX2, TRA-1-60, OCT4 and SSEA4) and trilineage differentiation markers (SOX17, FOXA2, Brachyury, TBX6, OTX2 and PAX6) hiPSCs were fixed with 4% paraformaldehyde for 15 min and washed with PBS. A buffer containing 2% BSA, 2% FBS and 0.05% Triton X-100 was used for blocking and permeabilization (1 h at room temperature). Primary antibodies (Table 1) were applied at 4°C overnight and diluted in the blocking solution. The day after, secondary antibodies (Table 1) were applied for 1 h at room temperature and nuclei were stained with DAPI solution (NucBlue™ Fixed Cell Stain, DAPI nuclear DNA stain, Thermo Fisher Scientific). The cells were observed using (Invitrogen) EVOS™ FL Digital Inverted Fluorescence Microscope (Invitrogen).

		Antibody	Dilution	Cas #; Company
Primary antibodies	Pluripotency markers	*Mouse anti-SSEA4*	1:100	*A24866;* Thermo Fisher Scientific*
		Rabbit anti-OCT4	1:200	*A24867;* Thermo Fisher Scientific*
		Rat anti-SOX2	1:100	*A24759;* Thermo Fisher Scientific*
		Mouse anti-TRA-1-60	1:100	*A24868;* Thermo Fisher Scientific*
	Trilineage differentiation markers	Goat anti-FOXA2	1:50	AF2400-SP; R&D Systems
		Goat anti-SOX17	1:50	AF1924-SP; R&D Systems
		Goat anti-Brachyury	1:100	AF2085; R&D Systems
		Goat anti-TBX6	1:100	AF4744; R&D Systems
		Goat anti-OTX2	1:50	AF1979; R&D Systems
		Rabbit anti-PAX-6	1:50	42-6600; Thermo Fisher Scientific
Secondary antibodies		Anti-mouse 488	1:250	A24877; Thermo Fisher Scientific*
		Anti-rat 488	1:250	A24876; Thermo Fisher Scientific*
		Anti-rabbit 555	1:250	A24869; Thermo Fisher Scientific*
		Anti-mouse 555	1:250	A24871; Thermo Fisher Scientific*
		Anti-goat 488	1:250	A11055; Thermo Fisher Scientific

Table 1. Antibodies used for immunocytochemistry. *Pluripotent Stem Cell 4-Marker Immunocytochemistry Kit (Thermo Fisher Scientific)

Trilineage differentiation

iPSCs were differentiated into the three germ layers using STEMdiff™ Trilineage Differentiation Kit (Stem Cell Technologies). Briefly, hiPSC colonies with 70–80% confluency were chemically dissociated using ethylenediaminetetraacetic acid solution (EDTA) diluted in PBS (0.5 μM) (Sigma), suspended into culture medium with 5μM of ROCK inhibitor (Y27632) and seeded as single cells onto Matrigel-coated wells of a 24-wells plate at a cell density of 100,000 cells/well for mesoderm and 400,000 cells/well for endoderm and ectoderm (day 0). The day after (day 1) the culture medium was changed with endoderm/ectoderm/mesoderm medium and refreshed every day, as indicated in the kit datasheet. The differentiated cells were fixed on day 5 (endoderm and mesoderm) or 7 (ectoderm) for immunofluorescence staining (Figure 21).

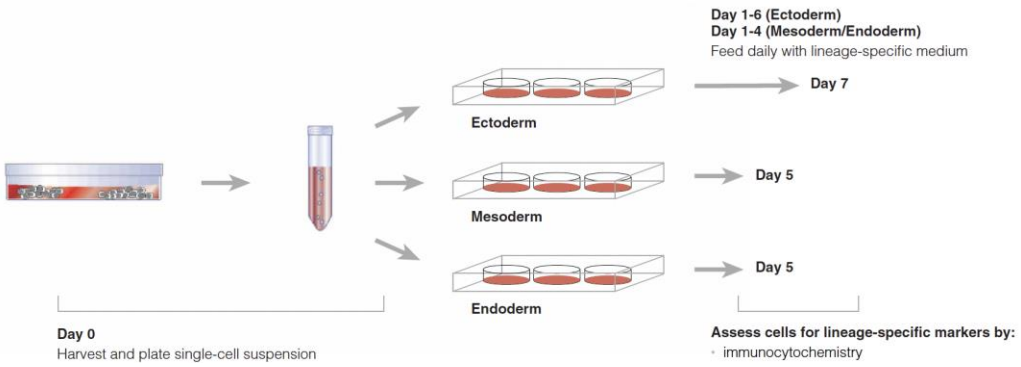

Figure 21. Schematic of STEMdiff™ Trilineage Differentiation Kit Assay. iPSCs are dissociated and seeded as single cells. After 24 h, the culture medium is changed with differentiation (endoderm/mesoderm/ectoderm) medium. After 5 days for Endoderm and Mesoderm or 7 days for Ectoderm, the cells are ready for experiments (from datasheet of STEMdiff™ Trilineage Differentiation Kit, Thermo Fisher Scientific).

RNA isolation, reverse transcription, and qPCR

RNA was extracted using Quick-RNA™ MiniPrep kit (Zymo Research) or RNeasy Plus Mini Kit (Qiagen) and transcribed to cDNA using qScript™ cDNA Synthesis Kits (QuantaBio) (cDNA 50 ng/μL). qPCR reactions were performed in duplicates using iQ™ SYBR Green supermix (Bio-Rad, 1708880) and run with the following protocol: 10 min at 95°C; 40 cycles of 15 s at 95°C and 60 s at 60°C (Mittal et al., 2022).

Karyotyping

Genomic DNA was extracted using Quick-DNA Miniprep Plus Kit (Zymo Research) or Blood & Cell Culture DNA Kit (Qiagen) for the digital karyotyping that was performed by Stem Genomics company.

STR analysis

Cells were dissociated with EDTA (0.5 μM) as single cells and spotted ($1x10^6$ cells/mL) on FTA paper, in order to perform the Short Tandem Repeat (STR) analysis by ATCC company.

3.3 Cardiac differentiation

hiPS cells (WTC11) were differentiated onto a Matrigel matrix by a monolayer-directed differentiation protocol, using the cardiac PSC Cardiomyocyte Differentiation Kit (Life Technologies, Thermo Fisher scientific, Carlsbad, CA, USA) following the manufacturer's instructions as previously described (Dell'Era et al. 2015, Pioner et al. 2019). Briefly, hiPSC colonies with 70–80% confluency were chemically dissociated using 1×TrypLE (Life Technologies, Thermo Fisher scientific, Carlsbad, CA, USA), suspended into mTeSR Plus with 5μM of ROCK inhibitor (Y27632) and seeded as single cells onto Matrigel-coated wells of a 24-wells plate at a cell density of 80,000 cells/well. At 70% of confluency (2–3 days) the medium is changed to Cardiomyocyte Differentiation Medium A (referred as day 0) to start cardiac induction. Medium A is replaced after two days with Medium B and following other 2 days with Medium C for final differentiation. hiPSC are fed every other day with Medium C until spontaneously beating monolayers appear (day 8–10). At day 12 and for further hiPSC-

cardiomyocyte (hiPSC-CM) maturation, Medium C is replaced with RPMI plus B27 supplement (Life Technologies, Thermo Fisher scientific, Carlsbad,CA, USA), which was refreshed every 2 days (Balducci et al., 2021). The cardiomyocytes were used on day 24-50 for electrophysiologic recordings (Figure 22).

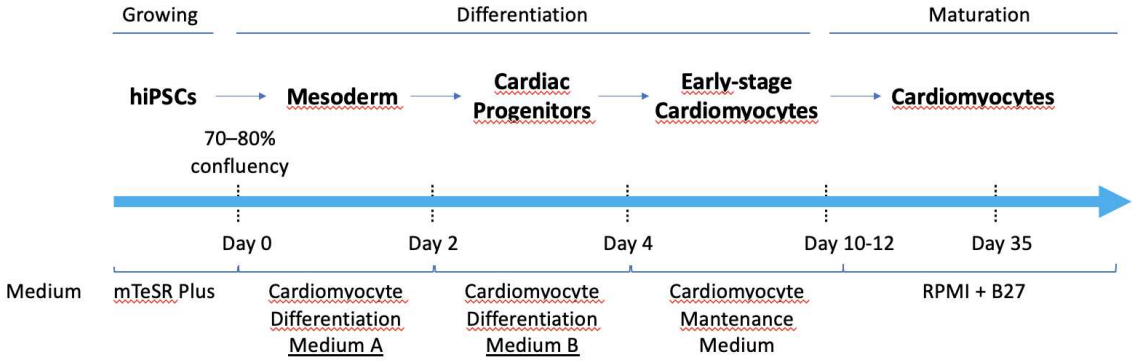

Figure 22. Monolayer-based cardiac differentiation protocol. hiPSC are differentiated into cardiomyocytes by sequential application of small molecules. Day 0 refers to Medium A. Media A, B and C mediate an induction of differentiation which recapitulates signaling pathways present during cardiogenesis: Wnt, Bone Morphogenetic Protein 4 (BPM4) and Activin A pathways induce embryonic to mesoderm germ layer transition; successive Wnt and Activin A inhibitions favor differentiation to cardiac progenitor. Around day 8, with Medium C, spontaneously beating monolayers appear, with variable percentage of primitive cardiomyocytes, that maintain in culture until electrophysiologic recordings.

4. Patch Clamp Recordings

Patch-clamp recordings were performed using the whole-cell configuration of the patch-clamp technique (Cerbai et al., 1996). Cells were placed in an experimental bath on the platform of an inverted microscope (Zeiss Axiovert 135, Germany; Nikon Diaphot TMD, Japan). Experiments were performed with a patch amplifier (Axopatch-200B series, Axon Instruments, CA) interfaced to a personal computer by means of a DAC/ACD interface (Labmaster, Tekmar, Scientific Solutions). Data were viewed on-line on a computer screen. Experimental control, data acquisition and preliminary analysis were performed by means of the integrated software package pClamp (Molecular Devices, Sunnyvale, CA, Unite States). Patch-clamp pipettes, prepared from glass capillary tubes (Harvard Apparatus Ltd, Kent, United Kingdom) by means of a two-stage horizontal puller (model P-87; Sutter Instruments, Novato, CA, United States), had a resistance of 4-6 MΩ for HEK293 cells and 3-4 MΩ for rDGR when filled with the internal solution (see “solutions”). Cells were continuously perfused by using a gravity-fed perfusion system with modified Tyrode solution (TIF) (see “solutions”) during measurements of the hyperpolarization-activated inward current (I_f). Temperature was maintained in the range of 37 ± 1°C.

Cell membrane capacitance (C_m) was measured by applying a ±10 mV pulse starting from a holding potential of -30 mV. A mono-exponential model was used to fit the current transient following the clamp protocol. Series resistance (R_s) and C_m were computed using the two equations:

$$R_s = \frac{\Delta V}{I_{peak}}$$

$$C_m = \frac{\tau}{R_S}$$

where I_{peak} is the maximum level of current (relative to the holding current) following the depolarization and τ is the time constant of the experimental current decay. Values of C_m were used to compute ionic current densities (I_f density expressed in pA/pF).
I_f was evoked from a holding potential of -20 mV to more negative voltage steps of -40 to -140/-150 mV in 10 mV increments. I_f amplitudes were calculated as the difference between the less negative value of current (or "peak") at the beginning of the test pulse and the value at steady state. Steady state values of the hyperpolarization-activated current were extrapolated by fitting the entire trace from the initial "peak" to the end of the step to a mono- (in HEK) or bi-exponential function (in DRG) with the Simplex fitting routine of the Clampfit program (pClamp ver. 11.0, Molecular Devices) and then normalized with respect to the C_m value.

The following equation shows how to determinate the conductance as a function of membrane potential:

$$G_f = \frac{I}{V_m - V_{rev}}$$

where G_f is the conductance (expressed in pS/pF) calculated at the membrane potential V_m, I the current (in pA/pF) and V_{rev} the reverse potential of the fully activated current (Cerbai et al., 1996).

Activation curves for HCN current were fitted with a Boltzmann's function:

$$y = \frac{1}{1+e^{(V-V_{1/2})/k}}$$

where V (in mV) is the test membrane potential, $V_{1/2}$ (in mV) is the fitted potential for half-maximal activation, and k (in mV) is the slope factor describing the slope of the activation curve.

In order to investigate the use-dependence of block, I_f was evoked by a series of 30 consecutive hyperpolarizing steps (-120 mV) at 1 Hz. Current amplitudes were calculated as the difference between the less negative current value and that at steady state and normalized to C_m.

Concentration-effect curves were fitted by Hill distribution:

$$y = Emax \frac{x^n}{k^n + x^n}$$

where E_{max} is the maximum effect, k corresponds to the concentration for half-maximal effect (IC_{50}), x is drug's concentration, and n is the Hill coefficient.

5. High Throughput System

MULTIPLE Optomechanical Design

As shown in Figure 23, the illumination for optical sensing and actuation is provided by a LED driver (DC20, Thorlabs, Newton, NJ, United States), that controls two high-power LEDs: the former is a LED operating at 623 nm (SOLIS 623C, Thorlabs), that provides the illumination for sensing and is followed by a band pass filter (625PB50, Omega Optical, Brattleboro, VT, United States); the latter is a LED operating at a wavelength centered at 470 nm (SOLIS-470C, Thorlabs) and provides optical actuation of ChR2. The light path for optical sensing is directed by a large-area dichroic mirror (550 DCLP, Omega Optical) mounted on a kinematic fluorescence cube (DFM2/M, Thorlabs), holding also a plane concave lens (f = 75 mm LC1315 A ML, Thorlabs) and an optical diffuser (DG20 1500, Thorlab s). The global and homogenous illumination of the multiwell plate (placed at ~12 mm distance onto a customized 3D printed holder) is achieved through the diverging lens and the diffuser. Emitted fluorescence is passed through a long pass filter (LP700, Omega Optical) and collected forward by a camera lens (f = 12 mm, MVL12M43, Thorlabs) placed in front of an sCMOS camera (ORCA Flash 4.0 V3, Hamamatsu Photonic Mamamatsu City, Japan) and operating at a frame rate of 100 Hz. The illumination, detection and sample holder block are vertically aligned on a construction rail carriage (XT95RC2/M, Thorlabs) for proper relative positioning between the blocks.

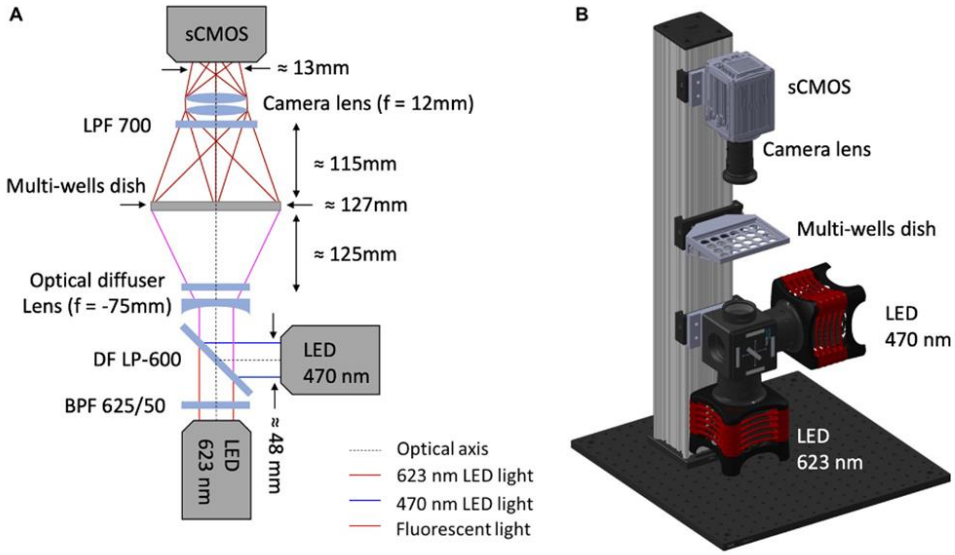

Figure 23. MULTIPLE optomechanical system design. (A) Optical scheme of MULTIPLE platform. A red LED followed by a band-pass filter (625/50 nm) with a blue LED, using a large-area dichroic beam mounted on a kinematic fluorescence cube (DFM2/M, Thorlabs), make up the excitation system of the MULTIPLE system. The light intensity, irradiating the multiwell plate, is homogenized by a divergent lens combined with an optical diffuser. The fluorescence signal is filtered with a long-pass filter and focused into a sCMOS camera sensor through a camera lens. (B) 3D mechanical scheme of MULTIPLE that consists of vertical alignment of the illumination, detection and sample holder blocks on a construction rail through drop on rail carriages (Credi *et al.*, 2021).

High Throughput Recordings

Recordings with the high-throughput screening approach was performed with MULTIPLE, which exploits high-power LED arrays to globally illuminate a multiwell plate and an sCMOS

sensor coupled with a camera lens for parallel detection of the fluorescence coming from multiple sites. hiPSC-CMs were loaded with a near-infrared fluorescent voltage-sensitive-dye (di-4-ANBDQPQ) and excited with red LED light in order to detect variations of membrane potential arising from spontaneous electrical activity. This allowed detection of repetitive membrane voltage variations that typically originated from clustered cells and propagated through the monolayer.

Initially, MULTIPLE has been tested on mouse atrial cardiomyocytes (HL-1) expressing blue light-activatable cation channels. To this aim, HL-1 cardiomyocytes were transduced with adeno-associated virus vector (AAVV) encoding mCherry-tagged ChR2(H134R) or with a lentiviral vector (LV) coding for eGFP-tagged CheRiff. The confocal imaging (Figure 24A) and flow cytometric analysis showed that the transduction with LV was more efficient than that with the AAVV, where only a subpopulation of the cells was transduced: flow cytometry resulted in the detection of 51.74% $mCherry^+$ cells and 97.52% $eGFP^+$ cells, respectively (Credi, Balducci et al., 2021). As shown in Figure 24B, MULTIPLE allows to optically induce and record action potential in HL-1 cardiomyocytes stably expressing CheRiff (stimulating channelrhodopsin activation with 30 ms blue light pulses at frequency of 1 Hz), showing a sensitivity in a significantly smaller area.

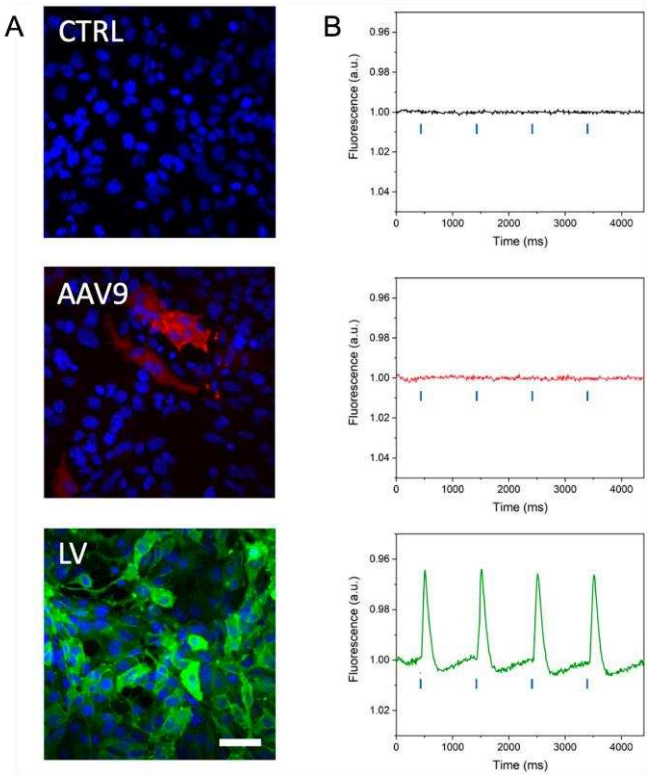

Figure 24. Optical recording of optogenetically induced APs in channelrhodopsin-expressing HL-1 cells. (A) Representative confocal microscope images of HL-1 cells wild type (negative control) and expressing blue light-activable ion channels after transduction with a commercial AAV serotype capsid 9-pseudotyped AAVV encoding mCherry-tagged ChR2 (red channel) and a custom-made LV encoding eGFP-tagged CheRiff expression (green channel). Cell nuclei were stained with DAPI (blue channel). The higher eGFP signal attests to the more efficient transduction of the HL-1 cells with the LV than with the AAVV. Scale bar = 25 mm. (B) Representative traces of optically induced APs registered in AAVV- and LV-transduced HL-1 cell layers after loading of the cells with VSD and stimulating with blue light pulses at 1 Hz (blue lines in the graph). Consistent with the higher transduction efficiency of the HL-1 cells, APs were registered only in the LV-transduced HL-1 cells. CTRL, untransduced HL-1 cells (Credi, Balducci et al., 2021).

The HT system presents a non-uniform illumination across the multiwell plate (as shown in paragraph "MULTIPLE High-Throughput System Development", Results), that does not affect the capacity of the system to also successfully track the effects of a drug (such as E-4031) on AP parameters (Credi, Balducci et al., 2021).

The HT recordings were carried out using a 24-well plate at the LEDs' maximum irradiance. A custom-developed script in LabVIEW (National Instruments, Austin, TX, United States) was used to maintain the optical sensing LED (blue LED) switched on and to trigger the camera which was programmed to record 10 s with 10-ms integration times through HC Image Live dedicated software (Hamamatsu Corporation, Sewickley, PA, United States) (Credi, Balducci et al., 2021). After images recording, a second LabVIEW script was used to select a region of interest (ROI) for each well and to extract associated traces reported in terms of percent change of fluorescence from baseline ($\Delta F/F_0$). Raw traces were processed by photobleaching correction and normalized using Fiji-ImageJ (National Institutes of Health, Bethesda, MD) and OriginLab (Northampton, MA, United States) software (Credi, Balducci et al., 2021).

6. Solutions

Extracellular solutions

Tyrode solution (mM): D-(+)-glucose 10, NaCl 140, KCl 5.4, $CaCl_2$ 1.8, $MgCl_2$ 1.2, HEPES 5, adjusted to pH 7,3 with NaOH.

Tyrode solution with low Calcium to resuspend the HEK293 cells. It was prepared as a normal Tyrode solution by changing the $CaCl_2$ concentration (300µM) and by adding Bovine Serum Albumin (1 mg/ml), then maintained at room temperature.

Modified Tyrode solution (TIF) to record I_f in HEK293 cells. It was obtained from the normal Tyrode solution supplemented with KCl 25 mM, necessary to amplify funny current.

Modified Tyrode solution (TIF) to record I_h in DRG neurons. It was obtained from the normal Tyrode solution supplemented with (mM): $BaCl_2$ 2, $MnCl_2$ 2, 4-aminopyridine 0.5, and KCl 25.

Drug solutions: PK19 (10^{-2} M), PK9 (10^{-2} M), ivabradine (iva, Sigma; 10^{-2} M), human Interleukine-6 (hIL-6, Sigma; 100 µg/mL) and tocilizumab (Toc, MedChemExpress; 10mg/mL) stock solutions were prepared in dimethylsulfoxide (DMSO; PK19 and PK9) or H_2O (iva) or PBS (hIL-6) and diluted in the different experimental solution to reach the desired final concentration.

Intracellular solutions

Pipette solution to record I_f current by Patch-Clamp recordings (mM): K-aspartate 130, Na_2-ATP 5, $MgCl_2$ 2, EGTA 11, $CaCl_2$ 5, HEPES 10, adjusted to pH 7,2 with KOH.

7. Data analysis and statistics

AP parameters (AP amplitude and duration and maximal diastolic potential) were automatically extracted from normalized traces.

For patch-clamp recordings only cells showing stable C_m and R_s were included in the analysis.

All data were analyzed using Origin 11 software (OriginLab, Northampton, MA, United States) and are expressed as mean±SEM.

Statistical analysis of data obtained from Patch-Clamp and High-Throughput recordings was performed, using GraphPad PRISM 7, by paired Student's t test and 1way ANOVA test, respectively. A p value <0.05 was taken to indicate statistical significance.

CHAPTER IV.
RESULTS

1. Two new HCN channel blockers

1.1. New zatebradine derivatives

Following the studies on verapamil-derived compounds, since 2005 at University of Florence new zatebradine analogues were identified, introducing chemical modifications in its structure. The aim was to increase the negative chronotropic activity in comparison to the other pharmacological properties, such as negative inotropism and smooth muscle relaxation (Romanelli *et al.*, 2016). Actually, the only HCN blocker clinically used as bradycardic agent, is ivabradine. However, ivabradine is not HCN isoform selective. This has led scientists to search HCN isoform-selective compounds through further structural changes. In particular, Prof. Romanelli and coworkers demonstrated that compounds, in which a 4,5 double bond was introduced in the benzazepinone ring, are more potent than their hydrogenated analogues (Romanelli *et al.*, 2005; Melchiorre *et al.*, 2010). The best substitution on the benzazepinone ring was achieved with electron-donating groups, such as methoxy, in position 8 or 7,8 (Romanelli *et al.*, 2016). Recently, the laboratory of Prof. Romanelli has synthetized two new compounds, called PK19 and PK9, obtained from zatebradine structure replacing the three-methylene chain (between the two nitrogen atoms) with a *cis*-butene group (Figure 25). These two compounds are enantiomers, in which a stereogenic center was introduced close to the exocyclic nitrogen atom in R configuration for PK19 and in S configuration for PK9. Our working hypothesis was to assess whether the use of the two enantiomers may help to disclose enantio-selective effects on HCN channels, in contrast with ivabradine, which presents an S configuration of the stereogenic center, like PK19, but does not have any HCN isoform preference.

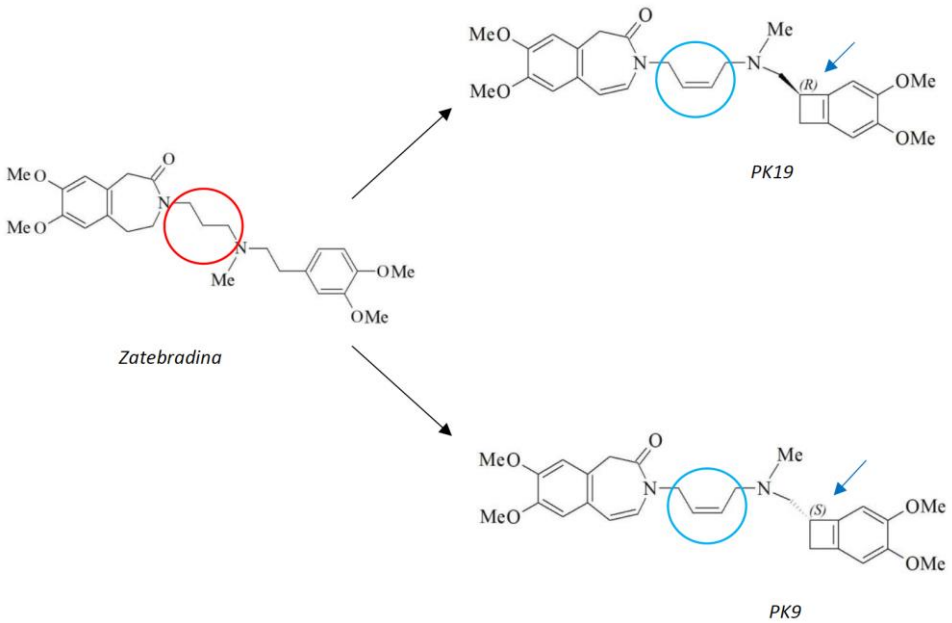

Figure 25. Structure of zatebradine and novel zatebradine derivatives PK19 and PK9. The structures of PK19 and PK9 were obtained through modifications of the zatebradine structure. The three methyl groups (in red) of the

zatebradine structure, linking two nitrogen atoms, were replaced from *cis*-butene group (in blue circle) in PK19 and PK9, in which the stereogenic centers were introduced in R and S configuration, respectively (indicated by the blue arrow). Compounds were drawn with software ACD/Chemsketch.

1.2 Effects of PK19 and PK9 on I_f of HEK293 cells

1.2.1 PK19

The effect of PK19 was characterized by measuring current (I-HCN) of single HEK293 cells expressing one of the cardiac HCN channel isoforms (HCN1, 2 or 4) by patch-clamp recordings (whole-cell configuration). PK19 was tested at several increasing concentrations (0, 0.001, 0.01, 0.1, 0.3, 1, 5, 10 and 30 μM). For each HCN isoform the mean activation curve is shown in Figure 26 in the presence and the absence of the novel compound. At physiological potential (-80 mV) and at 5 μM, PK19 showed a clear preference for HCN2 and HCN4, reducing current by 90% (n=7; p<0.01 vs respective control) and 86% (n=6; p<0.01 vs respective control) respectively. Similarly, at the same concentration (5 μM) but at maximal activation potential (-120 mV), current was reduced by 76% for I-HCN2 (n= 7; p<0.01 vs respective control) and 66% for I-HCN4 (n=6; p<0.01 vs respective control). Reduced blocking action was reported for I-HCN1 both at -80 mV (61%; n=8; p<0.01 vs respective control) and at -120 mV (44%; n=8; p<0.01 vs respective control).

Another effect of PK19 was the shift of the activation curve toward more negative hyperpolarized potential (Figure 27) that appeared to be concentration-dependent for all HCN isoforms, in particular for HCN2 and HCN4. Indeed, for I-HCN1, the potential of half-maximal activation ($V_{1/2}$), which was extrapolated by fitting current activation curves with a Boltzmann equation, was -76.15±2.61 mV in the control condition and -71.28±3.07 mV, -75.82±2.09 mV, -80.92±3.21 mV, -82.68±2.73 mV, -85.31±3.59 mV and -98.72±7.50 mV at 0.1, 0.3, 1, 5, 10 e 30 μM concentration (p<0.001 control vs 30 μM), respectively. Similarly, $V_{1/2}$ was also leftward shifted for I-HCN4 from -92.71±1.97 mV in control conditions to more negative values with PK19 (0.001 μM: -98.96±3.50 mV; 0.01μM: -102.51±2.51 mV; 0.1 μM: -100.68±2.73 mV; 0.3 μM: -101.27±2.91 mV; 1 μM: -102.97±2.76 mV; 5 μM: -106.79±4.08 mV; 10 μM: -112.52±5.87 mV; 30 μM: -103.16±3.77 mV) (p<0.01 control vs 5 μM; p<0.005 control vs 10 μM). Finally, for I-HCN2, $V_{1/2}$ shifted from -95.31±1.28 mV to -99.32±3.25 mV, -100.24±3.03 mV, -99.16±2.52 mV, -98.98±2.61 mV, -101.84±3.38 mV, -104.65±3.28 mV, -115.34±3.29 mV and -96.95±16.54 mV at 0, 0.001, 0.01, 0.1, 0.3, 1, 5, 10 e 30 μM (p<0.05 control vs 10 μM), respectively. As expected, the $V_{1/2}$ values of the three HCN isoforms are variable (see "voltage-dependent activation"); shift of $V_{1/2}$ to more hyperpolarized potentials at increasing compound concentrations could represent the result of alteration(s) of channel biophysical properties induced by the compound.

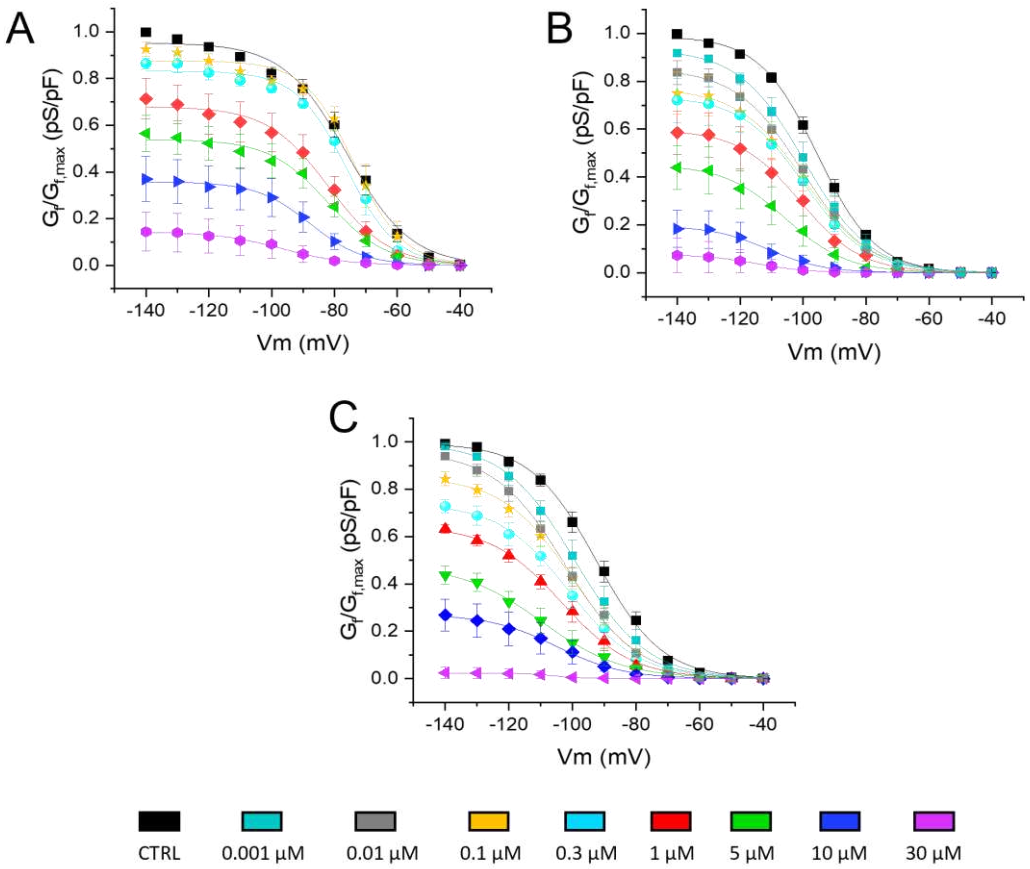

Figure 26. Effects of PK19 on I-HCNs mean activation curves obtained from HEK cells expressing single HCN isoforms. Plots report I-HCN current conductances before and after PK19 application at several concentrations (0, 0.1, 0.3, 1, 5, 10 and 30 µM for I-HCN1 (A); 0, 0.001, 0.01, 0.1, 0.3, 1, 5, 10 and 30 µM for I-HCN2 (B) and I-HCN4 (C)). I-HCN conductances were normalized with respect to maximal conductance ($G_f/G_{f,max}$) and plotted versus test membrane potential (mV) used to evoke current.

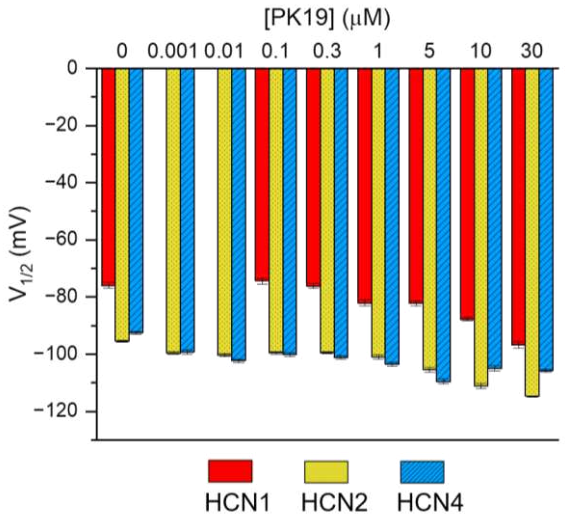

Figure 27. Effects of PK19 on I-HCNs activation mid potential obtained from HEK cells expressing single HCN isoforms. Bar graph (red, HCN1; yellow, HCN2 and blue, HCN4) represent voltage of half-maximal activation ($V_{1/2}$) for each I-HCN activation curve in the absence and the presence of PK19 (Balducci et al., 2021). HCN1, n=4-9; HCN2, n=4-12; HCN4 n=5-11.

Potency of PK19

PK19 was tested on I-HCN1 at seven concentrations (0, 0.1, 0.3, 1, 5, 10 and 30 μM) and on I-HCN2 and I-HCN4 at nine concentrations (0, 0.001, 0.01, 0.1, 0.3, 1, 5, 10 and 30 μM). This allowed to obtain a concentration-effect curve for each isoform. Residual current was normalized to maximal current ($I_{HCN}/I_{HCN,max}$) and plotted versus log_{10} of drug concentration. Fitting of experimental data by Hill equation (see "Materials and Methods") allowed to estimate half-maximal inhibitory concentration (IC_{50}) of PK19, which is inversely related to its potency. For HCN1, average IC_{50} values were 1.81±0.57 μM and 4.63±1.28 μM at -80 mV and -120 mV, respectively (Figure 28A). Instead, the IC_{50} values were 0.32±0.08 μM and 0.12±0.02 μM at -80 mV and 1.21±0.41 μM and 0.87±0.71 μM at -120 mV for HCN2 (Figure 27B) and HCN4 (Figure 27C), respectively. Therefore, average IC_{50} values showed that rank order of potency of PK19 is HCN4>HCN2>HCN1 at -80 and -120 mV.

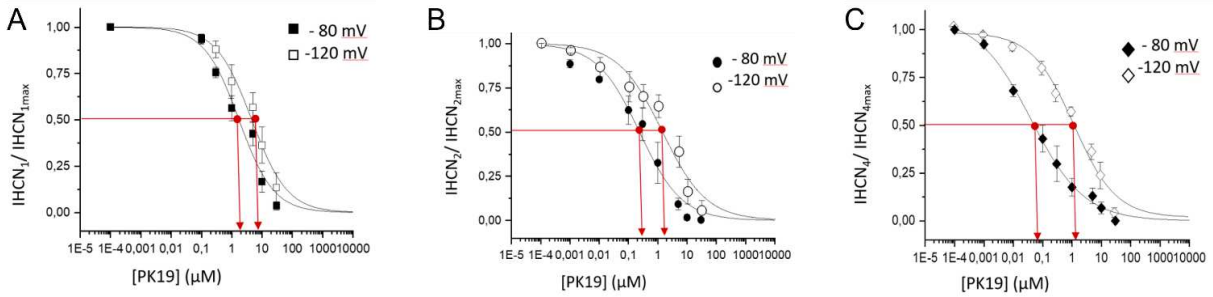

Figure 28. Concentration-effect curves of PK19 for I-HCNs obtained from HEK cells expressing single HCN isoforms. The inhibitory effect of PK19 was tested at 0, 0.1, 0.3, 1, 5, 10 and 30 μM concentrations on I-HCN1 (A, n=9) and at 0, 0.001, 0.01, 0.1, 0.3, 1, 5, 10 and 30 μM concentrations on I-HCN2 (B, n=8) and I-HCN4 (C, n=6). Concentration-effect curves of PK19 were calculated at -80 mV and -120 mV and both reported in the same graph for each channel isoform (modified from Balducci *et al.*, 2021).

Use- and state-dependency of PK19 effect

Bucchi and coworkers (2002) demonstrated that ivabradine is an open f-channel blocker that binds to the channel in the open state at hyperpolarized potentials. The ivabradine block develops preferentially when channel deactivates at depolarized voltages. Repetitive opening/closing cycles promote an efficient block. For this reason, ivabradine is defined as a strong "use-dependence" blocker of HCN channels (Bucchi *et al*., 2002). Despite ivabradine blocks all channel isoforms, the effect differs for the different isoforms. Indeed, while the block of mHCN1 requires a close configuration, that of hHCN4 occurs in the open state (Bucchi *et al.*, 2006). On the bases of these characteristics, use and state dependence of new zatebradine analogues were investigated. To this aim, a series of thirty consecutive activating steps at -120 mV (1 Hz) were used to evoke I-HCNs in control conditions. They were then followed by 2 minutes rest, in which channels were maintained at resting state (-30 mV) but in the presence of PK19 (30 μM). Stimulation protocol was then resumed, while exposure to the drug was maintained. I-HCNs were stable in control condition; after the rest, I-HCN2 and I-HCN4 showed amplitudes similar to those measured in the absence of PK19. Thereafter, a progressive inhibition appeared during the repetitive stimulation, indicating that the PK19 blockade of HCN2 and HCN4 was only use-dependent and not state-dependent. At the end of the protocol, the reduction of I-HCN2 and I-HCN4 was 73% (68% and 78%, n=2) and 55% (n=3), respectively. Conversely, for HCN1 isoform, when stimulation protocol was resumed after 2 minutes rest in

the presence of the inhibitor, a reduction of current was markedly detected compared to the current in control condition, that at the end of the protocol was reduced by 90% and 85% (n=2). This means that PK19 blockade of I-HCN1 is mainly state-dependent and only marginally use-dependent (Figure 29).

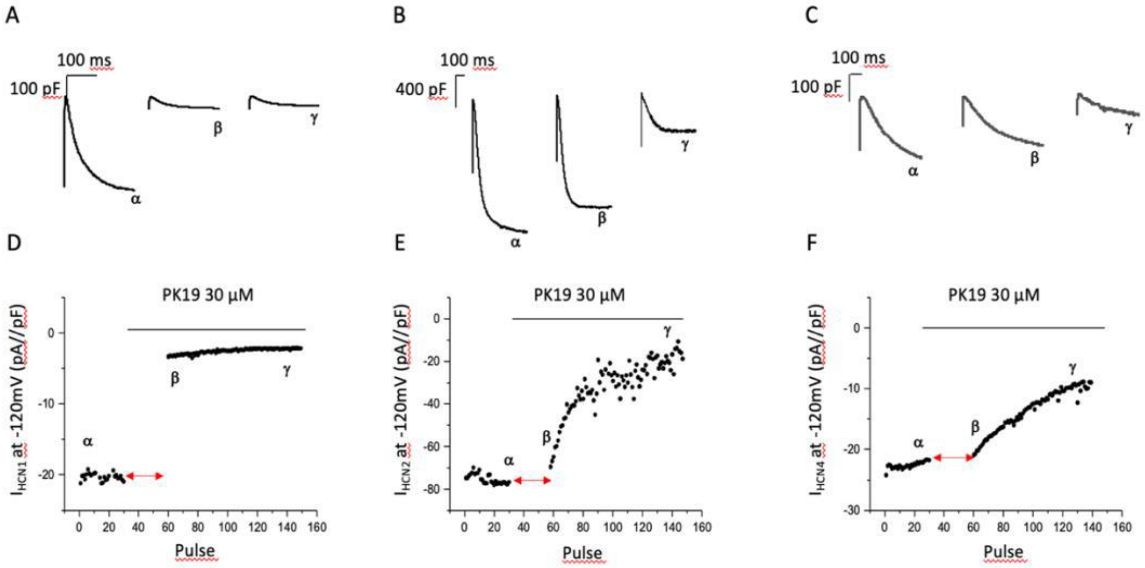

Figure 29. Use- and state-dependence of PK19 blockade of I-HCNs. Representative traces and time curses of maximal I-HCN1 (A and D, n=2), I-HCN2 (B and E, n=2) and I-HCN4 (C and F, n=3) evoked by a series of 30 consecutive hyperpolarizing steps at -120 mV in the absence (α) and in the presence (β, γ) of PK19 (30 µM). Blocker was perfused both during (red arrows) and after the two minutes stop of stimulation (Balducci *et al.*, 2021).

1.2.2 PK9

PK9 was tested at 0, 0.1, 0.3, 1, 5, 10, and 30 µM concentrations on I-HCN1 and I-HCN2 isoforms; while only 0, 0.1, 0.3, 1, 5 µM concentrations were tested on I-HCN4. Mean activation curves before and after PK9 perfusion are shown in Figure 30. At –80 mV and 5 µM, PK9 completely abrogated I-HCN2 conductance (99.94%; n=6; p<0.005), while I-HCN1 and I-HCN4 were reduced by 70% (n=5) and 65% (n= 6), respectively. Differently, at -120 mV, I-HCN2 was inhibited by 75% (n=6; p<0.0001), and I-HCN1 and I-HCN4 just by 42% (n= 5; p<0.0005) and 51% (n= 6; p<0.005), respectively.

PK9 induced a leftward shift of all I-HCNs activation curves (Figure 31), in a concentration-dependent manner, suggesting that similarly to PK19 it could affect the biophysical properties of HCN channels. For I-HCN1, $V_{1/2}$ value was -74.09±0.53 mV in the absence of PK9 and between -83.09±0.44 and -95.91±2.05 during the exposure to the inhibitor (0.1 µM: -86.66±0.29 mV; 0.3 µM: -89.35±0.36 mV; 1 µM: -83.09±0.44 mV; 5 µM: -83.19±0.35 mV; 10 µM: -91.35±0.55 mV; 30 µM: -95.91±2.05 mV). $V_{1/2}$ values of I-HCN2 were shifted from -86.72±1.06 mV in control condition to -90.75±1 mV, -93.64±0.93 mV, -95.47±1.39 mV, -104.33±1.89 mV, -103.87±3.28 mV and -94.20±3.05 mV at 0.1, 0.3, 1, 5, 10, and 30 µM concentrations (p<0.01 control vs 5 µM; p<0.005 control vs 10; p<0.001 control vs and 30 µM). Finally, $V_{1/2}$ values of I-HCN4 were shifted from -87.35±1.18 mV in control condition to -

102.33±0.74 mV, -104.78±0.85 mV, -107.39±0.92 mV, -105.14±1.22 mV at 0.1, 0.3, 1, 5, 10, and 30 μM concentrations.

Further experiments are required to confirm these data on I-HCN1 and I-HCN4.

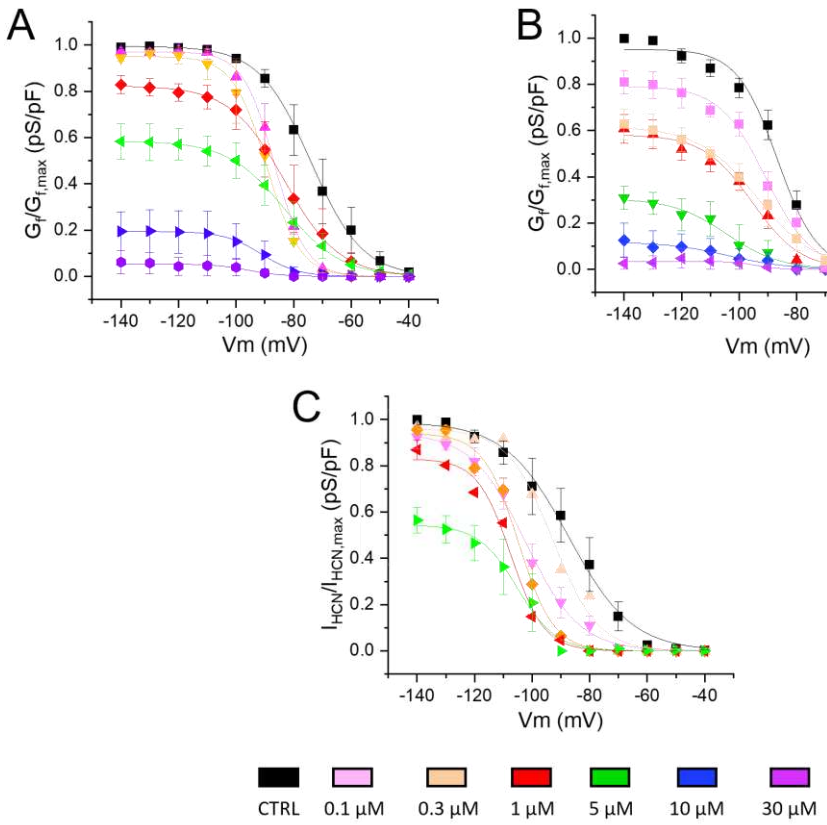

Figure 30. Effect of PK9 on I-HCN activation curve obtained from HEK cells expressing single HCN isoforms. Plots (A, HCN1; C, HCN2; E, HCN4) report I-HCN conductances, normalized with respect to I-HCN maximal conductance ($G_f/G_{f,max}$) versus test membrane potential (mV) used to evoke current in the absence and the presence of PK9 (0.1, 0.3, 1, 5, 10, and 30 μM). HCN1 n=2-5; HCN2 n=6; HCN4 n=2-5.

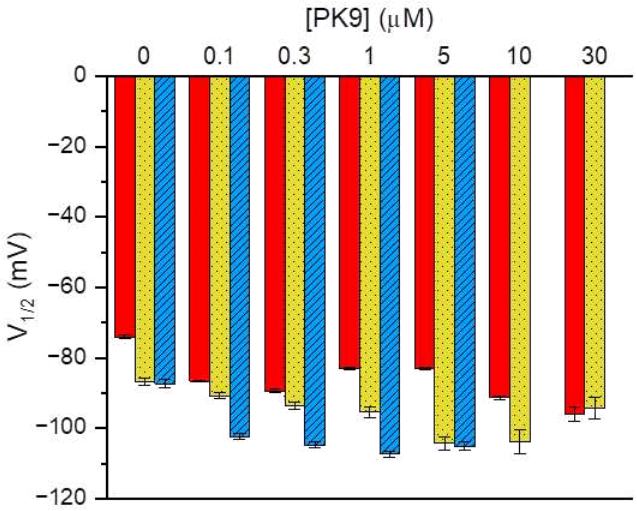

Figure 31. Effect of PK9 on I-HCN activation mid potential obtained from HEK cells expressing single HCN isoforms. Bar graphs (B, HCN1; D, HCN2; F, HCN4) represent voltage of half-maximal activation ($V_{1/2}$) of each activation curve before and after PK9 application. HCN1 n=2-5; HCN2 n=6; HCN4 n=2-5.

Potency of PK9

PK9 was tested at increasing concentrations (0, 0.1, 0.3, 1, 5, 10, and 30 μM) on HEK293 cells expressing one of the HCN channels isoforms to calculate compound potency. At physiological potential (-80 mV), PK9 was more potent on I-HCN4 and I-HCN2 (IC_{50}: 0.11±0.04 μM and 0.24±0.12 μM, respectively) than on I-HCN1 (IC_{50}: 1.64±0.86 μM). Differently, at more hyperpolarized potential (-120 mV), IC_{50} value was lower for I-HCN2 (1.50±0.41 μM) than for I-HCN4 (2.18±1.24 μM). However, PK9 was less potent on I-HCN1 also at -120 mV (IC_{50}: 5.31±1.12 μM) (Figure 32).

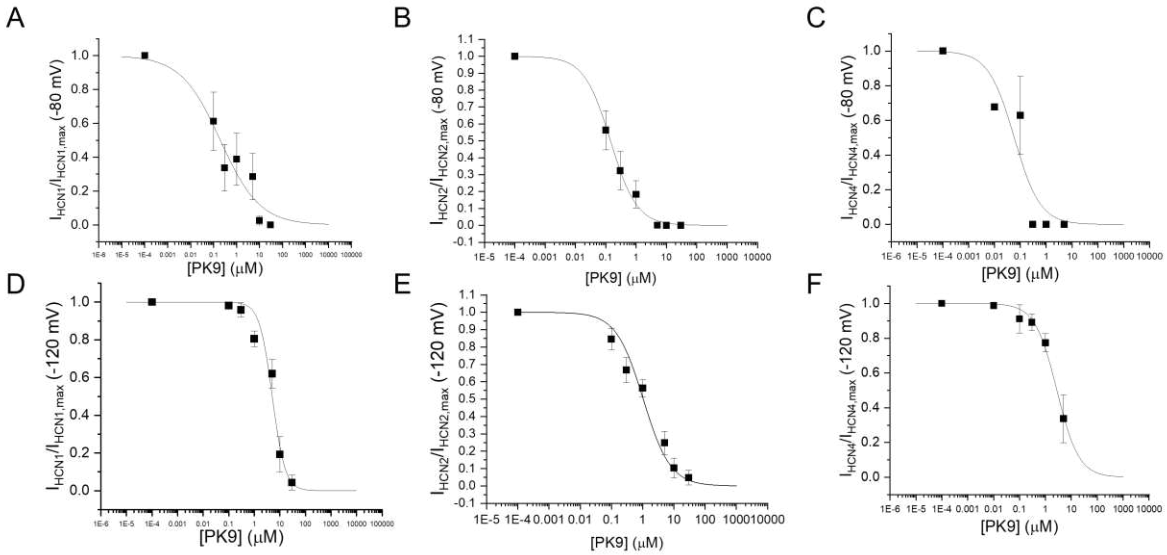

Figure 32. Concentration-effect curves of PK9 on I-HCNs obtained from HEK cells expressing single HCN isoforms. The inhibitory effect of PK9 was tested at 0, 0.1, 0.3, 1, 5, 10, and 30 μM concentrations. Graphs represent concentration-effect curves calculated for normalized I-HCN1 (n=4); I-HCN2 (n=6) and I-HCN4 (n=3) evoked at -80 mV (panels A, B and C) and at -120 mV (panels D, E and F) and fitted by Hill equation. At variance with PK19, graphs obtained at -80 and -120 mV are not overlapped because of data paucity.

Use- and state-dependency of PK9 effect

Use- and state-dependency of the PK9 were studied on each HCN isoforms, using the same experimental protocol described in the previous section. After the rest (two minutes), PK9 blocked I-HCNs when HCN channels are in the open state: when the stimulation was resumed, the amplitudes of I-HCNs were similar to those measured in the absence of PK9; subsequently, a progressive inhibition appeared during the repetitive stimulation (Figure 33). This data demonstrated that blockade of PK9 for I-HCNs is only use-dependent and not state-dependent.

Like its enantiomer, at the end of the high frequency stimulation PK9 shows higher effect on the open state of HCN1, reducing the current density by 78% and 46% (n=2); instead, I-HCN4 was reduced by 59% (57% and 60%, n=2), while I-HCN2 only by 27% (n=1).

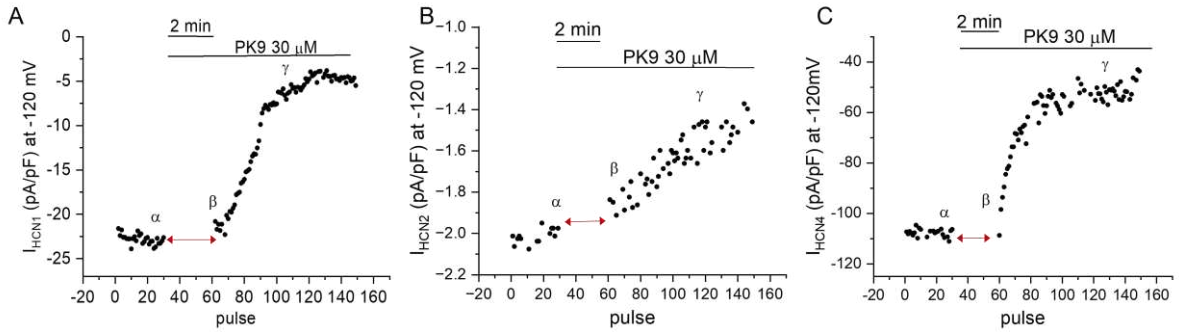

Figure 33. Use- and state-dependence of PK9 blockade of I-HCNs. Time curses of maximal I-HCN1 (A, n=1), I-HCN2 (B, n=1) and I-HCN4 (C, n=2) evoked by a series of thirty consecutive hyperpolarizing steps at -120 mV in the absence (α) and in the presence (β, γ) of PK9 (30 μM). The red arrows indicate the 2 minutes without stimulation but in the presence of the PK9.

1.3 Effects of PK19 and PK9 on I_h current of rat Dorsal Root Ganglia neurons

At variance with HEK293 cells expressing heterologous and homomeric HCN channels, rat Dorsal Root Ganglia (rDRG) neurons are used as physiological model to measure I_h. In fact, rDRG neurons express HCN1, HCN2 and HCN4 isoforms, that can assemble into functional homo- and/or hetero-tetramers. Importantly, recent experimental evidence obtained with this model have demonstrated that HCN channels are involved in the development of neuropathic pain (Dini *et al.*, 2018) and that their blockade obtained by zatebradine derivatives (MEL55A and MEL57A) is effective to control pain perception (Dini *et al.*, 2018; Resta *et al.*, 2018).

1.3.1 PK19

Effect of PK19 was tested at seven concentrations (0, 0.01, 0.1, 1, 5, 10 e 30 μM) on rDRG neurons using whole-cell patch-clamp recordings of I_h. Figure 34 shows the effect of increasing PK19 concentration on average I_h activation curves and kinetics. PK19 reduced I_h by 88% at 5 μM concentration (n=8; $p<0.05$ vs respective control) and at -80 mV and by 55% at the same concentration and at -120 mV (n=8; $p<0.05$ vs respective control).

PK19 shifted I_h activation curve toward more hyperpolarized potentials: in fact $V_{1/2}$ values, were -85.73±0.87 mV in control conditions and -87.92±0.98 mV (n=5), -90.08±1.18 mV (n=5), -92.9±1.21 mV (n=5), -94±0.61 mV (n=8), -93.70±0.60 mV (n=4), -110.6±1.22 mV (n=4) ($p<0.0005$ CTR vs 30 μM) at 0.01, 0.1, 1, 5, 10 and 30 μM, respectively (Figure 34). This result, as observed for currents measured on HEK cells expressing single channel isoforms, suggests that PK19 may change the biophysical properties of I_h, at least at high concentrations. Moreover, Figure 34C showed that the compound tended to slow activation kinetics, but without significant variations.

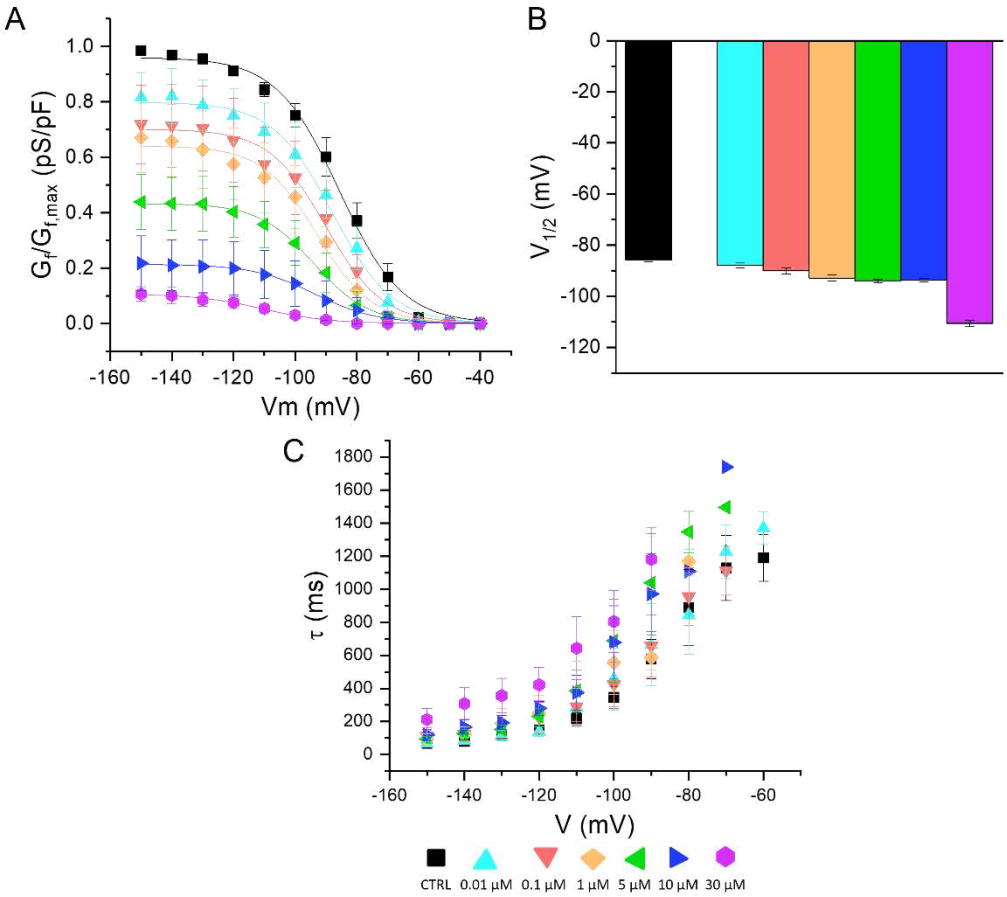

Figure 34. Effect of PK19 on I_h activation curve and time constant of activation in rDRG neurons. (A) Average activation curves of I_h recorded on DRG neurons in the absence and the presence of PK19 at several concentrations (0.01, 0.1, 1, 5, 10 e 30 µM). Plots report current conductances, normalized with respect to maximal conductance ($G_f/G_{f,max}$), versus test membrane potential (mV) used to evoke the current. (B) Bar graphs represent the voltage of half-maximal activation ($V_{1/2}$) for each current activation curve without or with PK19 (0, 0.01, 0.1, 1, 5, 10 e 30 µM). (C) Time constants (τ) of I_h activation in the presence or the absence of the inhibitor. n=5-9; ***p < 0.005 CTR vs PK19 10 µM; ^^p < 0.05 CTR vs PK 5, 30 µM; §p < 0.0005 CTR vs 30 µM.

Potency of PK19

Potency of PK19 was calculated by fitting concentration-effect data of normalized current by Hill equation, as previously described (see "materials and methods"). At physiological potential (-80 mV), PK19 appeared more potent (IC_{50}: 1.52±1.09 µM) than at -120 mV (IC_{50}: 5.15±1.48 µM) (Figure 35).

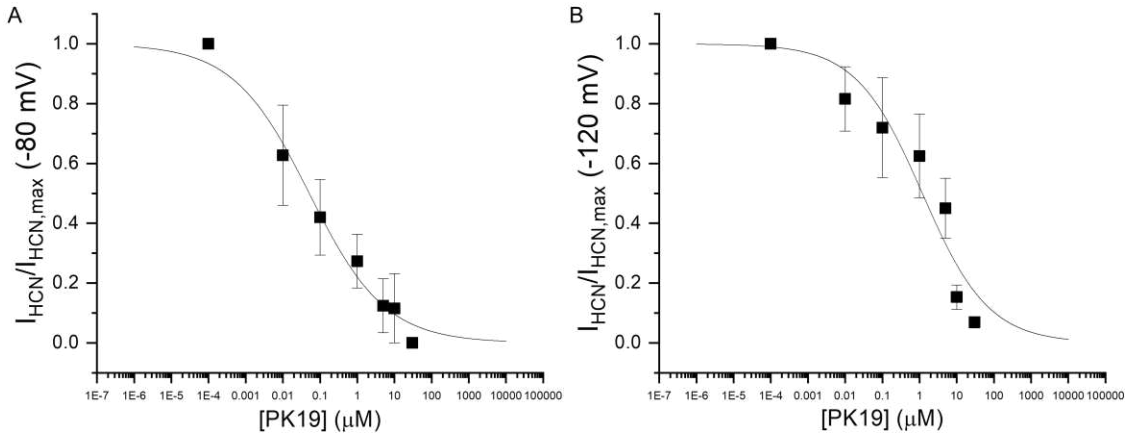

Figure 35. Concentration-effect curves of PK19 on I_h of rDRG neurons. The potency of PK19 was determined measuring current at -80 mV (A) and at -120 mV (B) with eight different PK19 concentrations (0, 0.01, 0.1, 1, 5, 10 and 30 μM). This allowed to fit concentration-effect curves by Hill equations that were used to calculate IC_{50}.

Use- and state-dependency of PK19 on I_h of rDRG neurons

In order to study use- and state-dependency of the new compound on I_h current of rDRG neurons, we used the same experimental protocol described in the previous sections. Results showed that PK19 blocked I_h when HCN channels are both in the open and the close state, thus demonstrating blockade is both use- and state-dependent (Figure 36). Overall, current blockade of the channel in the open state was 78% (n=3).

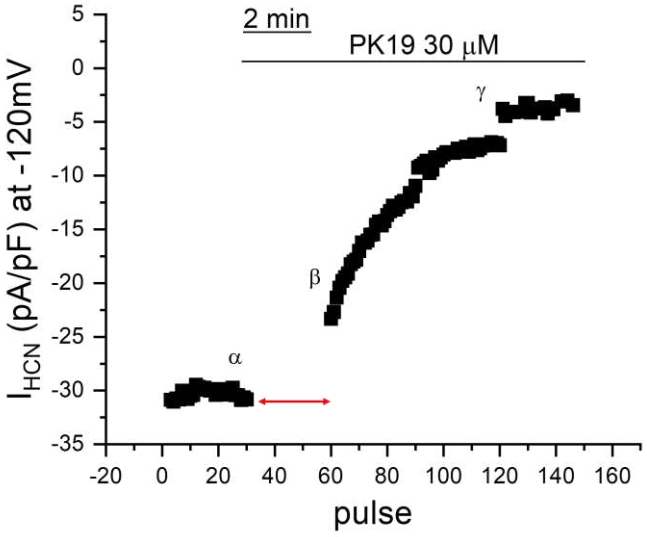

Figure 36. Use- and state-dependency of PK19 on I_h in rDRG neurons. Time curse of I_h evoked by a series of thirty consecutive steps at -120 mV in the absence (α) and in the presence (β, γ) of 30 μM PK19. The red arrow indicates the time interval (2 minutes) without stimulation but in the presence of the inhibitor. (n=3).

1.3.2 PK9

Figure 37 shows the typical activation curves of I_h evoked by increasingly hyperpolarizing steps in the absence and the presence of the S-enantiomer PK9 (0.01, 0.1, 1, 5, 10 e 30 μM). In particular, PK9 reduced I_h in a concentration-dependent manner. In presence of 5 μM PK9, reduction of I_h was of 92% (n=6; p<0.05 vs respective control) at -80 mV and of 70% at -120 mV (n=6; p<0.05 vs respective control). The activation curves were shifted to more hyperpolarized values ($V_{1/2}$ values from -91.83±1.02 mV in control condition to -95.95±0.98 mV, -97.03±0.68 mV, -95.20±0.86 mV, -98±1.02 mV, -100.86±1.02 mV and -100.81±1.93 mV in the presence of 0, 0.01, 0.1, 1, 5, 10 and 30 μM PK9, respectively; p<0.0001 CTR vs 30 μM). No significant variation was observed for the activation kinetics, similarly to what has been observed with the enantiomer PK19.

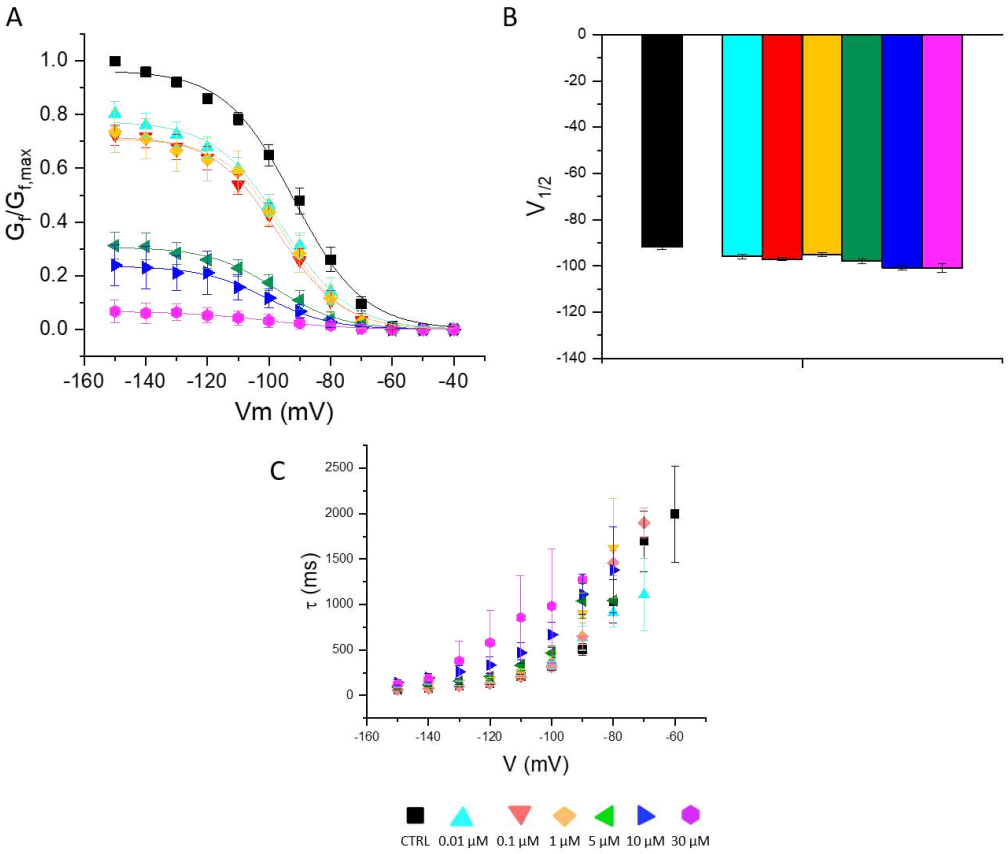

Figure 37. Effect of PK9 on I_h activation curve and time constant of activation on rDRG neurons. PK19 was tested at 0.01, 0.1, 1, 5, 10 e 30 μM. (A) Average activation curves of I_h in the absence and the presence of PK19. Plots report I-HCN conductances, normalized with respect to maximal conductance ($G_f/G_{f,max}$) and plotted versus test membrane potential (mV) used to evoke the current. (B) Bar graphs represent the voltages of half-maximal activation ($V_{1/2}$) for each current activation curve at 0, 0.01, 0.1, 1, 5, 10 e 30 μM PK19. (C) Time constants (τ) of I_h activation in the presence or absence of the inhibitor. n=4-10; °°°p<0.01 CTR vs PK19 0.01 μM; ***p<0.01 CTR vs PK19 0.1 μM; ^^^p<0.01 CTR vs PK19 1 μM; §§p<0.05 CTR vs PK 5, 10, 30 μM; *p<0.005 CTR vs 30 μM.

Potency of PK9

In order to study the potency of PK9 on I_h of rDRG neurons, the drug was tested at the concentrations described above (0, 0.01, 0.1, 1, 5, 10 and 30 µM). The IC_{50} values, extrapolated by the concentration-effect curves obtained by Hill equation fitting (Figure 38), were 0.36±0.17 µM at -80 mV and 2.20±1.20 µM at -120 mV.

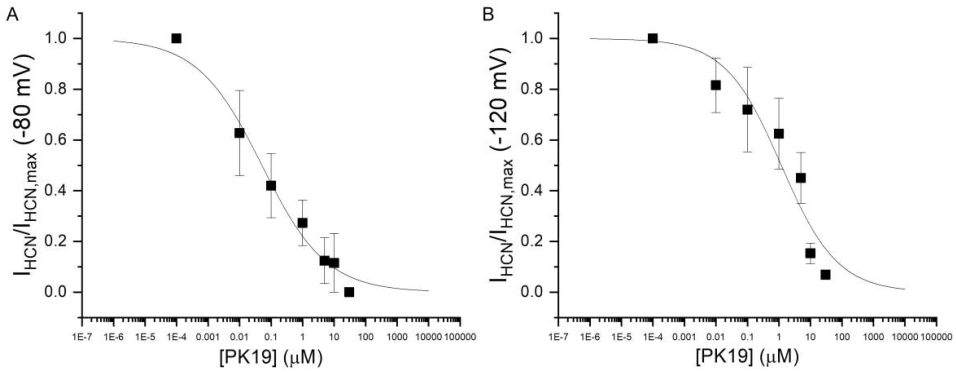

Figure 38. Concentration-effect curves of PK9 for I_h of rDRG neurons at -80 and -120 mV. Concentration-effect curves were obtained by testing the inhibitory effect of PK9 at several concentrations (0, 0.01, 0.1, 1, 5, 10 and 30 µM) on I_h current evoked at -80 mV (A) and -120 mV (B). n=8.

Use- and state-dependency of PK9

Using the same use- and state-dependency protocol described above for PK19, we studied PK9 blockade on I_h measured on rDRG neurons. Similarly to PK19, PK9 showed to interact with HCN channels in both the closed and open states. The inhibition was particularly fast during channel stimulation (Figure 39). This result indicates that in rDRG neurons, PK9 blockade of HCN current is state- and -use-dependent, showing similar properties compared to its enantiomer PK19. However, the effect of PK9 at the end of the use-dependency protocol on I_h was found to be greater (93%; n=3) compared to PK19.

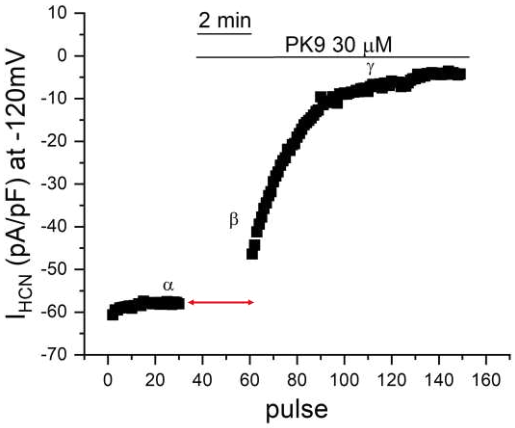

Figure 39. Use- and state-dependency of PK9 on I_h of rDRGs. A series of 30 consecutive hyperpolarizing steps at -120mV was used to evoked I_h in the absence (α) and in the presence (β, γ) of 30 µM PK9. After current stabilization in control conditions, the stimulation was stopped for 2 minutes (red arrow) and the perfusion with the inhibitor was started. After this time interval, PK9 perfusion continued, and the stimulation was resumed. n=3.

1.4 Effects of PK19 and PK9 on spontaneous action potentials of human cardiomyocytes differentiated from pluripotent stem cells

The new zatebradine analogues were also tested on a different physiological model, i.e. cardiomyocyte monolayers differentiated from human induced Pluripotent Stem Cells (hiPSC-CMs). hiPSC-CMs are biologically relevant as *in vitro* model of cardiac pacemakers, since they are able to develop spontaneous firing activity around day 8 of differentiation (see "materials and methods"), which maintains main properties of native human pacemaker centers. Some of these properties comprise the regulatory pathways controlled by the homo- and hetero-tetrameric HCN1, 2 and 4 channel activity and the response to cardiac rate-limiting drugs (Blazeski *et al.*, 2012; Horvath *et al.*, 2018; Karakikes *et al.*, 2015; Lemoine *et al.*, 2017; Lemoine *et al.*, 2018; Mandel *et al.*, 2012; Balducci *et al.*, 2021).

To perform the experiments with PK19 and PK9, I used the MULTIPLE High Throughput system, developed by Credi, Balducci and coworkers (2021). Using this approach, spontaneous electrical activity of hiPSC-CMs (at day 24-50 of maturation) was recorded by optical detection of a fluorescent red-shifted voltage-sensitive dye (di 4 ANBDQ PQ).

1.4.1. MULTIPLE High-Throughput System Development

In the last decades, optical techniques for electrophysiological studies represent a reference method for preclinical drug screening and cardiotoxicity testing (Dunlop et al., 2008). For this reason, several fast investigation platforms were developed, able to employ optical technologies to control and monitor features of action potentials both in single cells and cellular monolayers located in a multi-well plate (Klimas et al., 2016; Credi et al., 2021). Generally, these systems employ automated fluorescence microscopes to analyze single wells with high-speed investigation capacities. Recently, Credi, Balducci and coworkers (2021) developed a new optical system (MULTIPLE) able to illuminate globally a culture plate though high-power LED arrays and to detect parallelly the fluorescence coming from multiple wells, thanks to an sCMOS sensor.

Detection performance of MULTIPLE

The configuration of MULTIPLE, as described in "MULTIPLE Optomechanical Design" ("Materials and methods"), allows a maximum light intensity on the multiwell plane along the optical axis of the order of 30 and 60 mW/cm^2 for blue and red light, respectively (Credi *et al.*, 2021). However, this basic illumination scheme causes a radial intensity decrease with consequent non-uniform illumination across the multiwell plate (Figure 40). This leads to an intensity reduction below 50% across the 24-well plate for both light sources. This heterogeneity of the lights is not a critical issue for red light intensity, since potentiometric

optical recordings imply normalized fluorescent signals, but it could introduce inter well differences in the electrical response upon optical stimulation regarding the blue light.

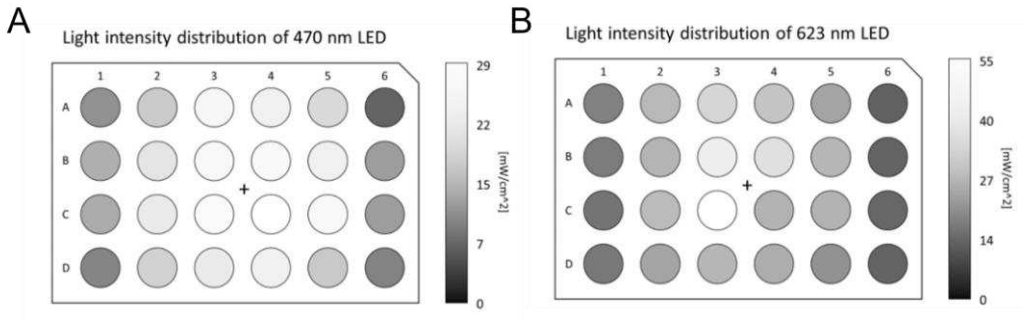

Figure 40. Illumination and detection performances of MULTIPLE. Light intensity distribution across the whole 24-well plate for blue (A) and red (B) LED light, using maximum LED power. The intensity of both LEDs radially decreases moving away from the optical axis causing a more than 50% reduction for the outermost wells (modified from Credi *et al.*, 2021).

Detection and Modulation of Spontaneous action potentials of hiPSC-CMs

This simple and cheap system use optical detection of action potential (AP) (Credi et al., 2021). In this way, MULTIPLE is able to identify spontaneous and/or optically-stimulated action potentials from spontaneously beating cells (such as hiPSC-CMs) or optically engineered cells (such as channelrhodopsin-expressing HL-1 cells). The APs detection takes place using a red-shifted voltage-sensitive fluorescent dye (di-4-ANBDQPQ), with which the cells are incubated for 10 minutes at 37°C. The dye is excited with red LED light in order to detect variations of membrane potential arising from spontaneous or induced electrical activity.

MULTIPLE platform was previously tested and characterized using VSD-loaded HL-1 cells stably expressing the blue light-activatable ion channel CheRiff (Credi et al., 2021) (see "materials and methods"). This phase of research enabled us to easily detect APs from monolayer of hiPSC-CMs at day 30 of maturation. hiPSC-CMs were loaded with di-4-ANBDQPQ and excited with red LED light, in order to detect membrane voltage variations arising from their spontaneous activity, maintaining the cells at 37°C. In this way, it was possible to record the propagation of AP, originating from clustered cells and propagating throughout the monolayer (Figure 41A). This experimental system was further exploited to test the activity of two negative modulators of the pacemaker activity, ivabradine (iva) and carbachol (CCh). While ivabradine effect pass through HCN channel direct blockade, the effect of carbachol is mediated by muscarinic receptor activation that reduces intracellular cyclic-AMP and thus HCN channel activity, as well as those of voltage activated calcium channels. We used the MULTIPLE system to detect the pharmacological responses of hiPSC-CM monolayers. Both iva and CCh induced a reduction of the spontaneous AP frequency, demonstrating that the biological system behaves as expected for a physiological pacemaker and the recording platform is a convenient approach to study this function (Credi *et al.*, 2021) (Figure 41B and C).

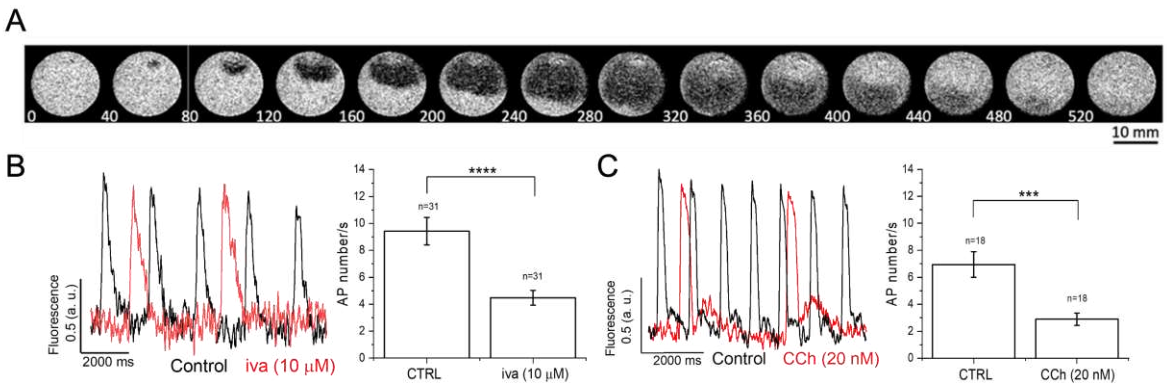

Figure 41. Effect of ivabradine and carbachol on spontaneously beating hiPSC-CMs. (A) Representative fluorescence imaging of spontaneous AP propagation in a hiPSC-CM monolayer (520 ms recording). Spontaneous AP traces recorded in hiPSC-CM monolayer (around day 30 of maturation) in the absence (black lines, CTR) and presence (red lines) of ivabradine (iva, 10 μM; B) or carbachol (CCh, 20 nM; C). AP number/seconds (mean±standard error) in absence and in the presence of respective drugs are represented in the histograms. ****p<0.0001 CTRL vs iva (10 μM); ***p<0.001 CTRL vs CCh (20 nM) (modified from Credi *et al.*, 2021).

1.4.2. Effect of the new HCN blockers on spontaneous AP frequency of hiPSC-CMs

By means of MULTIPLE high-throughput (HT) system, PK9 and PK19 were also tested on spontaneously beating hiPSC-CMs monolayers at day 24-50 of maturation. The HT recordings were performed by optical detection of the voltage-sensitive dye di-4-ANBDQPQ and applying in a cumulative manner the two new compounds at several concentrations (0, 0.001, 0.01, 0.1, 1, 10 and 30 μM). Ivabradine was used as reference compound. As shown in Figure 42, spontaneous AP firing rate decreased in a concentration-dependent manner for both enantiomers. Similarly to HEK293 cells and rDRG neurons, IC_{50} values were calculated from the concentration-effect curves obtained for PK19, PK9 and ivabradine, using Hill equation fitting. PK19 and PK9 resulted more potent than ivabradine, since IC_{50} values were 0.14±0.01 μM, 0.21±0.08 μM and 8.86±1.16 μM, respectively.

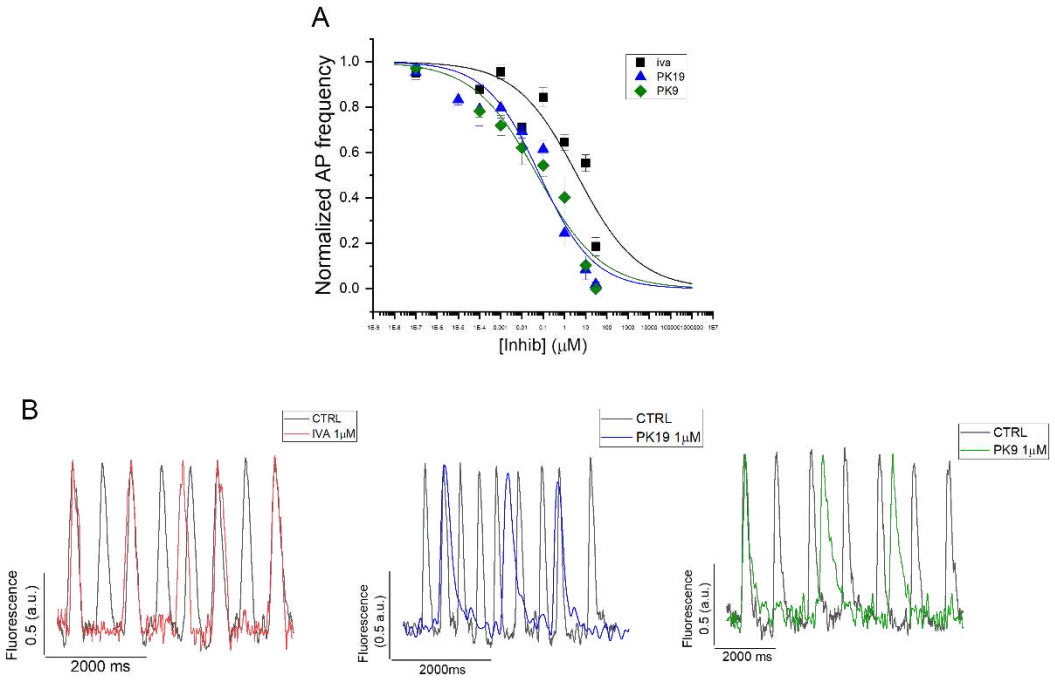

Figure 42. Concentration-effect curves of ivabradine, PK19 and PK9 on the spontaneous AP frequency detected in hiPSC-CMs. (A) The concentration-effect curves were obtained by Hill equation fitting of normalized AP frequencies obtained with ivabradine (iva, used as reference compound; n=19), PK19 (n=16) and PK9 (n=16) at several concentrations (0, 0.001, 0.01, 0.1, 1, 10 and 30 μM). (B) Representative traces of the spontaneous APs of hiPSC-CMs in the absence (black lines) and in presence of 1 μM of iva (red line), PK19 (blue line) and PK9 (green+ line).

2. Inhibition of pacemaker activity of hiPSC-CMs monolayers by the inflammatory cytokine Interleukin-6

Direct and indirect effects of cytokines, including interleukin 6 (IL-6), on ion channels are emerging as important mediators of arrhythmogenic remodeling. In particular, cytokines are capable of altering the function of ion channels and the homeostasis of intracellular calcium of cardiomyocytes. Additionally, a long-standing exposure of cardiac tissue to cytokine effects has been proposed to provide a basis to develop electrical and structural remodeling, which may induce arrhythmogenic alterations, cell apoptosis, myolysis and fibrosis (Hu et al., 2015). Indeed, elevated plasma levels of IL-6 are associated with an increase of cardiac arrhythmic events, such as atrial fibrillation (Marcus *et al.*, 2008; Roşianu *et al.*, 2013). However, despite many cardiac ion channels are known to represent direct targets of IL-6, no information are available on the direct effects of IL-6 on cardiac pacemaker activity.

To clarify this point, we tested the acute effects of cumulative growing concentrations (0, 50, 100, 500, 1000, 10000, 50000 and 100000 pg/mL) of human IL-6 (hIL-6) on the

spontaneous beating activity of hiPSC-CMs at day 30 of maturation. As described previously, hiPSC-CMs maintain the same ionic mechanisms, including those due to HCN channels, that regulate native pacemaker centers. The effects of IL-6 were studied by HT recordings on VSD-loaded hiPSC-CMs. Figure 43 shows the normalized spontaneous AP frequency as a function of hIL-6 concentrations. Spontaneous AP frequency was reduced in a concentration-dependent manner, and, compared to control condition, the effect became significant at 100 pg/mL hIL-6 concentration.

The potency of hIL-6 was evaluated by Hill fitting of concentration-effect curve. The half-maximal inhibitory concentration (IC_{50}) resulted 99.13±51.76 pg/mL. An interesting feature of hIL-6 effect is that maximal inhibition of the spontaneous firing was around 20%.

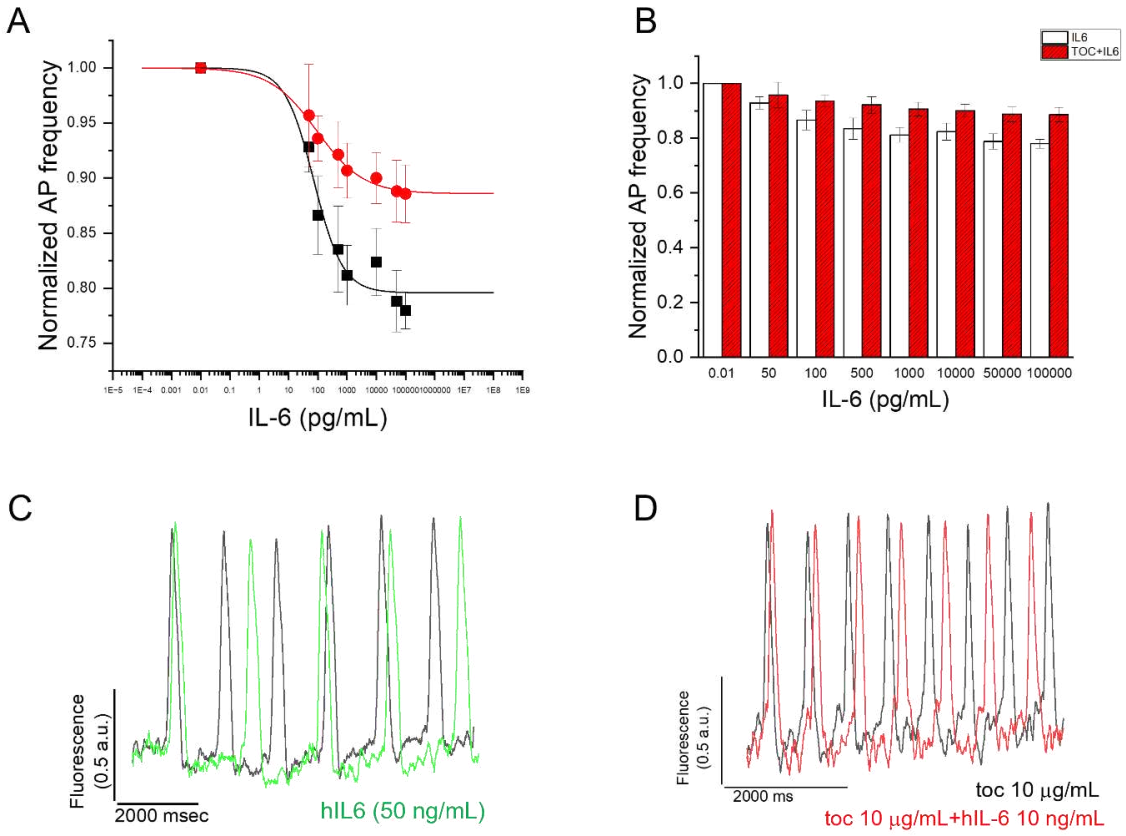

Figure 43. Effect of Interleukin-6 and tocilizumab on spontaneous AP frequency in hiPSC-CMs. (A) Concentration-effect curve of IL-6 (tested at 0, 50, 100, 500, 1000, 10000, 50000 and 100000 pg/mL) obtained by Hill equation fitting of fractional AP frequency without (black line) and with (red line) tocilizumab. (B) Bar graph represents the normalized spontaneous AP frequency of hiPSC-CMs measured at different drug concentration without (white bars) and with (red bars) tocilizumab. (C, D) Representative traces of spontaneous APs detected on hiPSC-CMs in control conditions without/with tocilizumab (black lines) and in the presence of 50 ng/mL (green line) or 10 ng/mL (red line) hIL-6. n=23; *p<0.05 CTR vs 500 pg/mL IL-6; **p<0.01 CTR vs 100 and 10000 pg/mL IL-6; ***p<0.0005 CTR vs 1000 pg/mL IL-6; ****p<0.0001 CTR vs 50000 and 100000 pg/mL IL-6.

The effect of hIL-6 was partially prevented by application of tocilizumab (used at 10 µM for 15 minutes before hIL-6), a recombinant humanized monoclonal antibody that acts as antagonist with the soluble and membrane bound IL-6 receptor. This indicates that at least part of the inhibitory effect of hIL-6 on the pacemaker activity is dependent on IL-6 receptor

activation. Tocilizumab alone reduces significantly spontaneous AP frequency ($p<0.05$ versus control).

The detailed analysis of spontaneous AP profile with hIL-6 also showed a concentration-dependent decrease of AP amplitude, that was significant at 100000 pg/mL IL-6 ($p<0.05$ vs control condition). On the contrary, no variations were observed for the Maximal Diastolic Potential (MDP) and durations at 20, 50 and 90% of AP repolarization (APD20, 50 and 90%; ms) (Figure 44).

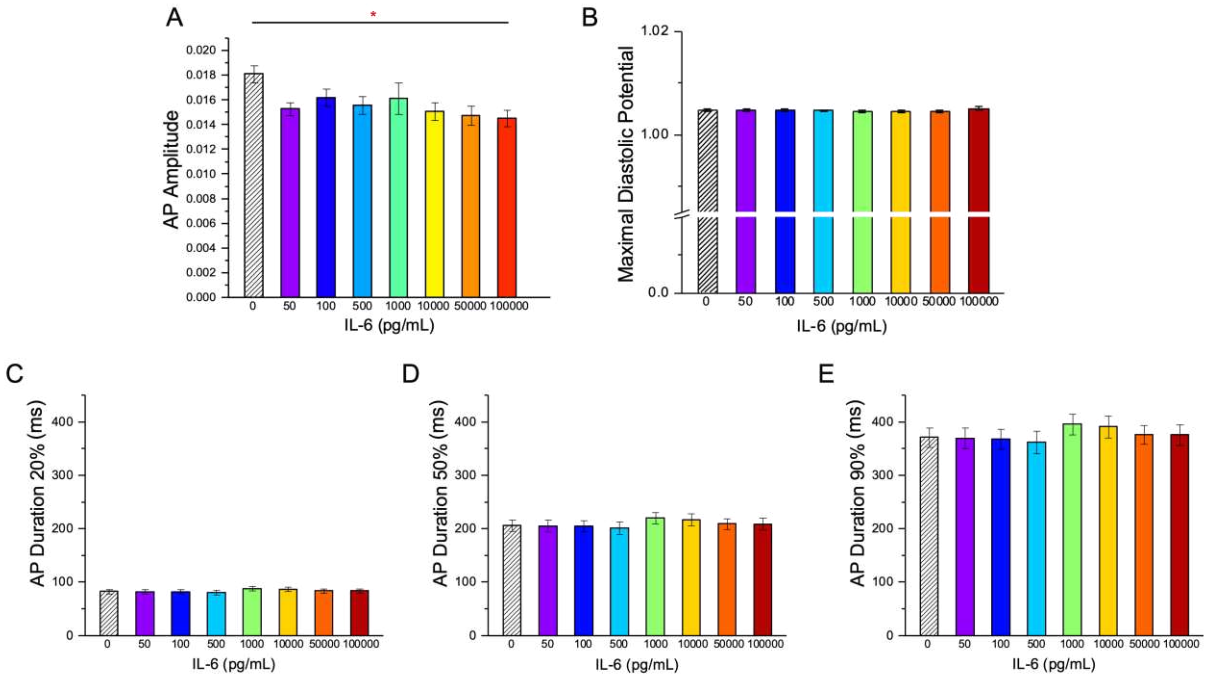

Figure 44. Effects of human IL-6 on spontaneous AP profile of hiPSC-CMs. Bar graphs show the effects of increasing hIL-6 concentration on the following parameters: (A) Action Potential Amplitude (APA), (B) Maximal Diastolic Potential (MDP) and (C, D and E) AP durations at 20, 50 and 90% of repolarization (APD20, 50 and 90; ms). n=23; *p<0.05 CTRL vs 100000 pg/mL.

3. Establishment and phenotypic characterization of novel hiPSCs lines

Since the first report of Takahashi and Yamanaka (2006), the reprogramming of somatic cells into induced pluripotent stem cells (iPSC) has becoming a widely used method. Moreover, ethical concerns regarding disruption of embryos were overpassed with hiPSCs that can be derived from patients or healthy donors, like embryonic stem cells (ESCs). Patient derived iPSCs (hiPSCs) has vast potential as an *in vitro* research tool as well as in regenerative medicine. However, many times, the reprogramming methods and the stress of *in vitro* culturing introduces genetic and epigenetic alterations that can change the cellular phenotype and

affect the integrity of experiments using these cell lines (Weissbein et al., 2017). Therefore, it is crucial that iPSCs are fully characterized as per regulatory requirements, in order to provide reliable scientific data and preclinical research model for clinical use (Garreta *et al.*, 2018).

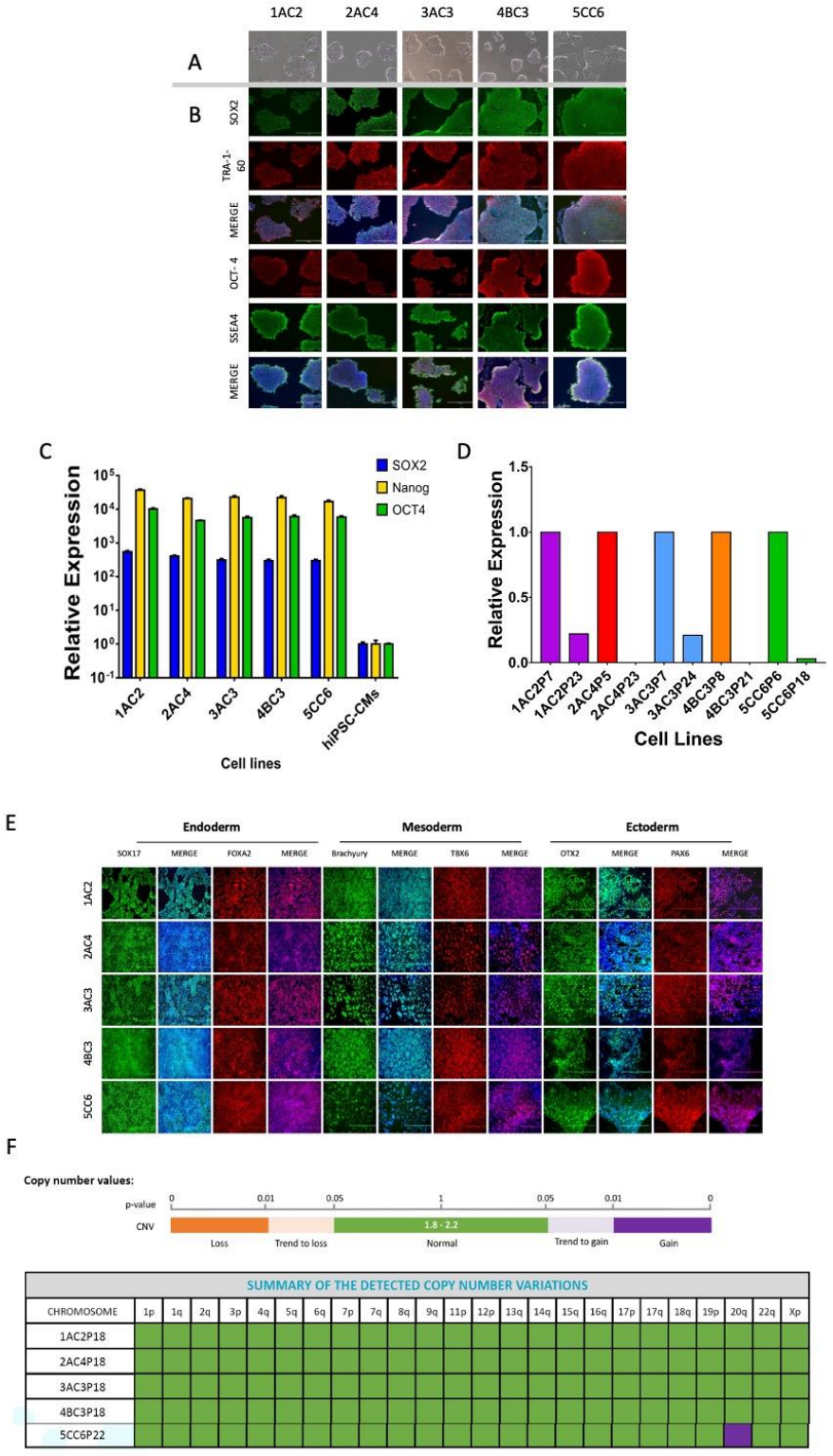

Figure 45. Characterization of hiPSCs lines performed at University Medical Center of Utrecht. (A) Brightfield microscopy shows hiPSCs colony morphology. (B) Immunostaining of pluripotency markers SOX2 (green), TRA-1-60 (red), OCT4 (red) and SSEA4 (green). (C) Relative expression of pluripotency markers SOX2, Nanog and OCT4,

compared to iPSC-derived cardiomyocytes, as measured by qPCR. (D) Absence or decrease of Sendai-viral transcript SeV confirmed by qPCR at low and high passages. (E) Immunostaining of trilineage differentiation markers: SOX17 (green) and FOXA2 (red) for endoderm; Brachyury (green) and TBX6 (red) for mesoderm; OTX2 (green) and PAX6 (red) for ectoderm. (F) Digital karyotype of new hiPSC lines. For each line the copy number variations (CNVs) in each chromosome are reported in the table: loss of CNVs in orange; normal CNVs in green; gain of CNVs in purple.

Based on this premise, during my stage of 6 months at the University Medical Center of Utrecht (UMCU), under the supervision of Prof. Stillitano, I carried out a series of assays necessary to characterize new human iPSC lines. All iPSC lines were obtained by reprogramming of peripheral blood mononuclear cells (PBMCs), using the CytoTuneTM-iPS 2.0 Sendai virus reprogramming system (see "materials and methods"). Subsequently, one clone from each line was selected and expanded under feeder-free conditions, splitting the cells every 3/4 days.

Figure 45 shows the results obtained during this characterization that was performed on five different new cell lines: 1AC2, 2AC4, 3AC3, 4BC3 and 5CC6. As evidenced in the images, cell line morphology is that typical of pluripotent cells, forming compact colonies with distinct borders and large nuclei (Figure 45A). Moreover, all cell lines displayed a pluripotent phenotype, since they express pluripotency genes, such as the membrane proteins TRA-1-60 and SSEA4 and the transcription factors SOX2, Nanog and OCT4 (Figure 45B and C). The expression of pluripotency markers was detected by positive immunostaining for SOX2, TRA-1-60, OCT4 and SSEA4 and quantitatively for SOX2, Nanog and OCT4 by RT-qPCR, comparing their expression to a reference hiPSC-CMs at day 170 of maturation.

Since it is important that the virus used in the reprogramming phase does not integrate into the genome of the stem cell lines, the absence (or the reduction) of the expression of Sendai-viral transcript SeV was investigated in low and high cell passages by qPCR. As shown in Figure 45D, with increasing cell passages the expression of viral transcript is absent (like in 2AC4 and 4BC3 lines) or decreased (like in 1AC2, 3AC3 and 5CC6). Sometimes virus is undetectable already at very low passages (i.e., P5; data not shown).

An important point in the characterization of novel pluripotent cell line relates to the pluripotency potential that should be necessarily displayed by the cell line. To this aim iPS cell lines are induced to differentiate toward the three germ layers (ectoderm, mesoderm, and endoderm). Accordingly, we performed the trilineage differentiation (see "materials and methods") for each cell line and positive immunostaining was studied for the following differentiation markers: SOX17 and FOXA2, endoderm markers; Brachyury and TBX6, mesoderm markers; OTX2 and PAX6, ectoderm markers (Figure 45E).

In addition, two quality tests are important to ultimate a thorough characterization. The first is digital karyotyping that revealed normal karyotype without evidence of structural or numerical chromosome aberrations for all cell line except the 5CC6 line (Figure 45F). The second test is the Short Tandem Repeat (STR) assay at high passages, that was performed on 16 genetic loci. Results (data not shown) ruled out cell-line cross-contaminations for each different cell line.

CHAPTER V. CONCLUSIONS AND DISCUSSION

Given the prominent role of HCN channels in various physiological and pathological conditions of the heart and the nervous system, their pharmacological blockade represents a promising field of exploration. Ivabradine is currently the only drug that specifically blocks HCN channels and entered in the clinical use as a bradycardic agent. Beyond the fact that ivabradine is, however, still confined to a second-line therapy in the treatment of heart failure, its inability to discriminate between different HCN channel isoforms reflects the occurrence of possible extra-cardiac effects (i.e., phosphenes) in the patients. To explore the full spectrum of possible indications covered by HCN channel blockade, second-generation compounds have to be designed.

Literature data suggest that structural modification of zatebradine could provide a successful strategy that has led to some new molecules able to preferentially target some HCN isoforms over the others (Sartiani et al., 2017). This isoform-selectivity may be related to the ability of these compounds to adopt different conformations and to interact with the channel through the presence of specific additional moieties. In this class of chemicals, an ongoing work is being done to derive solid structure-activity relationships, which are expected to optimize molecule potency and isoform or tissue selectivity. Using this strategy in the last decades, the research group I joined during my PhD has substantially grown up the possibility to develop new compounds, whose properties will be of interest for both *in vitro* and *in vivo* applications involving HCN channel function.

The electrophysiological evaluation of compounds tested in this thesis took advantage of the use of HEK-293 cell cultures. This experimental platform has long allowed the possibility to test molecules on heterologously expressed HCN channels and its simplicity well fits to be an effective model for screening pharmacological inhibitors. Of note, HCN channels can assemble both into homo- and hetero-tetramers, opening the possibility to test potential blockers in HEK cells expressing single homo-tetrameric HCN channels and thus obtaining important information on isoform selectivity/preference. Using this strategy, results obtained in this thesis demonstrated that appropriate modification of zatebradine chemical structure can lead to the enantiomeric derivatives PK9 and PK19 displaying a strong HCN isoform selectivity and a high potency compared to reference compounds ivabradine, zatebradine and cilobradine and to other zatebradine analogues, namely EC18, MEL57A and MEL55A, which were previously studied using a similar approach (Melchiorre et al., 2010; Del Lungo et al., 2012; Dini et al., 2018) (Figure 46).

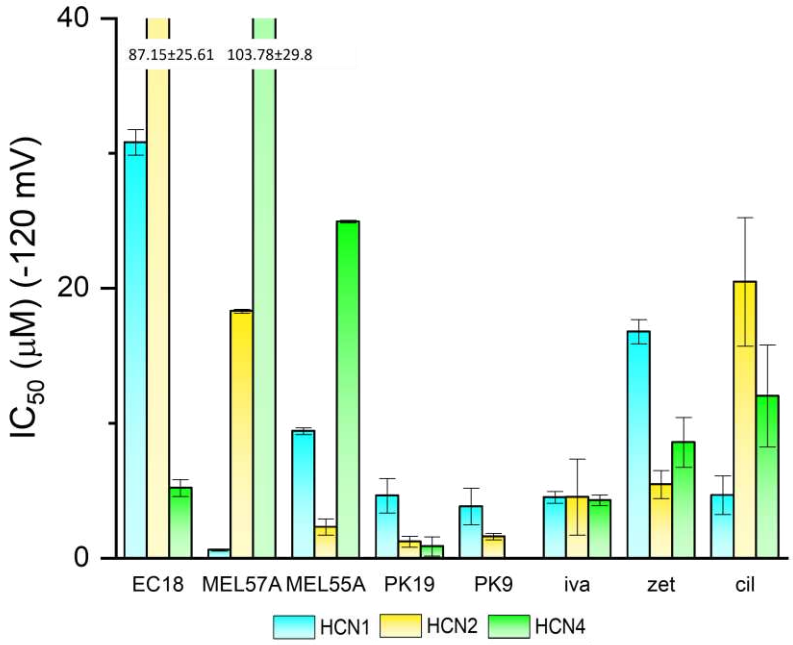

Figure 46. Mean values of IC_{50} of new and reference HCN blockers. IC_{50} values studied on I-HCNs at -120 mV for old and new zatebradine derivatives, reference compounds ivabradine (iva), zatebradine (Zat) and cilobradine (Cil), and other derivatives (EC18, MEL57A and MEL55A), described by Melchiorre et al., 2010; Del Lungo et al., 2012; Dini et al., 2018.

Indeed, analysis of IC_{50} values for different HCN-current measured at -120 mV (Figure 44) shows some peculiar properties of the newly tested compounds PK19 and PK9. Compared to the reference compounds and previously described zatebradine derivatives, both PK19 and PK9 show extremely low IC_{50} values (at least for the HCN2 and HCN4 isoforms); this indicates that the chemical modifications performed on zatebradine structure were effective to substantially increase blockade potencies. In particular, both PK9 and PK19 IC_{50} are lower than those calculated for the other zatebradine derivatives tested in previous studies, which were studied in similar experimental models using 1 µM as starting concentration. Differently, both PK9 and PK19 are able to block HCN channels even in the sub-µM range (see concentration-effect curve in the result section). Importantly, analysis of current at physiological potentials (-80 mV, Table 2), confirms the activity of both compounds in the sub-µM range and uncover a clear preference for HCN2 and HCN4 isoforms over HCN1.

IC_{50} (µM)	HCN1			HCN2			HCN4		
	-80 mV	-120 mV	n	-80 mV	-120 mV	n	-80 mV	-120 mV	n
PK19*	1.81 ± 0.57	4.63 ± 1.28	9	0.32 ± 0.08	1.21 ± 0.41	8	0.12 ± 0.02	0.87 ± 0.71	6
PK9	1.64 ± 0.86	5.31 ± 1.12	4	0.24 ± 0.12	1.50 ± 0.41	6	0.11 ± 0.04	2.18 ± 1. 24	3

Table 2. IC50 values of PK19 and PK9 on I-HCNs recorded in HEK293 at -80 mV and -120 mV.
*Published data (Balducci et al., 2021).

Taken together, these results lead us to make some conclusive considerations. To our knowledge, this is the first description of zatebradine derivatives endowing with a clear preference/selectivity toward the HCN2 and HCN4 isoforms. EC18, for example, proved to be much more selective for HCN4 compared to the other isoforms; differently MEL57A showed a strong activity on HCN1 respect to the other isoforms, while MEL55A is preferentially directed toward both HCN1 and HCN2. Given the elevate potency of PK9 and PK19 toward HCN2 isoform, we believe that both compounds may be useful to study the role of I_f within organs and conditions where this isoform is prominent and/or overexpressed, e.g., cardiac hypertrophy and neuropathic pain. At the same time, PK9 and PK19 could represent leading compounds to further investigate the physiologic role of HCN2/4 in cardiac and neuronal tissues and develop additional compounds with HCN2 or HCN4 inhibitory function.

Voltage protocols of use- and state-dependence evaluations demonstrated to be a precious tool for assessing the specific inhibitory properties of PK9 and PK19. Using these protocols, a series of studies (Bucchi *et al*., 2002) demonstrated that ivabradine effect on cardiac pacemaker occurs when channel is activated (use-dependence of blockade), meaning that decrease of pacemaker function by ivabradine is more potent at elevate cardiac rate. This important attribute is also present for PK19 and PK9, which showed a clear use-dependence. In particular, PK19 reduced HCN1 and 2 current densities more effectively than PK9; while I-HCN4 density was reduced similarly by both compounds. Additionally, and similarly to ivabradine, PK19 blockade occurs also in the close state of HCN1 channel, while for HCN2 and HCN4 isoforms and for HCN current measured in DRG neurons blockade is mainly use-dependent. In particular, in DRG neurons the use-dependent effect was stronger for PK9 than PK19. Differently, these results imply a more prominent effect of PK19 when the frequency of HCN2/4 channel opening is elevated and the channel is hyperactivated, two condition present in tachycardia and neuropathic pain. PK9 also displays a clear use dependence on current of DRG neurons, while further analysis is necessary to evaluate its use- and state dependence on single channel isoforms.

Data obtained on DRG neurons confirmed the findings observed in the recombinant systems. Notably, PK9 turned out to be 5-fold more potent than PK19 at physiological potential (IC_{50} 0.36 µM vs 1.52 µM), although reduction of current conductance at 5 µM was comparable (92% by PK9, 88% by PK19). These results are in line with those obtained in HEK cells, where 5 µM PK19 inhibited I-HCN2 by 90% but the same concentrations of PK9 blocked I-HCN2 by 100%.

Overall, despite further analysis is necessary to refine data, we believe that both PK19 and PK9 compounds deserve further investigation in appropriate animal models of neuropathic pain, where overexpression of HCN current in DRG neurons is reported to mediate excessive pain perception (Yagi and Sumino, 1998; Takeda et al., 2002). Previous studies on similar models have shown that pain is controlled by zatebradine derivatives showing preference for HCN1 and HCN2 (MEL55A) and HCN1 (MEL57A); our experiment will complement results obtained with MEL 55A and MEL 57A defining the potentials of the two novel analogues with elevate selectivity for HCN2 and HCN4.

Given the elevate preference of PK9 and PK19 also for HCN4, which is prominent in cardiac pacemaker, with the purpose of testing both compounds in a relevant physiologic model of pacemaking, I took advantage of the human induced pluripotent stem cell (hiPSC) technology to efficiently obtain *in vitro* cardiac myocytes. hiPSC-derived cardiomyocytes (hiPSC-CMs) at 24-50 day of differentiation (early differentiation) represent an optimal pacemaking model,

which retains the properties of hetero-tetrameric HCN1,2,4 channel regulation and the response to rate-lowering drugs. Beyond confirming to be a powerful tool to study cardiac morphogenesis, hiPSC-CMs offered the possibility to screen the ability of the zatebradine analogues to limit the spontaneous action potential frequency. To this aim, we used the MULTIPLE High Throughput system, developed during my PhD in collaboration with Prof. Sacconi and Dr. Credi (European Laboratory for Non-linear Spectroscopy). In particular, the MULTIPLE platform resulted very convenient to record spontaneous electrical activity of hiPSC-CMs by optical detection of a fluorescent red-shifted voltage-sensitive dye (di 4 ANBDQ PQ). As shown in Figure 39, similarly to ivabradine, PK9 and PK19 were effective to lower the number of action potential in the unit time. In line with the above-described elevate potency in recombinant channels, both PK9 and PK19 displayed a rate reduction potency that is 15- and 30-fold higher than that of ivabradine. These results further confirm the gain of potencies of PK9 and PK19 obtained by chemical modification of zatebradine structure. We believe these results represent a basis to identify the molecular determinant to achieve a stringent HCN2 and HCN4 selectivity and complement the knowledge acquired with the use of previous derivatives more selective for HCN1 and HCN2.

Inflammatory cytokines (i.e., TGF-β, IL-1β and IL-6) are polypeptide effectors of the immune system. Among them, IL-6 is particularly relevant in the promotion of arrhythmogenesis and its plasma levels in humans correlate with typical atrial arrhythmogenic alterations. Indeed, several experimental evidence indicates that IL-6 directly modifies cardiomyocyte electrogenesis through the acute interaction with their membrane associated channels. In particular, IL-6 increases L-Type Ca^{2+} current (I_{CaL}) and inhibits the rapid component of the delayed rectifier K^+ current (I_{Kr}), thus inducing prolongation of action potential, a recognized alteration leading to ventricular arrhythmias. Other important effects of IL-6 have been demonstrated for the expression and function of atrial connexins 40 and 43 (Lazzerini et al., 2019), data that consolidate the hypothesis of IL-6 as multichannel modulator with relevant effects on cardiac electrogenesis and impulse conduction. To date, it is unknown whether IL-6 acutely modifies the cardiac function of the HCN channels, which play a well-established role in cardiac pacemakers and is hypothesized to underlie and sustain some arrhythmias. Based on this evidence, we investigated whether IL-6 acutely affect spontaneous electrical activity of hiPSC-CMs. The effects of increasing concentrations of human IL-6 were evaluated using the MULTIPLE recording system and measuring the frequency and parameters (amplitude, maximum diastolic potential and durations at different repolarization values) of the action potentials. While the frequency is decreased in a dose-dependent manner, there was also a remarkable reduction of action potential amplitude; differently maximal diastolic potential and AP durations do not undergo significant changes. However, the slope of spontaneous depolarization appears clearly slowed by IL-6 application, uncovering a typical hallmark of HCN channel blockade. Since the frequency of action potentials is fundamentally regulated by the activity of HCN channels, it is possible that the acute effect observed after exposure to IL-6 is caused by a direct inhibition of HCN channels. However, since the observed reduction of AP amplitude may derive from Ca^{2+} and/or Na^+ channels blockade by hIL-6, it is possible that some or all these channels are involved in the effects of hIL-6 in AP frequency. While blockade of Ca^+ channels is in line with previous report for IL-6 obtained in other experimental setting, blockade of Na^+ channels has never been reported in previous studies. Despite further experiments are necessary to clarify the specific channels affected by hIL-6 in cardiomyocytes derived from hiPSCs, results obtained on the reduction of cardiac pacemaking

by IL-6 warrant further investigation in opportune animal models and in humans experiencing elevate inflammatory cytokines and IL-6. Such measurements would provide a basis to clarify a link between IL-6 - heart rate and HCN function.

Finally, data demonstrated that effects of IL-6 are partially prevented by tocilizumab, an IL-6 receptor antagonist, suggesting that the IL-6-induced decrease of the spontaneous rate is due to the interaction of IL-6 with its receptor. If confirmed by additional measurements, these results open the possibility for tocilizumab to revert bradycardia associated with inflammatory process. However, given the uncomplete prevention of hIL-6 effect by tocilizumab, it is also possible that hIL-6 interacts directly with ion channels responsible for the effects on pacemaking. Future experiments will clarify this point.

Experiment on acute effects of IL-6 relied on the properties of spontaneously beating cardiomyocytes differentiated from hiPSC, which at least in the differentiation stage examined in the thesis, represent a quite faithful model of cardiac pacemaking. However cardiac differentiation and selection of cell lines are time-consuming and still demanding to standardize, thus requiring consolidated knowledge of most appropriate technique in term of cell source generation, phenotypic characterization and stability. In general, hiPSC represent a valid *in vitro* experimental platform alternative to both embryonic stem cells and animal models. These cells have vast potential as a tool for *in vitro* research and in regenerative medicine. Indeed, they can be used for drug testing and discovery, cardiotoxicity screening, disease modelling, cell replacement therapy, by generating patient-specific cells and editing the genome of healthy cells. However, hiPSCs are intrinsically variable and can change during the manufacturing process with the introduction of genomic alterations that can modify the cellular phenotype and, consequentially, compromise the integrity of experiments using these cell lines. Based on this, during my stage of 6 months at the University Medical Center of Utrecht (UMCU), I carried out a specific training to characterize new human hiPSCs lines. This enabled me to study and identify the typical morphology of hiPSC lines by using brightfield microscopy, while the pluripotency was studied investigating the gene and protein expression of pluripotency markers (such as SOX2, Nanog, OCT4, TRA-1-60 and SSEA4) by RT-qPCR and immunofluorescence, respectively. I also assessed whether Sendai virus used to reprogram somatic cells in iPSCs was integrated in the cell genome, using qPCR performed on high passages cells. Importantly, I verified all cell line pluripotency potential by differentiation into the three germ layers (ectoderm, mesoderm and endoderm). In this case phenotype was investigated using immunofluorescence. Finally, collection and analysis of DNA-samples was used to successfully verify both the absence of cross-contamination and the genetic integrity after long-term cell culturing. Overall, this phase of my study enabled me to consolidate the knowledge on pluripotent stem cell biology and to progress quickly in the phenotypic study of cardiac pacemaking.

As a general conclusion, results obtained in this thesis provide a solid basis to test PK9 and PK19 in opportune animal models suitable to study the action of HCN channels in heart function and pain transmission. Whether successful, these experiments will contribute to progress the knowledge of HCN channel pharmacology holding elevate translational potential for human diseases. Finally, results obtained with IL-6 uncovered a novel modulatory signal of cardiac pacemaking that represent a basis for further investigations aiming to clarify the control of heart rate during inflammatory diseases.

CHAPTER VI.
REFERENCES

Abbas A., Lichtman A, Pillai S. Cellular and molecular Immunology. 2005. Philadelphia: W.B. Saunders Company.

Accili EA, Proenza C, Baruscotti M, DiFrancesco D. From funny current to HCN channels: 20 years of excitation. News Physiol Sci. 2002 Feb;17:32-7. doi: 10.1152/physiologyonline.2002.17.1.32.

Acosta C, McMullan S, Djouhri L, Gao L, Watkins R, Berry C, Dempsey K, Lawson SN. HCN1 and HCN2 in Rat DRG neurons: levels in nociceptors and non-nociceptors, NT3-dependence and influence of CFA-induced skin inflammation on HCN2 and NT3 expression. PLoS One. 2012;7(12):e50442. doi: 10.1371/journal.pone.0050442.

Akira S, Isshiki H, Sugita T, Tanabe O, Kinoshita S, Nishio Y, Nakajima T, Hirano T, Kishimoto T. A nuclear factor for IL-6 expression (NF-IL6) is a member of a C/EBP family. EMBO J. 1990 Jun;9(6):1897-906. doi: 10.1002/j.1460-2075.1990.tb08316.x.

Akira S, Nishio Y, Inoue M, Wang XJ, Wei S, Matsusaka T, Yoshida K, Sudo T, Naruto M, Kishimoto T. Molecular cloning of APRF, a novel IFN-stimulated gene factor 3 p91-related transcription factor involved in the gp130-mediated signaling pathway. Cell. 1994 Apr 8;77(1):63-71. doi: 10.1016/0092-8674(94)90235-6.

Alí A, Boutjdir M, Aromolaran AS. Cardiolipotoxicity, Inflammation, and Arrhythmias: Role for Interleukin-6 Molecular Mechanisms. Front Physiol. 2019 Jan 7;9:1866. doi: 10.3389/fphys.2018.01866.

Alonso A, Llinás RR. Subthreshold Na+-dependent theta-like rhythmicity in stellate cells of entorhinal cortex layer II. Nature. 1989 Nov 9;342(6246):175-7. doi: 10.1038/342175a0.

Altomare C, Bucchi A, Camatini E, Baruscotti M, Viscomi C, Moroni A, DiFrancesco D. Integrated allosteric model of voltage gating of HCN channels. J Gen Physiol. 2001 Jun;117(6):519-32. doi: 10.1085/jgp.117.6.519.

Altomare C, Terragni B, Brioschi C, Milanesi R, Pagliuca C, Viscomi C, Moroni A, Baruscotti M, DiFrancesco D. Heteromeric HCN1-HCN4 channels: a comparison with native pacemaker channels from the rabbit sinoatrial node. J Physiol. 2003 Jun 1;549(Pt 2):347-59. doi: 10.1113/jphysiol.2002.027698.

Anderson RH, Yanni J, Boyett MR, Chandler NJ, Dobrzynski H. The anatomy of the cardiac conduction system. Clin Anat. 2009 Jan;22(1):99-113. doi: 10.1002/ca.20700.

Arnsten AF, Jin LE. Molecular influences on working memory circuits in dorsolateral prefrontal cortex. Prog Mol Biol Transl Sci. 2014;122:211-31. doi: 10.1016/B978-0-12-420170-5.00008-8.

Aromolaran AS, Srivastava U, Alí A, Chahine M, Lazaro D, El-Sherif N, Capecchi PL, Laghi-Pasini F, Lazzerini PE, Boutjdir M. Interleukin-6 inhibition of hERG underlies risk for acquired long QT in cardiac and systemic inflammation. PLoS One. 2018 Dec 6;13(12):e0208321. doi: 10.1371/journal.pone.0208321.

Balducci V, Credi C, Sacconi L, Romanelli MN, Sartiani L, Cerbai E. The HCN channel as a pharmacological target: Why, where, and how to block it. Prog Biophys Mol Biol. 2021 Nov;166:173-181. doi: 10.1016/j.pbiomolbio.2021.07.010.

Barbuti A, Baruscotti M, DiFrancesco D. The pacemaker current: from basics to the clinics. J Cardiovasc Electrophysiol. 2007 Mar;18(3):342-7. doi: 10.1111/j.1540-8167.2006.00736.x.

Barbuti A, Gravante B, Riolfo M, Milanesi R, Terragni B, DiFrancesco D. Localization of pacemaker channels in lipid rafts regulates channel kinetics. Circ Res. 2004 May 28;94(10):1325-31. doi: 10.1161/01.RES.0000127621.54132.AE.

Bartos DC, Grandi E, Ripplinger CM. Ion Channels in the Heart. Compr Physiol. 2015 Jul 1;5(3):1423-64. doi: 10.1002/cphy.c140069.

Baruscotti M, Barbuti A, Bucchi A. The cardiac pacemaker current. J Mol Cell Cardiol. 2010 Jan;48(1):55-64. doi: 10.1016/j.yjmcc.2009.06.019.

Baruscotti M, Bucchi A, Difrancesco D. Physiology and pharmacology of the cardiac pacemaker ("funny") current. Pharmacol Ther. 2005 Jul;107(1):59-79. doi: 10.1016/j.pharmthera.2005.01.005.

Bédard C, Kröger H, Destexhe A. Model of low-pass filtering of local field potentials in brain tissue. Phys Rev E Stat Nonlin Soft Matter Phys. 2006 May;73(5 Pt 1):051911. doi: 10.1103/PhysRevE.73.051911.

Bellin M, Marchetto MC, Gage FH, Mummery CL. Induced pluripotent stem cells: the new patient? Nat Rev Mol Cell Biol. 2012 Nov;13(11):713-26. doi: 10.1038/nrm3448.

Bender RA, Brewster A, Santoro B, Ludwig A, Hofmann F, Biel M, Baram TZ. Differential and age-dependent expression of hyperpolarization-activated, cyclic nucleotide-gated cation channel isoforms 1-4 suggests evolving roles in the developing rat hippocampus. Neuroscience. 2001;106(4):689-98. doi: 10.1016/s0306-4522(01)00314-1.

Benetos A, Rudnichi A, Thomas F, Safar M, Guize L. Influence of heart rate on mortality in a French population: role of age, gender, and blood pressure. Hypertension. 1999 Jan;33(1):44-52. doi: 10.1161/01.hyp.33.1.44.

Bernard Healey SA, Scholtes I, Abrahams M, McNaughton PA, Menon DK, Lee MC. Role of hyperpolarization-activated cyclic nucleotide-gated ion channels in neuropathic pain: a proof-of-concept study of ivabradine in patients with chronic peripheral neuropathic pain. Pain Rep. 2021 Oct 18;6(4):e967. doi: 10.1097/PR9.0000000000000967.

Bers DM, Perez-Reyes E. Ca channels in cardiac myocytes: structure and function in Ca influx and intracellular Ca release. Cardiovasc Res. 1999 May;42(2):339-60. doi: 10.1016/s0008-6363(99)00038-3.

Bhatla A, Mayer MM, Adusumalli S, Hyman MC, Oh E, Tierney A, Moss J, Chahal AA, Anesi G, Denduluri S, Domenico CM, Arkles J, Abella BS, Bullinga JR, Callans DJ, Dixit S, Epstein AE, Frankel DS, Garcia FC, Kumareswaram R, Nazarian S, Riley MP, Santangeli P, Schaller RD,

Supple GE, Lin D, Marchlinski F, Deo R. COVID-19 and cardiac arrhythmias. Heart Rhythm. 2020 Sep;17(9):1439-1444. doi: 10.1016/j.hrthm.2020.06.016.

Biel M, Michalakis S. Function and dysfunction of CNG channels: insights from channelopathies and mouse models. Mol Neurobiol. 2007 Jun;35(3):266-77. doi: 10.1007/s12035-007-0025-y.

Biel M, Schneider A, Wahl C. Cardiac HCN channels: structure, function, and modulation. Trends Cardiovasc Med. 2002 Jul;12(5):206-12. doi: 10.1016/s1050-1738(02)00162-7.

Biel M, Wahl-Schott C, Michalakis S, Zong X. Hyperpolarization-activated cation channels: from genes to function. Physiol Rev. 2009 Jul;89(3):847-85. doi: 10.1152/physrev.00029.2008.

Blazeski A, Zhu R, Hunter DW, Weinberg SH, Zambidis ET, Tung L. Cardiomyocytes derived from human induced pluripotent stem cells as models for normal and diseased cardiac electrophysiology and contractility. Prog Biophys Mol Biol. 2012 Oct-Nov;110(2-3):166-77. doi: 10.1016/j.pbiomolbio.2012.07.013.

Böhm M, Swedberg K, Komajda M, Borer JS, Ford I, Dubost-Brama A, Lerebours G, Tavazzi L; SHIFT Investigators. Heart rate as a risk factor in chronic heart failure (SHIFT): the association between heart rate and outcomes in a randomised placebo-controlled trial. Lancet. 2010 Sep 11;376(9744):886-94. doi: 10.1016/S0140-6736(10)61259-7.

Borish LC, Steinke JW. 2. Cytokines and chemokines. J Allergy Clin Immunol. 2003 Feb;111(2 Suppl):S460-75. doi: 10.1067/mai.2003.

BoSmith RE, Briggs I, Sturgess NC. Inhibitory actions of ZENECA ZD7288 on whole-cell hyperpolarization activated inward current (If) in guinea-pig dissociated sinoatrial node cells. Br J Pharmacol. 1993 Sep;110(1):343-9. doi: 10.1111/j.1476-5381.1993.tb13815.x.

Boyes J, Bolam JP, Shigemoto R, Stanford IM. Functional presynaptic HCN channels in the rat globus pallidus. Eur J Neurosci. 2007 Apr;25(7):2081-92. doi: 10.1111/j.1460-9568.2007.05463.x.

Brown H, Difrancesco D. Voltage-clamp investigations of membrane currents underlying pace-maker activity in rabbit sino-atrial node. J Physiol. 1980 Nov;308:331-51. doi: 10.1113/jphysiol.1980.sp013474.

Brown HF, DiFrancesco D, Noble SJ. How does adrenaline accelerate the heart? Nature. 1979 Jul 19;280(5719):235-6. doi: 10.1038/280235a0.

Bucchi A, Baruscotti M, DiFrancesco D. Current-dependent block of rabbit sino-atrial node I(f) channels by ivabradine. J Gen Physiol. 2002 Jul;120(1):1-13. doi: 10.1085/jgp.20028593.

Bucchi A, Baruscotti M, Nardini M, Barbuti A, Micheloni S, Bolognesi M, DiFrancesco D. Identification of the molecular site of ivabradine binding to HCN4 channels. PLoS One. 2013;8(1):e53132. doi: 10.1371/journal.pone.0053132.

Bucchi A, Tognati A, Milanesi R, Baruscotti M, DiFrancesco D. Properties of ivabradine-induced block of HCN1 and HCN4 pacemaker channels. J Physiol. 2006 Apr 15;572(Pt 2):335-46. doi: 10.1113/jphysiol.2005.100776.

Burridge PW, Matsa E, Shukla P, Lin ZC, Churko JM, Ebert AD, Lan F, Diecke S, Huber B, Mordwinkin NM, Plews JR, Abilez OJ, Cui B, Gold JD, Wu JC. Chemically defined generation of human cardiomyocytes. Nat Methods. 2014 Aug;11(8):855-60. doi: 10.1038/nmeth.2999.

Cacheaux LP, Topf N, Tibbs GR, Schaefer UR, Levi R, Harrison NL, Abbott GW, Goldstein PA. Impairment of hyperpolarization-activated, cyclic nucleotide-gated channel function by the intravenous general anesthetic propofol. J Pharmacol Exp Ther. 2005 Nov;315(2):517-25. doi: 10.1124/jpet.105.091801.

Cerbai E, Barbieri M, Mugelli A. Characterization of the hyperpolarization-activated current, I(f), in ventricular myocytes isolated from hypertensive rats. J Physiol. 1994 Dec 15;481 (Pt 3)(Pt 3):585-91. doi: 10.1113/jphysiol.1994.sp020465.

Cerbai E, Barbieri M, Mugelli A. Occurrence and properties of the hyperpolarization-activated current If in ventricular myocytes from normotensive and hypertensive rats during aging. Circulation. 1996 Oct 1;94(7):1674-81. doi: 10.1161/01.cir.94.7.1674.

Cerbai E, Mugelli A. I(f) in non-pacemaker cells: role and pharmacological implications. Pharmacol Res. 2006 May;53(5):416-23. doi: 10.1016/j.phrs.2006.03.015.

Cerbai E, Pino R, Porciatti F, Sani G, Toscano M, Maccherini M, Giunti G, Mugelli A. Characterization of the hyperpolarization-activated current, I(f), in ventricular myocytes from human failing heart. Circulation. 1997 Feb 4;95(3):568-71. doi: 10.1161/01.cir.95.3.568.

Cerbai E, Pino R, Rodriguez ML, Mugelli A. Modulation of the pacemaker current If by beta-adrenoceptor subtypes in ventricular myocytes isolated from hypertensive and normotensive rats. Cardiovasc Res. 1999 Apr;42(1):121-9. doi: 10.1016/s0008-6363(98)00291-0.

Cervetto L, Demontis GC, Gargini C. Cellular mechanisms underlying the pharmacological induction of phosphenes. Br J Pharmacol. 2007 Feb;150(4):383-90. doi: 10.1038/sj.bjp.0706998.

Chaplan SR, Guo HQ, Lee DH, Luo L, Liu C, Kuei C, Velumian AA, Butler MP, Brown SM, Dubin AE. Neuronal hyperpolarization-activated pacemaker channels drive neuropathic pain. J Neurosci. 2003 Feb 15;23(4):1169-78. doi: 10.1523/JNEUROSCI.23-04-01169.2003.

Chen J, Mitcheson JS, Lin M, Sanguinetti MC. Functional roles of charged residues in the putative voltage sensor of the HCN2 pacemaker channel. J Biol Chem. 2000 Nov 17;275(46):36465-71. doi: 10.1074/jbc.M007034200.

Chen S, Wang J, Siegelbaum SA. Properties of hyperpolarization-activated pacemaker current defined by coassembly of HCN1 and HCN2 subunits and basal modulation by cyclic nucleotide. J Gen Physiol. 2001 May;117(5):491-504. doi: 10.1085/jgp.117.5.491.

Chen X, Zhang Q, Su Y, Zhao W, Li Y, Du B, Deng X, Ji F, Dong Q, Chen C, Li J. Evidence for the contribution of HCN1 gene polymorphism (rs1501357) to working memory at both behavioral and neural levels in schizophrenia patients and healthy controls. Schizophrenia (Heidelb). 2022 Aug 20;8(1):66. doi: 10.1038/s41537-022-00271-7.

Cheng Q, Zhou Y. Novel role of KT5720 on regulating hyperpolarization-activated cyclic nucleotide-gated channel activity and dorsal root ganglion neuron excitability. DNA Cell Biol. 2013 Jun;32(6):320-8. doi: 10.1089/dna.2013.2021.

Cong L, Ran FA, Cox D, Lin S, Barretto R, Habib N, Hsu PD, Wu X, Jiang W, Marraffini LA, Zhang F. Multiplex genome engineering using CRISPR/Cas systems. Science. 2013 Feb 15;339(6121):819-23. doi: 10.1126/science.1231143.

Corrigan-Curay J, O'Reilly M, Kohn DB, Cannon PM, Bao G, Bushman FD, Carroll D, Cathomen T, Joung JK, Roth D, Sadelain M, Scharenberg AM, von Kalle C, Zhang F, Jambou R, Rosenthal E, Hassani M, Singh A, Porteus MH. Genome editing technologies: defining a path to clinic. Mol Ther. 2015 May;23(5):796-806. doi: 10.1038/mt.2015.54.

Coutaux A, Adam F, Willer JC, Le Bars D. Hyperalgesia and allodynia: peripheral mechanisms. Joint Bone Spine. 2005 Oct;72(5):359-71. doi: 10.1016/j.jbspin.2004.01.010.

Credi C, Balducci V, Munagala U, Cianca C, Bigiarini S, de Vries AAF, Loew LM, Pavone FS, Cerbai E, Sartiani L, Sacconi L. Fast Optical Investigation of Cardiac Electrophysiology by Parallel Detection in Multiwell Plates. Front Physiol. 2021 Sep 3;12:692496. doi: 10.3389/fphys.2021.692496.

Crumb WJ Jr, Vicente J, Johannesen L, Strauss DG. An evaluation of 30 clinical drugs against the comprehensive in vitro proarrhythmia assay (CiPA) proposed ion channel panel. J Pharmacol Toxicol Methods. 2016 Sep-Oct;81:251-62. doi: 10.1016/j.vascn.2016.03.009.

Cyganek L, Tiburcy M, Sekeres K, Gerstenberg K, Bohnenberger H, Lenz C, Henze S, Stauske M, Salinas G, Zimmermann WH, Hasenfuss G, Guan K. Deep phenotyping of human induced pluripotent stem cell-derived atrial and ventricular cardiomyocytes. JCI Insight. 2018 Jun 21;3(12):e99941. doi: 10.1172/jci.insight.99941.

Dell'Era P, Benzoni P, Crescini E, Valle M, Xia E, Consiglio A, Memo M. Cardiac disease modeling using induced pluripotent stem cell-derived human cardiomyocytes. World J Stem Cells. 2015 Mar 26;7(2):329-42. doi: 10.4252/wjsc.v7.i2.329.

Del Lungo M, Melchiorre M, Guandalini L, Sartiani L, Mugelli A, Koncz I, Szel T, Varro A, Romanelli MN, Cerbai E. Novel blockers of hyperpolarization-activated current with isoform selectivity in recombinant cells and native tissue. Br J Pharmacol. 2012 May;166(2):602-16. doi: 10.1111/j.1476-5381.2011.01782.x.

Delpón E, Valenzuela C, Pérez O, Franqueza L, Gay P, Snyders DJ, Tamargo J. Mechanisms of block of a human cloned potassium channel by the enantiomers of a new bradycardic agent: S-16257-2 and S-16260-2. Br J Pharmacol. 1996 Mar;117(6):1293-301. doi: 10.1111/j.1476-5381.1996.tb16728.x.

Devalla HD, Schwach V, Ford JW, Milnes JT, El-Haou S, Jackson C, Gkatzis K, Elliott DA, Chuva de Sousa Lopes SM, Mummery CL, Verkerk AO, Passier R. Atrial-like cardiomyocytes from human pluripotent stem cells are a robust preclinical model for assessing atrial-selective pharmacology. EMBO Mol Med. 2015 Apr;7(4):394-410. doi: 10.15252/emmm.201404757.

DiFrancesco D. A new interpretation of the pace-maker current in calf Purkinje fibres. J Physiol. 1981 May;314:359-76. doi: 10.1113/jphysiol.1981.sp013713.

DiFrancesco D. Characterization of single pacemaker channels in cardiac sino-atrial node cells. Nature. 1986 Dec 4-10;324(6096):470-3. doi: 10.1038/324470a0.

DiFrancesco D. Pacemaker mechanisms in cardiac tissue. Annu Rev Physiol. 1993;55:455-72. doi: 10.1146/annurev.ph.55.030193.002323.

DiFrancesco D. Dual allosteric modulation of pacemaker (f) channels by cAMP and voltage in rabbit SA node. J Physiol. 1999 Mar 1;515 (Pt 2) (Pt 2):367-76. doi: 10.1111/j.1469-7793.1999.367ac.x.

DiFrancesco D. Serious workings of the funny current. Prog Biophys Mol Biol. 2006 Jan-Apr;90(1-3):13-25. doi: 10.1016/j.pbiomolbio.2005.05.001.

DiFrancesco D. The role of the funny current in pacemaker activity. Circ Res. 2010 Feb 19;106(3):434-46. doi: 10.1161/CIRCRESAHA.109.208041.

DiFrancesco D, Borer JS. The funny current: cellular basis for the control of heart rate. Drugs. 2007;67 Suppl 2:15-24. doi: 10.2165/00003495-200767002-00003.

DiFrancesco JC, DiFrancesco D. Dysfunctional HCN ion channels in neurological diseases. Front Cell Neurosci. 2015 Mar 10;6:174. doi: 10.3389/fncel.2015.00071.

DiFrancesco D, Ducouret P, Robinson RB. Muscarinic modulation of cardiac rate at low acetylcholine concentrations. Science. 1989 Feb 3;243(4891):669-71. doi: 10.1126/science.2916119.

DiFrancesco D, Noble D. A model of cardiac electrical activity incorporating ionic pumps and concentration changes. Philos Trans R Soc Lond B Biol Sci. 1985 Jan 10;307(1133):353-98. doi: 10.1098/rstb.1985.0001.

DiFrancesco D, Noble D. The funny current has a major pacemaking role in the sinus node. Heart Rhythm. 2012 Feb;9(2):299-301. doi: 10.1016/j.hrthm.2011.09.021.

DiFrancesco D, Tortora P. Direct activation of cardiac pacemaker channels by intracellular cyclic AMP. Nature. 1991 May 9;351(6322):145-7. doi: 10.1038/351145a0.

DiFrancesco D, Tromba C. Inhibition of the hyperpolarization-activated current (if) induced by acetylcholine in rabbit sino-atrial node myocytes. J Physiol. 1988 Nov;405:477-91. doi: 10.1113/jphysiol.1988.sp017343.

Dinarello CA. Historical insights into cytokines. Eur J Immunol. 2007 Nov;37 Suppl 1(Suppl 1):S34-45. doi: 10.1002/eji.200737772.

Dinarello CA. Overview of the IL-1 family in innate inflammation and acquired immunity. Immunol Rev. 2018 Jan;281(1):8-27. doi: 10.1111/imr.12621.

Dini L, Del Lungo M, Resta F, Melchiorre M, Spinelli V, Di Cesare Mannelli L, Ghelardini C, Laurino A, Sartiani L, Coppini R, Mannaioni G, Cerbai E, Romanelli MN. Selective Blockade of

HCN1/HCN2 Channels as a Potential Pharmacological Strategy Against Pain. Front Pharmacol. 2018 Nov 8;9:1252. doi: 10.3389/fphar.2018.01252.

Doan TN, Kunze DL. Contribution of the hyperpolarization-activated current to the resting membrane potential of rat nodose sensory neurons. J Physiol. 1999 Jan 1;514 (Pt 1)(Pt 1):125-38. doi: 10.1111/j.1469-7793.1999.125af.x.

Driggin E, Madhavan MV, Bikdeli B, Chuich T, Laracy J, Biondi-Zoccai G, Brown TS, Der Nigoghossian C, Zidar DA, Haythe J, Brodie D, Beckman JA, Kirtane AJ, Stone GW, Krumholz HM, Parikh SA. Cardiovascular Considerations for Patients, Health Care Workers, and Health Systems During the COVID-19 Pandemic. J Am Coll Cardiol. 2020 May 12;75(18):2352-2371. doi: 10.1016/j.jacc.2020.03.031.

Dunlop J, Bowlby M, Peri R, Vasilyev D, Arias R. High-throughput electrophysiology: an emerging paradigm for ion-channel screening and physiology. Nat Rev Drug Discov. 2008 Apr;7(4):358-68. doi: 10.1038/nrd2552.

Dyhrfjeld-Johnsen J, Morgan RJ, Soltesz I. Double Trouble? Potential for Hyperexcitability Following Both Channelopathic up- and Downregulation of I(h) in Epilepsy. Front Neurosci. 2009 May 1;3(1):25-33. doi: 10.3389/neuro.01.005.2009.

Fabiato A, Fabiato F. Calcium and cardiac excitation-contraction coupling. Annu Rev Physiol. 1979;41:473-84. doi: 10.1146/annurev.ph.41.030179.002353.

FDA, 2015 https://www.fda.gov/drugs/new-drugs-fda-cders-new-molecular-entities-and-new-therapeutic-biological-products/novel-drug-approvals-2015

Fenske S, Krause SC, Hassan SI, Becirovic E, Auer F, Bernard R, Kupatt C, Lange P, Ziegler T, Wotjak CT, Zhang H, Hammelmann V, Paparizos C, Biel M, Wahl-Schott CA. Sick sinus syndrome in HCN1-deficient mice. Circulation. 2013 Dec 17;128(24):2585-94. doi: 10.1161/CIRCULATIONAHA.113.003712.

Feric NT, Radisic M. Maturing human pluripotent stem cell-derived cardiomyocytes in human engineered cardiac tissues. Adv Drug Deliv Rev. 2016 Jan 15;96:110-34. doi: 10.1016/j.addr.2015.04.019.

Flynn GE, Black KD, Islas LD, Sankaran B, Zagotta WN. Structure and rearrangements in the carboxy-terminal region of SpIH channels. Structure. 2007 Jun;15(6):671-82. doi: 10.1016/j.str.2007.04.008.

Flynn GE, Zagotta WN. Insights into the molecular mechanism for hyperpolarization-dependent activation of HCN channels. Proc Natl Acad Sci U S A. 2018 Aug 21;115(34):E8086-E8095. doi: 10.1073/pnas.1805596115.

Fontes JA, Rose NR, Čiháková D. The varying faces of IL-6: From cardiac protection to cardiac failure. Cytokine. 2015 Jul;74(1):62-8. doi: 10.1016/j.cyto.2014.12.024.

Fox K, Ford I, Steg PG, Tardif JC, Tendera M, Ferrari R; SIGNIFY Investigators. Ivabradine in stable coronary artery disease without clinical heart failure. N Engl J Med. 2014 Sep 18;371(12):1091-9. doi: 10.1056/NEJMoa1406430.

Fox K, Ford I, Steg PG, Tendera M, Ferrari R; BEAUTIFUL Investigators. Ivabradine for patients with stable coronary artery disease and left-ventricular systolic dysfunction (BEAUTIFUL): a randomised, double-blind, placebo-controlled trial. Lancet. 2008 Sep 6;372(9641):807-16. doi: 10.1016/S0140-6736(08)61170-8.

Freemantle N, Cleland J, Young P, Mason J, Harrison J. beta Blockade after myocardial infarction: systematic review and meta regression analysis. BMJ. 1999 Jun 26;318(7200):1730-7. doi: 10.1136/bmj.318.7200.1730.

Frishman WH, Pepine CJ, Weiss RJ, Baiker WM. Addition of zatebradine, a direct sinus node inhibitor, provides no greater exercise tolerance benefit in patients with angina taking extended-release nifedipine: results of a multicenter, randomized, double-blind, placebo-controlled, parallel-group study. The Zatebradine Study Group. J Am Coll Cardiol. 1995 Aug;26(2):305-12. doi: 10.1016/0735-1097(95)80000-7.

Fürst O, D'Avanzo N. Isoform dependent regulation of human HCN channels by cholesterol. Sci Rep. 2015 Sep 25;5:14270. doi: 10.1038/srep14270.

Gao LL, McMullan S, Djouhri L, Acosta C, Harper AA, Lawson SN. Expression and properties of hyperpolarization-activated current in rat dorsal root ganglion neurons with known sensory function. J Physiol. 2012 Oct 1;590(19):4691-705. doi: 10.1113/jphysiol.2012.238485.

Garreta E, Sanchez S, Lajara J, Montserrat N, Belmonte JCI. Roadblocks in the Path of iPSC to the Clinic. Curr Transplant Rep. 2018;5(1):14-18. doi: 10.1007/s40472-018-0177-x.

Gasparini S, DiFrancesco D. Action of the hyperpolarization-activated current (Ih) blocker ZD 7288 in hippocampal CA1 neurons. Pflugers Arch. 1997 Dec;435(1):99-106. doi: 10.1007/s004240050488.

Gauss R, Seifert R, Kaupp UB. Molecular identification of a hyperpolarization-activated channel in sea urchin sperm. Nature. 1998 Jun 11;393(6685):583-7. doi: 10.1038/31248.

Gibson JK, Yue Y, Bronson J, Palmer C, Numann R. Human stem cell-derived cardiomyocytes detect drug-mediated changes in action potentials and ion currents. J Pharmacol Toxicol Methods. 2014 Nov-Dec;70(3):255-67. doi: 10.1016/j.vascn.2014.09.005.

Giocomo LM, Hasselmo ME. Knock-out of HCN1 subunit flattens dorsal-ventral frequency gradient of medial entorhinal neurons in adult mice. J Neurosci. 2009 Jun 10;29(23):7625-30. doi: 10.1523/JNEUROSCI.0609-09.2009.

Giocomo LM, Hussaini SA, Zheng F, Kandel ER, Moser MB, Moser EI. Grid cells use HCN1 channels for spatial scaling. Cell. 2011 Nov 23;147(5):1159-70. doi: 10.1016/j.cell.2011.08.051.

Gold MS, Reichling DB, Shuster MJ, Levine JD. Hyperalgesic agents increase a tetrodotoxin-resistant Na+ current in nociceptors. Proc Natl Acad Sci U S A. 1996 Feb 6;93(3):1108-12. doi: 10.1073/pnas.93.3.1108.

Gravante B, Barbuti A, Milanesi R, Zappi I, Viscomi C, DiFrancesco D. Interaction of the pacemaker channel HCN1 with filamin A. J Biol Chem. 2004 Oct 15;279(42):43847-53. doi: 10.1074/jbc.M401598200.

Hagiwara Y, Miyoshi S, Fukuda K, Nishiyama N, Ikegami Y, Tanimoto K, Murata M, Takahashi E, Shimoda K, Hirano T, Mitamura H, Ogawa S. SHP2-mediated signaling cascade through gp130 is essential for LIF-dependent I CaL, [Ca2+]i transient, and APD increase in cardiomyocytes. J Mol Cell Cardiol. 2007 Dec;43(6):710-6. doi: 10.1016/j.yjmcc.2007.09.004.

Hanna A, Frangogiannis NG. Inflammatory Cytokines and Chemokines as Therapeutic Targets in Heart Failure. Cardiovasc Drugs Ther. 2020 Dec;34(6):849-863. doi: 10.1007/s10557-020-07071-0.

Harnett MT, Magee JC, Williams SR. Distribution and function of HCN channels in the apical dendritic tuft of neocortical pyramidal neurons. J Neurosci. 2015 Jan 21;35(3):1024-37. doi: 10.1523/JNEUROSCI.2813-14.2015.

Hawkins VE, Hawryluk JM, Takakura AC, Tzingounis AV, Moreira TS, Mulkey DK. HCN channels contribute to serotonergic modulation of ventral surface chemosensitive neurons and respiratory activity. J Neurophysiol. 2015 Feb 15;113(4):1195-205. doi: 10.1152/jn.00487.2014.

He C, Chen F, Li B, Hu Z. Neurophysiology of HCN channels: from cellular functions to multiple regulations. Prog Neurobiol. 2014 Jan;112:1-23. doi: 10.1016/j.pneurobio.2013.10.001.

He JT, Li XY, Zhao X, Liu X. Hyperpolarization-activated and cyclic nucleotide-gated channel proteins as emerging new targets in neuropathic pain. Rev Neurosci. 2019 Jul 26;30(6):639-649. doi: 10.1515/revneuro-2018-0094.

Heinrich PC, Behrmann I, Haan S, Hermanns HM, Müller-Newen G, Schaper F. Principles of interleukin (IL)-6-type cytokine signalling and its regulation. Biochem J. 2003 Aug 15;374(Pt 1):1-20. doi: 10.1042/BJ20030407.

Herrmann S, Hofmann F, Stieber J, Ludwig A. HCN channels in the heart: lessons from mouse mutants. Br J Pharmacol. 2012 May;166(2):501-9. doi: 10.1111/j.1476-5381.2011.01798.x.

Herrmann S, Schnorr S, Ludwig A. HCN channels--modulators of cardiac and neuronal excitability. Int J Mol Sci. 2015 Jan 8;16(1):1429-47. doi: 10.3390/ijms16011429.

Hirano T, Nakajima K, Hibi M. Signaling mechanisms through gp130: a model of the cytokine system. Cytokine Growth Factor Rev. 1997 Dec;8(4):241-52. doi: 10.1016/s1359-6101(98)80005-1.

Hoekstra M, Mummery CL, Wilde AA, Bezzina CR, Verkerk AO. Induced pluripotent stem cell derived cardiomyocytes as models for cardiac arrhythmias. Front Physiol. 2012 Aug 31;3:346. doi: 10.3389/fphys.2012.00346.

Hoppe UC, Jansen E, Südkamp M, Beuckelmann DJ. Hyperpolarization-activated inward current in ventricular myocytes from normal and failing human hearts. Circulation. 1998 Jan 6-13;97(1):55-65. doi: 10.1161/01.cir.97.1.55.

Horváth A, Lemoine MD, Löser A, Mannhardt I, Flenner F, Uzun AU, Neuber C, Breckwoldt K, Hansen A, Girdauskas E, Reichenspurner H, Willems S, Jost N, Wettwer E, Eschenhagen T, Christ T. Low Resting Membrane Potential and Low Inward Rectifier Potassium Currents Are Not Inherent Features of hiPSC-Derived Cardiomyocytes. Stem Cell Reports. 2018 Mar 13;10(3):822-833. doi: 10.1016/j.stemcr.2018.01.012.

Hu YF, Chen YJ, Lin YJ, Chen SA. Inflammation and the pathogenesis of atrial fibrillation. Nat Rev Cardiol. 2015 Apr;12(4):230-43. doi: 10.1038/nrcardio.2015.2.

Huang Z, Lujan R, Kadurin I, Uebele VN, Renger JJ, Dolphin AC, Shah MM. Presynaptic HCN1 channels regulate Cav3.2 activity and neurotransmission at select cortical synapses. Nat Neurosci. 2011 Apr;14(4):478-86. doi: 10.1038/nn.2757.

Huo S, Shi W, Ma H, Yan D, Luo P, Guo J, Li C, Lin J, Zhang C, Li S, Lv J, Lin L. Alleviation of Inflammation and Oxidative Stress in Pressure Overload-Induced Cardiac Remodeling and Heart Failure via IL-6/STAT3 Inhibition by Raloxifene. Oxid Med Cell Longev. 2021 Mar 20;2021:6699054. doi: 10.1155/2021/6699054.

Hutcheon B, Miura RM, Puil E. Models of subthreshold membrane resonance in neocortical neurons. J Neurophysiol. 1996 Aug;76(2):698-714. doi: 10.1152/jn.1996.76.2.698.

Hwang HS, Kryshtal DO, Feaster TK, Sánchez-Freire V, Zhang J, Kamp TJ, Hong CC, Wu JC, Knollmann BC. Comparable calcium handling of human iPSC-derived cardiomyocytes generated by multiple laboratories. J Mol Cell Cardiol. 2015 Aug;85:79-88. doi: 10.1016/j.yjmcc.2015.05.003.

Ingram SL, Williams JT. Opioid inhibition of Ih via adenylyl cyclase. Neuron. 1994 Jul;13(1):179-86. doi: 10.1016/0896-6273(94)90468-5.

Ip RJ, Ali A, Baloch ZQ, Al-Abcha A, Jacob C, Arnautovic J, Boumegouas M, Do S, Meka K, Wilcox M, Ip J. Atrial Fibrillation as a Predictor of Mortality in High Risk COVID-19 Patients: A Multicentre Study of 171 Patients. Heart Lung Circ. 2021 Aug;30(8):1151-1156. doi: 10.1016/j.hlc.2021.02.010.

Ishii TM, Takano M, Xie LH, Noma A, Ohmori H. Molecular characterization of the hyperpolarization-activated cation channel in rabbit heart sinoatrial node. J Biol Chem. 1999 Apr 30;274(18):12835-9. doi: 10.1074/jbc.274.18.12835.

Itzhaki I, Maizels L, Huber I, Zwi-Dantsis L, Caspi O, Winterstern A, Feldman O, Gepstein A, Arbel G, Hammerman H, Boulos M, Gepstein L. Modelling the long QT syndrome with induced pluripotent stem cells. Nature. 2011 Mar 10;471(7337):225-9. doi: 10.1038/nature09747.

Ivanova E, Müller F. Retinal bipolar cell types differ in their inventory of ion channels. Vis Neurosci. 2006 Mar-Apr;23(2):143-54. doi: 10.1017/S0952523806232048.

Jiang Y, Park P, Hong SM, Ban K. Maturation of Cardiomyocytes Derived from Human Pluripotent Stem Cells: Current Strategies and Limitations. Mol Cells. 2018 Jul 31;41(7):613-621. doi: 10.14348/molcells.2018.0143.

Kajstura J, Cigola E, Malhotra A, Li P, Cheng W, Meggs LG, Anversa P. Angiotensin II induces apoptosis of adult ventricular myocytes in vitro. J Mol Cell Cardiol. 1997 Mar;29(3):859-70. doi: 10.1006/jmcc.1996.0333.

Karakikes I, Ameen M, Termglinchan V, Wu JC. Human induced pluripotent stem cell-derived cardiomyocytes: insights into molecular, cellular, and functional phenotypes. Circ Res. 2015 Jun 19;117(1):80-8. doi: 10.1161/CIRCRESAHA.117.305365.

Karakikes I, Senyei GD, Hansen J, Kong CW, Azeloglu EU, Stillitano F, Lieu DK, Wang J, Ren L, Hulot JS, Iyengar R, Li RA, Hajjar RJ. Small molecule-mediated directed differentiation of human embryonic stem cells toward ventricular cardiomyocytes. Stem Cells Transl Med. 2014 Jan;3(1):18-31. doi: 10.5966/sctm.2013-0110.

Kase D, Imoto K. The Role of HCN Channels on Membrane Excitability in the Nervous System. J Signal Transduct. 2012;2012:619747. doi: 10.1155/2012/619747.

Keung W, Boheler KR, Li RA. Developmental cues for the maturation of metabolic, electrophysiological and calcium handling properties of human pluripotent stem cell-derived cardiomyocytes. Stem Cell Res Ther. 2014 Jan 28;5(1):17. doi: 10.1186/scrt406.

Kim S, Iwao H. Molecular and cellular mechanisms of angiotensin II-mediated cardiovascular and renal diseases. Pharmacol Rev. 2000 Mar;52(1):11-34.

Kim YK, Na KS, Myint AM, Leonard BE. The role of pro-inflammatory cytokines in neuroinflammation, neurogenesis and the neuroendocrine system in major depression. Prog Neuropsychopharmacol Biol Psychiatry. 2016 Jan 4;64:277-84. doi: 10.1016/j.pnpbp.2015.06.008.

Kimura K, Kitano J, Nakajima Y, Nakanishi S. Hyperpolarization-activated, cyclic nucleotide-gated HCN2 cation channel forms a protein assembly with multiple neuronal scaffold proteins in distinct modes of protein-protein interaction. Genes Cells. 2004 Jul;9(7):631-40. doi: 10.1111/j.1356-9597.2004.00752.x.

Kitano J, Yamazaki Y, Kimura K, Masukado T, Nakajima Y, Nakanishi S. Tamalin is a scaffold protein that interacts with multiple neuronal proteins in distinct modes of protein-protein association. J Biol Chem. 2003 Apr 25;278(17):14762-8. doi: 10.1074/jbc.M300184200.

Klimas A, Ambrosi CM, Yu J, Williams JC, Bien H, Entcheva E. OptoDyCE as an automated system for high-throughput all-optical dynamic cardiac electrophysiology. Nat Commun. 2016 May 10;7:11542. doi: 10.1038/ncomms11542.

Knollmann BC. Induced pluripotent stem cell-derived cardiomyocytes: boutique science or valuable arrhythmia model? Circ Res. 2013 Mar 15;112(6):969-76; discussion 976. doi: 10.1161/CIRCRESAHA.112.300567.

Ko KW, Rasband MN, Meseguer V, Kramer RH, Golding NL. Serotonin modulates spike probability in the axon initial segment through HCN channels. Nat Neurosci. 2016 Jun;19(6):826-34. doi: 10.1038/nn.4293.

Kondapuram M, Frieg B, Yüksel S, Schwabe T, Sattler C, Lelle M, Schweinitz A, Schmauder R, Benndorf K, Gohlke H, Kusch J. Functional and structural characterization of interactions between opposite subunits in HCN pacemaker channels. Commun Biol. 2022 May 9;5(1):430. doi: 10.1038/s42003-022-03360-6.

Kourliouros A, Savelieva I, Kiotsekoglou A, Jahangiri M, Camm J. Current concepts in the pathogenesis of atrial fibrillation. Am Heart J. 2009 Feb;157(2):243-52. doi: 10.1016/j.ahj.2008.10.009.

Kumar V, Cotran RS, Robbins SL. Basic Pathology Robbins. 2003. Saunders

Lam CK, Wu JC. Disease modelling and drug discovery for hypertrophic cardiomyopathy using pluripotent stem cells: how far have we come? Eur Heart J. 2018 Nov 14;39(43):3893-3895. doi: 10.1093/eurheartj/ehy388.

Lazzerini PE, Accioli R, Acampa M, Zhang WH, Verrengia D, Cartocci A, Bacarelli MR, Xin X, Salvini V, Chen KS, Salvadori F, D'errico A, Bisogno S, Cevenini G, Marzotti T, Capecchi M, Laghi-Pasini F, Chen L, Capecchi PL, Boutjdir M. Interleukin-6 Elevation Is a Key Pathogenic Factor Underlying COVID-19-Associated Heart Rate-Corrected QT Interval Prolongation. Front Cardiovasc Med. 2022 May 19;9:893681. doi: 10.3389/fcvm.2022.893681.

Lazzerini PE, Boutjdir M, Capecchi PL. COVID-19, Arrhythmic Risk, and Inflammation: Mind the Gap! Circulation. 2020 Jul 7;142(1):7-9. doi: 10.1161/CIRCULATIONAHA.120.047293.

Lazzerini PE, Capecchi PL, Laghi-Pasini F. Systemic inflammation and arrhythmic risk: lessons from rheumatoid arthritis. Eur Heart J. 2017 Jun 7;38(22):1717-1727. doi: 10.1093/eurheartj/ehw208.

Lazzerini PE, Laghi-Pasini F, Acampa M, Srivastava U, Bertolozzi I, Giabbani B, Finizola F, Vanni F, Dokollari A, Natale M, Cevenini G, Selvi E, Migliacci N, Maccherini M, Boutjdir M, Capecchi PL. Systemic Inflammation Rapidly Induces Reversible Atrial Electrical Remodeling: The Role of Interleukin-6-Mediated Changes in Connexin Expression. J Am Heart Assoc. 2019 Aug 20;8(16):e011006. doi: 10.1161/JAHA.118.011006.

Lazzerini PE, Laghi-Pasini F, Boutjdir M, Capecchi PL. Inflammatory cytokines and cardiac arrhythmias: the lesson from COVID-19. Nat Rev Immunol. 2022 May;22(5):270-272. doi: 10.1038/s41577-022-00714-3.

Lee CH, MacKinnon R. Structures of the Human HCN1 Hyperpolarization-Activated Channel. Cell. 2017 Jan 12;168(1-2):111-120.e11. doi: 10.1016/j.cell.2016.12.023.

Lemoine MD, Krause T, Koivumäki JT, Prondzynski M, Schulze ML, Girdauskas E, Willems S, Hansen A, Eschenhagen T, Christ T. Human Induced Pluripotent Stem Cell-Derived Engineered Heart Tissue as a Sensitive Test System for QT Prolongation and Arrhythmic Triggers. Circ Arrhythm Electrophysiol. 2018 Jul;11(7):e006035. doi: 10.1161/CIRCEP.117.006035.

Lemoine MD, Mannhardt I, Breckwoldt K, Prondzynski M, Flenner F, Ulmer B, Hirt MN, Neuber C, Horváth A, Kloth B, Reichenspurner H, Willems S, Hansen A, Eschenhagen T, Christ T. Human iPSC-derived cardiomyocytes cultured in 3D engineered heart tissue show physiological

upstroke velocity and sodium current density. Sci Rep. 2017 Jul 14;7(1):5464. doi: 10.1038/s41598-017-05600-w.

León-Aparicio D, Salvador C, Aparicio-Trejo OE, Briones-Herrera A, Pedraza-Chaverri J, Vaca L, Sampieri A, Padilla-Flores T, López-González Z, León-Contreras JC, Hernández-Pando R, Escobar LI. Novel Potassium Channels in Kidney Mitochondria: The Hyperpolarization-Activated and Cyclic Nucleotide-Gated HCN Channels. Int J Mol Sci. 2019 Oct 9;20(20):4995. doi: 10.3390/ijms20204995.

Lewandowski J, Rozwadowska N, Kolanowski TJ, Malcher A, Zimna A, Rugowska A, Fiedorowicz K, Łabędź W, Kubaszewski Ł, Chojnacka K, Bednarek-Rajewska K, Majewski P, Kurpisz M. The impact of in vitro cell culture duration on the maturation of human cardiomyocytes derived from induced pluripotent stem cells of myogenic origin. Cell Transplant. 2018 Jul;27(7):1047-1067. doi: 10.1177/0963689718779346.

Lewis AS, Chetkovich DM. HCN channels in behavior and neurological disease: too hyper or not active enough? Mol Cell Neurosci. 2011 Feb;46(2):357-67. doi: 10.1016/j.mcn.2010.11.007.

Li M, Kanda Y, Ashihara T, Sasano T, Nakai Y, Kodama M, Hayashi E, Sekino Y, Furukawa T, Kurokawa J. Overexpression of KCNJ2 in induced pluripotent stem cell-derived cardiomyocytes for the assessment of QT-prolonging drugs. J Pharmacol Sci. 2017 Jun;134(2):75-85. doi: 10.1016/j.jphs.2017.05.004.

Li CH, Zhang Q, Teng B, Mustafa SJ, Huang JY, Yu HG. Src tyrosine kinase alters gating of hyperpolarization-activated HCN4 pacemaker channel through Tyr531. Am J Physiol Cell Physiol. 2008 Jan;294(1):C355-62. doi: 10.1152/ajpcell.00236.2007.

Lieu DK, Liu J, Siu CW, McNerney GP, Tse HF, Abu-Khalil A, Huser T, Li RA. Absence of transverse tubules contributes to non-uniform Ca(2+) wavefronts in mouse and human embryonic stem cell-derived cardiomyocytes. Stem Cells Dev. 2009 Dec;18(10):1493-500. doi: 10.1089/scd.2009.0052.

Lörincz A, Notomi T, Tamás G, Shigemoto R, Nusser Z. Polarized and compartment-dependent distribution of HCN1 in pyramidal cell dendrites. Nat Neurosci. 2002 Nov;5(11):1185-93. doi: 10.1038/nn962.

Ludwig A, Budde T, Stieber J, Moosmang S, Wahl C, Holthoff K, Langebartels A, Wotjak C, Munsch T, Zong X, Feil S, Feil R, Lancel M, Chien KR, Konnerth A, Pape HC, Biel M, Hofmann F. Absence epilepsy and sinus dysrhythmia in mice lacking the pacemaker channel HCN2. EMBO J. 2003 Jan 15;22(2):216-24. doi: 10.1093/emboj/cdg032.

Ludwig A, Zong X, Jeglitsch M, Hofmann F, Biel M. A family of hyperpolarization-activated mammalian cation channels. Nature. 1998 Jun 11;393(6685):587-91. doi: 10.1038/31255.

Ludwig A, Zong X, Stieber J, Hullin R, Hofmann F, Biel M. Two pacemaker channels from human heart with profoundly different activation kinetics. EMBO J. 1999 May 4;18(9):2323-9. doi: 10.1093/emboj/18.9.2323.

Lundy SD, Zhu WZ, Regnier M, Laflamme MA. Structural and functional maturation of cardiomyocytes derived from human pluripotent stem cells. Stem Cells Dev. 2013 Jul 15;22(14):1991-2002. doi: 10.1089/scd.2012.0490.

Luo L, Chang L, Brown SM, Ao H, Lee DH, Higuera ES, Dubin AE, Chaplan SR. Role of peripheral hyperpolarization-activated cyclic nucleotide-modulated channel pacemaker channels in acute and chronic pain models in the rat. Neuroscience. 2007 Feb 23;144(4):1477-85. doi: 10.1016/j.neuroscience.2006.10.048.

Luo P, Guo L (2015) HCN Channels: From the Role in Chronic Cerebral Hypoperfusion-Induced Cognitive Impairments to a New Therapeutic Target for Vascular Dementia. J Neurol Neurophysiol 6: 308. doi:10.4172/2155-9562.1000308

Lütticken C, Wegenka UM, Yuan J, Buschmann J, Schindler C, Ziemiecki A, Harpur AG, Wilks AF, Yasukawa K, Taga T, et al. Association of transcription factor APRF and protein kinase Jak1 with the interleukin-6 signal transducer gp130. Science. 1994 Jan 7;263(5143):89-92. doi: 10.1126/science.8272872.

Ma J, Guo L, Fiene SJ, Anson BD, Thomson JA, Kamp TJ, Kolaja KL, Swanson BJ, January CT. High purity human-induced pluripotent stem cell-derived cardiomyocytes: electrophysiological properties of action potentials and ionic currents. Am J Physiol Heart Circ Physiol. 2011 Nov;301(5):H2006-17. doi: 10.1152/ajpheart.00694.2011.

Maccaferri G, Mangoni M, Lazzari A, DiFrancesco D. Properties of the hyperpolarization-activated current in rat hippocampal CA1 pyramidal cells. J Neurophysiol. 1993 Jun;69(6):2129-36. doi: 10.1152/jn.1993.69.6.2129.

Maltsev VA, Lakatta EG. The funny current in the context of the coupled-clock pacemaker cell system. Heart Rhythm. 2012 Feb;9(2):302-7. doi: 10.1016/j.hrthm.2011.09.022.

Mandel Y, Weissman A, Schick R, Barad L, Novak A, Meiry G, Goldberg S, Lorber A, Rosen MR, Itskovitz-Eldor J, Binah O. Human embryonic and induced pluripotent stem cell-derived cardiomyocytes exhibit beat rate variability and power-law behavior. Circulation. 2012 Feb 21;125(7):883-93. doi: 10.1161/CIRCULATIONAHA.111.045146.

Männikkö R, Pandey S, Larsson HP, Elinder F. Hysteresis in the voltage dependence of HCN channels: conversion between two modes affects pacemaker properties. J Gen Physiol. 2005 Mar;125(3):305-26. doi: 10.1085/jgp.200409130.

Marcus GM, Whooley MA, Glidden DV, Pawlikowska L, Zaroff JG, Olgin JE. Interleukin-6 and atrial fibrillation in patients with coronary artery disease: data from the Heart and Soul Study. Am Heart J. 2008 Feb;155(2):303-9. doi: 10.1016/j.ahj.2007.09.006.

Marshall PW, Rouse W, Briggs I, Hargreaves RB, Mills SD, McLoughlin BJ. ICI D7288, a novel sinoatrial node modulator. J Cardiovasc Pharmacol. 1993 Jun;21(6):902-6. doi: 10.1097/00005344-199306000-00008.

Matsa E, Ahrens JH, Wu JC. Human Induced Pluripotent Stem Cells as a Platform for Personalized and Precision Cardiovascular Medicine. Physiol Rev. 2016 Jul;96(3):1093-126. doi: 10.1152/physrev.00036.2015.

McCormick DA, Pape HC. Noradrenergic and serotonergic modulation of a hyperpolarization-activated cation current in thalamic relay neurones. J Physiol. 1990a Dec;431:319-42. doi: 10.1113/jphysiol.1990.sp018332.

McCormick DA, Pape HC. Properties of a hyperpolarization-activated cation current and its role in rhythmic oscillation in thalamic relay neurones. J Physiol. 1990b Dec;431:291-318. doi: 10.1113/jphysiol.1990.sp018331.

Medzhitov R. Origin and physiological roles of inflammation. Nature. 2008 Jul 24;454(7203):428-35. doi: 10.1038/nature07201.

Melchiorre M, Del Lungo M, Guandalini L, Martini E, Dei S, Manetti D, Scapecchi S, Teodori E, Sartiani L, Mugelli A, Cerbai E, Romanelli MN. Design, synthesis, and preliminary biological evaluation of new isoform-selective f-current blockers. J Med Chem. 2010 Sep 23;53(18):6773-7. doi: 10.1021/jm1006758.

Mengesha HG, Tafesse TB, Bule MH. If Channel as an Emerging Therapeutic Target for Cardiovascular Diseases: A Review of Current Evidence and Controversies. Front Pharmacol. 2017 Nov 24;8:874. doi: 10.3389/fphar.2017.00874.

Metcalf D. Leukemia inhibitory factor--a puzzling polyfunctional regulator. Growth Factors. 1992;7(3):169-73. doi: 10.3109/08977199209046921.

Michels G, Er F, Khan IF, Endres-Becker J, Brandt MC, Gassanov N, Johns DC, Hoppe UC. K+ channel regulator KCR1 suppresses heart rhythm by modulating the pacemaker current If. PLoS One. 2008 Jan 30;3(1):e1511. doi: 10.1371/journal.pone.0001511. Erratum in: PLoS One. 2012;7(8): doi/10.1371/annotation/ff27c2a4-7732-4c32-88da-c412f1cced0c.

Michels G, Herzig S, Hoppe UC. Levosimendan [Levosimendan]. Dtsch Med Wochenschr. 2005 Oct 28;130(43):2444-6. German. doi: 10.1055/s-2005-918588.

Mihara M, Hashizume M, Yoshida H, Suzuki M, Shiina M. IL-6/IL-6 receptor system and its role in physiological and pathological conditions. Clin Sci (Lond). 2012 Feb;122(4):143-59. doi: 10.1042/CS20110340.

Mihara M, Nishimoto N, Ohsugi Y. The therapy of autoimmune diseases by anti-interleukin-6 receptor antibody. Expert Opin Biol Ther. 2005 May;5(5):683-90. doi: 10.1517/14712598.5.5.683.

Mistrík P, Pfeifer A, Biel M. The enhancement of HCN channel instantaneous current facilitated by slow deactivation is regulated by intracellular chloride concentration. Pflugers Arch. 2006 Sep;452(6):718-27. doi: 10.1007/s00424-006-0095-0.

Mittal N, Dave J, Harakalova M, van Tintelen JP, Asselbergs FW, Doevendans PA, Costa KD, Turnbull IC, Stillitano F. Generation of human induced pluripotent stem cell (iPSC) lines derived from five patients carrying the pathogenic phospholamban-R14del (PLN-R14del) variant and

three non-carrier family members. Stem Cell Res. 2022 Apr;60:102737. doi: 10.1016/j.scr.2022.102737.

Moehle EA, Rock JM, Lee YL, Jouvenot Y, DeKelver RC, Gregory PD, Urnov FD, Holmes MC. Targeted gene addition into a specified location in the human genome using designed zinc finger nucleases. Proc Natl Acad Sci U S A. 2007 Feb 27;104(9):3055-60. doi: 10.1073/pnas.0611478104.

Momin A, Cadiou H, Mason A, McNaughton PA. Role of the hyperpolarization-activated current Ih in somatosensory neurons. J Physiol. 2008 Dec 15;586(24):5911-29. doi: 10.1113/jphysiol.2008.163154.

Monnerat G, Alarcón ML, Vasconcellos LR, Hochman-Mendez C, Brasil G, Bassani RA, Casis O, Malan D, Travassos LH, Sepúlveda M, Burgos JI, Vila-Petroff M, Dutra FF, Bozza MT, Paiva CN, Carvalho AB, Bonomo A, Fleischmann BK, de Carvalho ACC, Medei E. Macrophage-dependent IL-1β production induces cardiac arrhythmias in diabetic mice. Nat Commun. 2021 Dec 8;12(1):7261. doi: 10.1038/s41467-021-27508-w.

Moosmang S, Stieber J, Zong X, Biel M, Hofmann F, Ludwig A. Cellular expression and functional characterization of four hyperpolarization-activated pacemaker channels in cardiac and neuronal tissues. Eur J Biochem. 2001 Mar;268(6):1646-52. doi: 10.1046/j.1432-1327.2001.02036.x.

Moroni A, Barbuti A, Altomare C, Viscomi C, Morgan J, Baruscotti M, DiFrancesco D. Kinetic and ionic properties of the human HCN2 pacemaker channel. Pflugers Arch. 2000 Mar;439(5):618-26. doi: 10.1007/s004249900225.

Moser MB, Rowland DC, Moser EI. Place cells, grid cells, and memory. Cold Spring Harb Perspect Biol. 2015 Feb 2;7(2):a021808. doi: 10.1101/cshperspect.a021808.

Much B, Wahl-Schott C, Zong X, Schneider A, Baumann L, Moosmang S, Ludwig A, Biel M. Role of subunit heteromerization and N-linked glycosylation in the formation of functional hyperpolarization-activated cyclic nucleotide-gated channels. J Biol Chem. 2003 Oct 31;278(44):43781-6. doi: 10.1074/jbc.M306958200.

Mussolino C, Morbitzer R, Lütge F, Dannemann N, Lahaye T, Cathomen T. A novel TALE nuclease scaffold enables high genome editing activity in combination with low toxicity. Nucleic Acids Res. 2011 Nov;39(21):9283-93. doi: 10.1093/nar/gkr597.

Naka T, Narazaki M, Hirata M, Matsumoto T, Minamoto S, Aono A, Nishimoto N, Kajita T, Taga T, Yoshizaki K, Akira S, Kishimoto T. Structure and function of a new STAT-induced STAT inhibitor. Nature. 1997 Jun 26;387(6636):924-9. doi: 10.1038/43219.

Nathan C. Points of control in inflammation. Nature. 2002 Dec 19-26;420(6917):846-52. doi: 10.1038/nature01320.

Nazzari H, Angoli D, Chow SS, Whitaker G, Leclair L, McDonald E, Macri V, Zahynacz K, Walker V, Accili EA. Regulation of cell surface expression of functional pacemaker channels by a motif

in the B-helix of the cyclic nucleotide-binding domain. Am J Physiol Cell Physiol. 2008 Sep;295(3):C642-52. doi: 10.1152/ajpcell.00062.2008.

Nerbonne JM, Kass RS. Molecular physiology of cardiac repolarization. Physiol Rev. 2005 Oct;85(4):1205-53. doi: 10.1152/physrev.00002.2005.

Noam Y, Ehrengruber MU, Koh A, Feyen P, Manders EM, Abbott GW, Wadman WJ, Baram TZ. Filamin A promotes dynamin-dependent internalization of hyperpolarization-activated cyclic nucleotide-gated type 1 (HCN1) channels and restricts Ih in hippocampal neurons. J Biol Chem. 2014 Feb 28;289(9):5889-903. doi: 10.1074/jbc.M113.522060.

Noble D, Tsien RW. The kinetics and rectifier properties of the slow potassium current in cardiac Purkinje fibres. J Physiol. 1968 Mar;195(1):185-214. doi: 10.1113/jphysiol.1968.sp008454.

Nolan MF, Malleret G, Dudman JT, Buhl DL, Santoro B, Gibbs E, Vronskaya S, Buzsáki G, Siegelbaum SA, Kandel ER, Morozov A. A behavioral role for dendritic integration: HCN1 channels constrain spatial memory and plasticity at inputs to distal dendrites of CA1 pyramidal neurons. Cell. 2004 Nov 24;119(5):719-32. doi: 10.1016/j.cell.2004.11.020.

Nolan MF, Malleret G, Lee KH, Gibbs E, Dudman JT, Santoro B, Yin D, Thompson RF, Siegelbaum SA, Kandel ER, Morozov A. The hyperpolarization-activated HCN1 channel is important for motor learning and neuronal integration by cerebellar Purkinje cells. Cell. 2003 Nov 26;115(5):551-64. doi: 10.1016/s0092-8674(03)00884-5.

Noma A. Ionic mechanisms of the cardiac pacemaker potential. Jpn Heart J. 1996 Sep;37(5):673-82. doi: 10.1536/ihj.37.673.

Nunes SS, Miklas JW, Liu J, Aschar-Sobbi R, Xiao Y, Zhang B, Jiang J, Massé S, Gagliardi M, Hsieh A, Thavandiran N, Laflamme MA, Nanthakumar K, Gross GJ, Backx PH, Keller G, Radisic M. Biowire: a platform for maturation of human pluripotent stem cell-derived cardiomyocytes. Nat Methods. 2013 Aug;10(8):781-7. doi: 10.1038/nmeth.2524.

Opthof T. The membrane current (I(f)) in human atrial cells: implications for atrial arrhythmias. Cardiovasc Res. 1998 Jun;38(3):537-40. doi: 10.1016/s0008-6363(98)00089-3.

Pape HC. Queer current and pacemaker: the hyperpolarization-activated cation current in neurons. Annu Rev Physiol. 1996;58:299-327. doi: 10.1146/annurev.ph.58.030196.001503.

Papp I, Holló K, Antal M. Plasticity of hyperpolarization-activated and cyclic nucleotid-gated cation channel subunit 2 expression in the spinal dorsal horn in inflammatory pain. Eur J Neurosci. 2010 Oct;32(7):1193-201. doi: 10.1111/j.1460-9568.2010.07370.x.

Pian P, Bucchi A, Robinson RB, Siegelbaum SA. Regulation of gating and rundown of HCN hyperpolarization-activated channels by exogenous and endogenous PIP2. J Gen Physiol. 2006 Nov;128(5):593-604. doi: 10.1085/jgp.200609648.

Pioner JM, Santini L, Palandri C, Martella D, Lupi F, Langione M, Querceto S, Grandinetti B, Balducci V, Benzoni P, Landi S, Barbuti A, Ferrarese Lupi F, Boarino L, Sartiani L, Tesi C, Mack DL, Regnier M, Cerbai E, Parmeggiani C, Poggesi C, Ferrantini C, Coppini R. Optical Investigation

of Action Potential and Calcium Handling Maturation of hiPSC-Cardiomyocytes on Biomimetic Substrates. Int J Mol Sci. 2019 Aug 3;20(15):3799. doi: 10.3390/ijms20153799.

Porciatti F, Pelzmann B, Cerbai E, Schaffer P, Pino R, Bernhart E, Koidl B, Mugelli A. The pacemaker current I(f) in single human atrial myocytes and the effect of beta-adrenoceptor and A1-adenosine receptor stimulation. Br J Pharmacol. 1997 Nov;122(5):963-9. doi: 10.1038/sj.bjp.0701473.

Postea O, Biel M. Exploring HCN channels as novel drug targets. Nat Rev Drug Discov. 2011 Nov 18;10(12):903-14. doi: 10.1038/nrd3576.

Pourrier M, Fedida D. The Emergence of Human Induced Pluripotent Stem Cell-Derived Cardiomyocytes (hiPSC-CMs) as a Platform to Model Arrhythmogenic Diseases. Int J Mol Sci. 2020 Jan 19;21(2):657. doi: 10.3390/ijms21020657.

Proenza C, Angoli D, Agranovich E, Macri V, Accili EA. Pacemaker channels produce an instantaneous current. J Biol Chem. 2002 Feb 15;277(7):5101-9. doi: 10.1074/jbc.M106974200.

Protze SI, Liu J, Nussinovitch U, Ohana L, Backx PH, Gepstein L, Keller GM. Sinoatrial node cardiomyocytes derived from human pluripotent cells function as a biological pacemaker. Nat Biotechnol. 2017 Jan;35(1):56-68. doi: 10.1038/nbt.3745.

Ramírez D, Zúñiga R, Concha G, Zúñiga L. HCN Channels: New Therapeutic Targets for Pain Treatment. Molecules. 2018 Aug 21;23(9):2094. doi: 10.3390/molecules23092094.

Ravens U, Cerbai E. Role of potassium currents in cardiac arrhythmias. Europace. 2008 Oct;10(10):1133-7. doi: 10.1093/europace/eun193.

Renwick J, Kerr C, McTaggart R, Yeung J. Cardiac electrophysiology and conduction pathway ablation. Can J Anaesth. 1993 Nov;40(11):1053-64. doi: 10.1007/BF03009477.

Resta F, Micheli L, Laurino A, Spinelli V, Mello T, Sartiani L, Di Cesare Mannelli L, Cerbai E, Ghelardini C, Romanelli MN, Mannaioni G, Masi A. Selective HCN1 block as a strategy to control oxaliplatin-induced neuropathy. Neuropharmacology. 2018 Mar 15;131:403-413. doi: 10.1016/j.neuropharm.2018.01.014.

Ribeiro AJS, Guth BD, Engwall M, Eldridge S, Foley CM, Guo L, Gintant G, Koerner J, Parish ST, Pierson JB, Brock M, Chaudhary KW, Kanda Y, Berridge B. Considerations for an In Vitro, Cell-Based Testing Platform for Detection of Drug-Induced Inotropic Effects in Early Drug Development. Part 2: Designing and Fabricating Microsystems for Assaying Cardiac Contractility With Physiological Relevance Using Human iPSC-Cardiomyocytes. Front Pharmacol. 2019 Aug 29;10:934. doi: 10.3389/fphar.2019.00934.

Robinson RB, Brink PR, Cohen IS, Rosen MR. I(f) and the biological pacemaker. Pharmacol Res. 2006 May;53(5):407-15. doi: 10.1016/j.phrs.2006.03.007.

Robinson RB, Siegelbaum SA. Hyperpolarization-activated cation currents: from molecules to physiological function. Annu Rev Physiol. 2003;65:453-80. doi: 10.1146/annurev.physiol.65.092101.142734.

Robinson RB, Yu H, Chang F, Cohen IS. Developmental change in the voltage-dependence of the pacemaker current, if, in rat ventricle cells. Pflugers Arch. 1997 Feb;433(4):533-5. doi: 10.1007/s004240050309.

Romanelli MN, Del Lungo M, Guandalini L, Zobeiri M, Gyökeres A, Árpádffy-Lovas T, Koncz I, Sartiani L, Bartolucci G, Dei S, Manetti D, Teodori E, Budde T, Cerbai E. EC18 as a Tool To Understand the Role of HCN4 Channels in Mediating Hyperpolarization-Activated Current in Tissues. ACS Med Chem Lett. 2019 Feb 6;10(4):584-589. doi: 10.1021/acsmedchemlett.8b00587.

Romanelli MN, Cerbai E, Dei S, Guandalini L, Martelli C, Martini E, Scapecchi S, Teodori E, Mugelli A. Design, synthesis and preliminary biological evaluation of zatebradine analogues as potential blockers of the hyperpolarization-activated current. Bioorg Med Chem. 2005 Feb 15;13(4):1211-20. doi: 10.1016/j.bmc.2004.11.017.

Romanelli MN, Sartiani L, Masi A, Mannaioni G, Manetti D, Mugelli A, Cerbai E. HCN Channels Modulators: The Need for Selectivity. Curr Top Med Chem. 2016;16(16):1764-91. doi: 10.2174/1568026616999160315130832.

Roşianu ŞH, Roşianu AN, Aldica M, Căpâlneanu R, Buzoianu AD. Inflammatory markers in paroxysmal atrial fibrillation and the protective role of renin-angiotensin-aldosterone system inhibitors. Clujul Med. 2013;86(3):217-21. Epub 2013 Aug 5.

Rothberg BS, Shin KS, Phale PS, Yellen G. Voltage-controlled gating at the intracellular entrance to a hyperpolarization-activated cation channel. J Gen Physiol. 2002 Jan;119(1):83-91. doi: 10.1085/jgp.119.1.83.

Sadoshima J, Izumo S. Molecular characterization of angiotensin II--induced hypertrophy of cardiac myocytes and hyperplasia of cardiac fibroblasts. Critical role of the AT1 receptor subtype. Circ Res. 1993 Sep;73(3):413-23. doi: 10.1161/01.res.73.3.413.

Sala L, Gnecchi M, Schwartz PJ. Long QT Syndrome Modelling with Cardiomyocytes Derived from Human-induced Pluripotent Stem Cells. Arrhythm Electrophysiol Rev. 2019 May;8(2):105-110. doi: 10.15420/aer.2019.1.1.

Sánchez-Alonso JL, Halliwell JV, Colino A. ZD 7288 inhibits T-type calcium current in rat hippocampal pyramidal cells. Neurosci Lett. 2008 Jul 18;439(3):275-80. doi: 10.1016/j.neulet.2008.05.016.

Santoro B, Liu DT, Yao H, Bartsch D, Kandel ER, Siegelbaum SA, Tibbs GR. Identification of a gene encoding a hyperpolarization-activated pacemaker channel of brain. Cell. 1998 May 29;93(5):717-29. doi: 10.1016/s0092-8674(00)81434-8.

Santoro B, Wainger BJ, Siegelbaum SA. Regulation of HCN channel surface expression by a novel C-terminal protein-protein interaction. J Neurosci. 2004 Nov 24;24(47):10750-62. doi: 10.1523/JNEUROSCI.3300-04.2004.

Sartiani L, Mannaioni G, Masi A, Novella Romanelli M, Cerbai E. The Hyperpolarization-Activated Cyclic Nucleotide-Gated Channels: from Biophysics to Pharmacology of a Unique Family of Ion Channels. Pharmacol Rev. 2017 Oct;69(4):354-395. doi: 10.1124/pr.117.014035.

Sartiani L, Romanelli MN, Mugelli A, Cerbai E. Updates on HCN Channels in the Heart: Function, Dysfunction and Pharmacology. Curr Drug Targets. 2015;16(8):868-76. doi: 10.2174/1389450116666150531152047.

Satoh H, Hashimoto K. Electrophysiological study of alinidine in voltage clamped rabbit sino-atrial node cells. Eur J Pharmacol. 1986 Feb 18;121(2):211-9. doi: 10.1016/0014-2999(86)90492-9.

Scroggs RS, Todorovic SM, Anderson EG, Fox AP. Variation in IH, IIR, and ILEAK between acutely isolated adult rat dorsal root ganglion neurons of different size. J Neurophysiol. 1994 Jan;71(1):271-9. doi: 10.1152/jn.1994.71.1.271.

Scuderi GJ, Butcher J. Naturally Engineered Maturation of Cardiomyocytes. Front Cell Dev Biol. 2017 May 5;5:50. doi: 10.3389/fcell.2017.00050.

Seccareccia F, Pannozzo F, Dima F, Minoprio A, Menditto A, Lo Noce C, Giampaoli S; Malattie Cardiovascolari Aterosclerotiche Istituto Superiore di Sanita Project. Heart rate as a predictor of mortality: the MATISS project. Am J Public Health. 2001 Aug;91(8):1258-63. doi: 10.2105/ajph.91.8.1258.

Seeger T, Porteus M, Wu JC. Genome Editing in Cardiovascular Biology. Circ Res. 2017 Mar 3;120(5):778-780. doi: 10.1161/CIRCRESAHA.116.310197.

Seifert R, Scholten A, Gauss R, Mincheva A, Lichter P, Kaupp UB. Molecular characterization of a slowly gating human hyperpolarization-activated channel predominantly expressed in thalamus, heart, and testis. Proc Natl Acad Sci U S A. 1999 Aug 3;96(16):9391-6. doi: 10.1073/pnas.96.16.9391.

Serhan CN, Savill J. Resolution of inflammation: the beginning programs the end. Nat Immunol. 2005 Dec;6(12):1191-7. doi: 10.1038/ni1276.

Shah MM. Hyperpolarization-Activated Cyclic Nucleotide-Gated Channel Currents in Neurons. Cold Spring Harb Protoc. 2016 Jul 1;2016(7). doi: 10.1101/pdb.top087346.

Sharma A, Mücke M, Seidman CE. Human Induced Pluripotent Stem Cell Production and Expansion from Blood using a Non-Integrating Viral Reprogramming Vector. Curr Protoc Mol Biol. 2018 Apr;122(1):e58. doi: 10.1002/cpmb.58.

Sheets PL, Suter BA, Kiritani T, Chan CS, Surmeier DJ, Shepherd GM. Corticospinal-specific HCN expression in mouse motor cortex: I(h)-dependent synaptic integration as a candidate microcircuit mechanism involved in motor control. J Neurophysiol. 2011 Nov;106(5):2216-31. doi: 10.1152/jn.00232.2011.

Shiba Y, Hauch KD, Laflamme MA. Cardiac applications for human pluripotent stem cells. Curr Pharm Des. 2009;15(24):2791-806. doi: 10.2174/138161209788923804.

Shin KS, Rothberg BS, Yellen G. Blocker state dependence and trapping in hyperpolarization-activated cation channels: evidence for an intracellular activation gate. J Gen Physiol. 2001 Feb;117(2):91-101. doi: 10.1085/jgp.117.2.91.

Smith AS, Macadangdang J, Leung W, Laflamme MA, Kim DH. Human iPSC-derived cardiomyocytes and tissue engineering strategies for disease modeling and drug screening. Biotechnol Adv. 2017 Jan-Feb;35(1):77-94. doi: 10.1016/j.biotechadv.2016.12.002.

Snyders DJ, Van Bogaert PP. Alinidine modifies the pacemaker current in sheep Purkinje fibers. Pflugers Arch. 1987 Sep;410(1-2):83-91. doi: 10.1007/BF00581900.

Spain WJ, Schwindt PC, Crill WE. Anomalous rectification in neurons from cat sensorimotor cortex in vitro. J Neurophysiol. 1987 May;57(5):1555-76. doi: 10.1152/jn.1987.57.5.1555.

Stahl N, Boulton TG, Farruggella T, Ip NY, Davis S, Witthuhn BA, Quelle FW, Silvennoinen O, Barbieri G, Pellegrini S, et al. Association and activation of Jak-Tyk kinases by CNTF-LIF-OSM-IL-6 beta receptor components. Science. 1994 Jan 7;263(5143):92-5. doi: 10.1126/science.8272873.

Stevens DR, Seifert R, Bufe B, Müller F, Kremmer E, Gauss R, Meyerhof W, Kaupp UB, Lindemann B. Hyperpolarization-activated channels HCN1 and HCN4 mediate responses to sour stimuli. Nature. 2001 Oct 11;413(6856):631-5. doi: 10.1038/35098087.

Stillitano F, Lonardo G, Zicha S, Varro A, Cerbai E, Mugelli A, Nattel S. Molecular basis of funny current (If) in normal and failing human heart. J Mol Cell Cardiol. 2008 Aug;45(2):289-99. doi: 10.1016/j.yjmcc.2008.04.013.

Strong A, Musunuru K. Genome editing in cardiovascular diseases. Nat Rev Cardiol. 2017 Jan;14(1):11-20. doi: 10.1038/nrcardio.2016.139.

Swynghedauw B. Molecular mechanisms of myocardial remodeling. Physiol Rev. 1999 Jan;79(1):215-62. doi: 10.1152/physrev.1999.79.1.215.

Taga T, Kishimoto T. Gp130 and the interleukin-6 family of cytokines. Annu Rev Immunol. 1997;15:797-819. doi: 10.1146/annurev.immunol.15.1.797.

Takahashi E, Fukuda K, Miyoshi S, Murata M, Kato T, Ita M, Tanabe T, Ogawa S. Leukemia inhibitory factor activates cardiac L-Type Ca2+ channels via phosphorylation of serine 1829 in the rabbit Cav1.2 subunit. Circ Res. 2004 May 14;94(9):1242-8. doi: 10.1161/01.RES.0000126405.38858.BC.

Takahashi K, Yamanaka S. Induction of pluripotent stem cells from mouse embryonic and adult fibroblast cultures by defined factors. Cell. 2006 Aug 25;126(4):663-76. doi: 10.1016/j.cell.2006.07.024.

Takigawa T, Alzheimer C, Quasthoff S, Grafe P. A special blocker reveals the presence and function of the hyperpolarization-activated cation current IH in peripheral mammalian nerve fibres. Neuroscience. 1998 Feb;82(3):631-4. doi: 10.1016/s0306-4522(97)00383-7.

Tanaka T, Narazaki M, Kishimoto T. IL-6 in inflammation, immunity, and disease. Cold Spring Harb Perspect Biol. 2014 Sep 4;6(10):a016295. doi: 10.1101/cshperspect.a016295.

Thuringer D, Sauvé R. A patch-clamp study of the Ca2+ mobilization from internal stores in bovine aortic endothelial cells. I. Effects of caffeine on intracellular Ca2+ stores. J Membr Biol. 1992 Nov;130(2):125-37. doi: 10.1007/BF00231891.

Tibbs GR, Rowley TJ, Sanford RL, Herold KF, Proekt A, Hemmings HC Jr, Andersen OS, Goldstein PA, Flood PD. HCN1 channels as targets for anesthetic and nonanesthetic propofol analogs in the amelioration of mechanical and thermal hyperalgesia in a mouse model of neuropathic pain. J Pharmacol Exp Ther. 2013 Jun;345(3):363-73. doi: 10.1124/jpet.113.203620.

Tu H, Deng L, Sun Q, Yao L, Han JS, Wan Y. Hyperpolarization-activated, cyclic nucleotide-gated cation channels: roles in the differential electrophysiological properties of rat primary afferent neurons. J Neurosci Res. 2004 Jun 1;76(5):713-22. doi: 10.1002/jnr.20109.

Vaccari T, Moroni A, Rocchi M, Gorza L, Bianchi ME, Beltrame M, DiFrancesco D. The human gene coding for HCN2, a pacemaker channel of the heart. Biochim Biophys Acta. 1999 Sep 3;1446(3):419-25. doi: 10.1016/s0167-4781(99)00092-5.

Vaidyanathan R, Markandeya YS, Kamp TJ, Makielski JC, January CT, Eckhardt LL. IK1-enhanced human-induced pluripotent stem cell-derived cardiomyocytes: an improved cardiomyocyte model to investigate inherited arrhythmia syndromes. Am J Physiol Heart Circ Physiol. 2016 Jun 1;310(11):H1611-21. doi: 10.1152/ajpheart.00481.2015.

Van Bogaert PP, Pittoors F. Use-dependent blockade of cardiac pacemaker current (If) by cilobradine and zatebradine. Eur J Pharmacol. 2003 Oct 8;478(2-3):161-71. doi: 10.1016/j.ejphar.2003.08.083.

Van Hook MJ, Nawy S, Thoreson WB. Voltage- and calcium-gated ion channels of neurons in the vertebrate retina. Prog Retin Eye Res. 2019 Sep;72:100760. doi: 10.1016/j.preteyeres.2019.05.001.

Varró A, Tomek J, Nagy N, Virág L, Passini E, Rodriguez B, Baczkó I. Cardiac transmembrane ion channels and action potentials: cellular physiology and arrhythmogenic behavior. Physiol Rev. 2021 Jul 1;101(3):1083-1176. doi: 10.1152/physrev.00024.2019.

Vasilyev DV, Shan Q, Lee Y, Mayer SC, Bowlby MR, Strassle BW, Kaftan EJ, Rogers KE, Dunlop J. Direct inhibition of Ih by analgesic loperamide in rat DRG neurons. J Neurophysiol. 2007 May;97(5):3713-21. doi: 10.1152/jn.00841.2006.

Villalba-Galea CA, Chiem AT. Hysteretic Behavior in Voltage-Gated Channels. Front Pharmacol. 2020 Nov 2;11:579596. doi: 10.3389/fphar.2020.579596.

Villière V, McLachlan EM. Electrophysiological properties of neurons in intact rat dorsal root ganglia classified by conduction velocity and action potential duration. J Neurophysiol. 1996 Sep;76(3):1924-41. doi: 10.1152/jn.1996.76.3.1924.

Vinogradova TM, Brochet DX, Sirenko S, Li Y, Spurgeon H, Lakatta EG. Sarcoplasmic reticulum Ca2+ pumping kinetics regulates timing of local Ca2+ releases and spontaneous beating rate

of rabbit sinoatrial node pacemaker cells. Circ Res. 2010 Sep 17;107(6):767-75. doi: 10.1161/CIRCRESAHA.110.220517.

Wahl-Schott C, Baumann L, Zong X, Biel M. An arginine residue in the pore region is a key determinant of chloride dependence in cardiac pacemaker channels. J Biol Chem. 2005 Apr 8;280(14):13694-700. doi: 10.1074/jbc.M413197200.

Wahl-Schott C, Biel M. HCN channels: structure, cellular regulation and physiological function. Cell Mol Life Sci. 2009 Feb;66(3):470-94. doi: 10.1007/s00018-008-8525-0.

Wahl-Schott C, Fenske S, Biel M. HCN channels: new roles in sinoatrial node function. Curr Opin Pharmacol. 2014 Apr;15:83-90. doi: 10.1016/j.coph.2013.12.005.

Wainger BJ, DeGennaro M, Santoro B, Siegelbaum SA, Tibbs GR. Molecular mechanism of cAMP modulation of HCN pacemaker channels. Nature. 2001 Jun 14;411(6839):805-10. doi: 10.1038/35081088.

Wang M, Ramos BP, Paspalas CD, Shu Y, Simen A, Duque A, Vijayraghavan S, Brennan A, Dudley A, Nou E, Mazer JA, McCormick DA, Arnsten AF. Alpha2A-adrenoceptors strengthen working memory networks by inhibiting cAMP-HCN channel signaling in prefrontal cortex. Cell. 2007 Apr 20;129(2):397-410. doi: 10.1016/j.cell.2007.03.015.

Wang J, Wang H, Zhang Y, Gao H, Nattel S, Wang Z. Impairment of HERG K(+) channel function by tumor necrosis factor-alpha: role of reactive oxygen species as a mediator. J Biol Chem. 2004 Apr 2;279(14):13289-92. doi: 10.1074/jbc.C400025200.

Weissbein U, Plotnik O, Vershkov D, Benvenisty N. Culture-induced recurrent epigenetic aberrations in human pluripotent stem cells. PLoS Genet. 2017 Aug 24;13(8):e1006979. doi: 10.1371/journal.pgen.1006979.

Wemhöner K, Silbernagel N, Marzian S, Netter MF, Rinné S, Stansfeld PJ, Decher N. A leucine zipper motif essential for gating of hyperpolarization-activated channels. J Biol Chem. 2012 Nov 23;287(48):40150-60. doi: 10.1074/jbc.M112.378513.

Weng Z, Kong CW, Ren L, Karakikes I, Geng L, He J, Chow MZ, Mok CF, Chan HYS, Webb SE, Keung W, Chow H, Miller AL, Leung AY, Hajjar RJ, Li RA, Chan CW. A simple, cost-effective but highly efficient system for deriving ventricular cardiomyocytes from human pluripotent stem cells. Stem Cells Dev. 2014 Jul 15;23(14):1704-16. doi: 10.1089/scd.2013.0509.

Womble MD, Moises HC. Hyperpolarization-activated currents in neurons of the rat basolateral amygdala. J Neurophysiol. 1993 Nov;70(5):2056-65. doi: 10.1152/jn.1993.70.5.2056.

Woodroofe MN. Cytokine production in the central nervous system. Neurology. 1995 Jun;45(6 Suppl 6):S6-10. doi: 10.1212/wnl.45.6_suppl_6.s6.

Workman AJ, Rankin AC. Serotonin, I(f) and human atrial arrhythmia. Cardiovasc Res. 1998 Dec;40(3):436-7. doi: 10.1016/s0008-6363(98)00258-2.

Wu X, Liao L, Liu X, Luo F, Yang T, Li C. Is ZD7288 a selective blocker of hyperpolarization-activated cyclic nucleotide-gated channel currents? Channels (Austin). 2012 Nov-Dec;6(6):438-42. doi: 10.4161/chan.22209.

Wu N, Xu B, Xiang Y, Wu L, Zhang Y, Ma X, Tong S, Shu M, Song Z, Li Y, Zhong L. Association of inflammatory factors with occurrence and recurrence of atrial fibrillation: a meta-analysis. Int J Cardiol. 2013 Oct 25;169(1):62-72. doi: 10.1016/j.ijcard.2013.08.078.

Xu C. Differentiation and enrichment of cardiomyocytes from human pluripotent stem cells. J Mol Cell Cardiol. 2012 Jun;52(6):1203-12. doi: 10.1016/j.yjmcc.2012.03.012.

Yagi J, Sumino R. Inhibition of a hyperpolarization-activated current by clonidine in rat dorsal root ganglion neurons. J Neurophysiol. 1998 Sep;80(3):1094-104. doi: 10.1152/jn.1998.80.3.1094.

Yamanaka Y, Nakajima K, Fukada T, Hibi M, Hirano T. Differentiation and growth arrest signals are generated through the cytoplasmic region of gp130 that is essential for Stat3 activation. EMBO J. 1996 Apr 1;15(7):1557-65.

Yang X, Pabon L, Murry CE. Engineering adolescence: maturation of human pluripotent stem cell-derived cardiomyocytes. Circ Res. 2014 Jan 31;114(3):511-23. doi: 10.1161/CIRCRESAHA.114.300558.

Yang X, Rodriguez ML, Leonard A, Sun L, Fischer KA, Wang Y, Ritterhoff J, Zhao L, Kolwicz SC Jr, Pabon L, Reinecke H, Sniadecki NJ, Tian R, Ruohola-Baker H, Xu H, Murry CE. Fatty Acids Enhance the Maturation of Cardiomyocytes Derived from Human Pluripotent Stem Cells. Stem Cell Reports. 2019 Oct 8;13(4):657-668. doi: 10.1016/j.stemcr.2019.08.013.

Yang X, Rodriguez M, Pabon L, Fischer KA, Reinecke H, Regnier M, Sniadecki NJ, Ruohola-Baker H, Murry CE. Tri-iodo-l-thyronine promotes the maturation of human cardiomyocytes-derived from induced pluripotent stem cells. J Mol Cell Cardiol. 2014 Jul;72:296-304. doi: 10.1016/j.yjmcc.2014.04.005.

Yao H, Donnelly DF, Ma C, LaMotte RH. Upregulation of the hyperpolarization-activated cation current after chronic compression of the dorsal root ganglion. J Neurosci. 2003 Mar 15;23(6):2069-74. doi: 10.1523/JNEUROSCI.23-06-02069.2003.

Yeon KY, Chung G, Kim YH, Hwang JH, Davies AJ, Park MK, Ahn DK, Kim JS, Jung SJ, Oh SB. Eugenol reverses mechanical allodynia after peripheral nerve injury by inhibiting hyperpolarization-activated cyclic nucleotide-gated (HCN) channels. Pain. 2011 Sep;152(9):2108-2116. doi: 10.1016/j.pain.2011.05.018.

Ying SW, Tibbs GR, Picollo A, Abbas SY, Sanford RL, Accardi A, Hofmann F, Ludwig A, Goldstein PA. PIP2-mediated HCN3 channel gating is crucial for rhythmic burst firing in thalamic intergeniculate leaflet neurons. J Neurosci. 2011 Jul 13;31(28):10412-23. doi: 10.1523/JNEUROSCI.0021-11.2011.

Yoshida Y, Yamanaka S. iPS cells: a source of cardiac regeneration. J Mol Cell Cardiol. 2011 Feb;50(2):327-32. doi: 10.1016/j.yjmcc.2010.10.026.

Yoshida K, Taga T, Saito M, Suematsu S, Kumanogoh A, Tanaka T, Fujiwara H, Hirata M, Yamagami T, Nakahata T, Hirabayashi T, Yoneda Y, Tanaka K, Wang WZ, Mori C, Shiota K, Yoshida N, Kishimoto T. Targeted disruption of gp130, a common signal transducer for the interleukin 6 family of cytokines, leads to myocardial and hematological disorders. Proc Natl Acad Sci U S A. 1996 Jan 9;93(1):407-11. doi: 10.1073/pnas.93.1.407.

Young GT, Emery EC, Mooney ER, Tsantoulas C, McNaughton PA. Inflammatory and neuropathic pain are rapidly suppressed by peripheral block of hyperpolarisation-activated cyclic nucleotide-gated ion channels. Pain. 2014 Sep;155(9):1708-1719. doi: 10.1016/j.pain.2014.05.021.

Yu X, Duan KL, Shang CF, Yu HG, Zhou Z. Calcium influx through hyperpolarization-activated cation channels (I(h) channels) contributes to activity-evoked neuronal secretion. Proc Natl Acad Sci U S A. 2004 Jan 27;101(4):1051-6. doi: 10.1073/pnas.0305167101.

Zhang Q, Jiang J, Han P, Yuan Q, Zhang J, Zhang X, Xu Y, Cao H, Meng Q, Chen L, Tian T, Wang X, Li P, Hescheler J, Ji G, Ma Y. Direct differentiation of atrial and ventricular myocytes from human embryonic stem cells by alternating retinoid signals. Cell Res. 2011 Apr;21(4):579-87. doi: 10.1038/cr.2010.163.

Zhao L, Cheng G, Jin R, Afzal MR, Samanta A, Xuan YT, Girgis M, Elias HK, Zhu Y, Davani A, Yang Y, Chen X, Ye S, Wang OL, Chen L, Hauptman J, Vincent RJ, Dawn B. Deletion of Interleukin-6 Attenuates Pressure Overload-Induced Left Ventricular Hypertrophy and Dysfunction. Circ Res. 2016 Jun 10;118(12):1918-1929. doi: 10.1161/CIRCRESAHA.116.308688. Epub 2016 Apr 28. Erratum in: Circ Res. 2020 Mar 27;126(7):e35.

Zhao Z, Lan H, El-Battrawy I, Li X, Buljubasic F, Sattler K, Yücel G, Lang S, Tiburcy M, Zimmermann WH, Cyganek L, Utikal J, Wieland T, Borggrefe M, Zhou XB, Akin I. Ion Channel Expression and Characterization in Human Induced Pluripotent Stem Cell-Derived Cardiomyocytes. Stem Cells Int. 2018 Jan 8;2018:6067096. doi: 10.1155/2018/6067096.

Zhou C, Ke B, Zhao Y, Liang P, Liao D, Li T, Liu J, Chen X. Hyperpolarization-activated cyclic nucleotide-gated channels may contribute to regional anesthetic effects of lidocaine. Anesthesiology. 2015 Mar;122(3):606-18. doi: 10.1097/ALN.0000000000000557.

Zolles G, Klöcker N, Wenzel D, Weisser-Thomas J, Fleischmann BK, Roeper J, Fakler B. Pacemaking by HCN channels requires interaction with phosphoinositides. Neuron. 2006 Dec 21;52(6):1027-36. doi: 10.1016/j.neuron.2006.12.005.

Zong X, Stieber J, Ludwig A, Hofmann F, Biel M. A single histidine residue determines the pH sensitivity of the pacemaker channel HCN2. J Biol Chem. 2001 Mar 2;276(9):6313-9. doi: 10.1074/jbc.M010326200.